Creating a simplified and standardised bioreactor system for tissue-engineered vascular graft culturing and characterisation

by

Dmitri Visser

in partial fulfilment of the requirements for the degree of

Master of Science

in Biomedical Engineering

at the Delft University of Technology to be defended publicly on Wednesday, 5th of December 2018 at 14:00.

Student number: 4279913

Submission date: 25th of November 2018

Sending institution

Delft University of Technology, Delft, The Netherlands Faculty of Mechanical, Maritime, and Materials Engineering (3mE) Department of Biomechanical Engineering Section of Biomaterials & Tissue Biomechanics

MSc-thesis advisor: dr. ir. Lidy Fratila-Apachitei
Chair examining committee: Prof. dr. Amir Zadpoor
External committee member: dr. ing. Saša Kenjereš

Receiving institution

Natural and Medical Sciences Institute at the Univ. of Tübingen (NMI), Reutlingen, Germany Department of Functional Surfaces and Biomaterials Section of Biomaterials Engineering

Supervision: Dr. Svenja Hinderer

Responsible person at receiving institution: Prof. Dr. Katja Schenke-Layland





Acknowledgements

First of all, I would like to express my gratitude to Prof. Dr. Katja Schenke-Layland and Dr. Svenja Hinderer, as well as to my thesis advisors from Delft (dr. Lidy Fratila-Apachitei and Prof. dr. Amir Zadpoor) for the opportunity to work in the Schenke-Layland Lab group, where I started at the location in Stuttgart as student intern and laboratory assistant and continued at the location in Reutlingen as a master thesis student. I want to express special gratitude to Svenja for her role as supervisor during this master thesis. I want to thank her for her valuable feedback and for her scientific and organisational support.

I want to thank 'die Spinner': Ruben Daum, Nora Feuerer, Kathrin Stadelmann, and Johannes Morschl for the great atmosphere at the NMI in Reutlingen, for all the support and time I have spent with them so far both during and outside work hours. Special thanks to Ruben, with whom I have been working together since the start at Fraunhofer IGB in Stuttgart. I would like to extend my gratitude to all staff members who supported me at the NMI, especially to Sebastian Wagner and Simon Werner, without whom this project would not have been possible. They have made a tremendous contribution by providing technical assistance whenever I knocked on their door. I want to thank them for the numerous discussions I had with them and for the introduction to the machinery and electrical equipment at the NMI. Additionally, my special gratitude towards Dr. Martin Stelzle, for showing the value of cooperation, for the effort in the organisation of the Friday's seminars, and for all the inspiring talks about physics during lunchtime. Furthermore, I would like to thank all members of the Schenke-Layland Lab group at the laboratory in Tübingen, especially Simone Liebscher, Daniel Carvajal Berrio, and Dr. med. Martin Weiss for whenever I needed something in the lab or from the university hospital Tübingen.

Abstract

With the recent developments in tissue-engineered organ substitutes, there has been an increasing demand for novel culturing techniques to create biological substitutes in vitro, as well as reliable and efficient test methods that can assess their biocompatibility and mechanical performance. In the past two decades, perfusion bioreactors have proved to be important tools in the creation, control, and evaluation of cell cultures and engineered tissues under precisely controlled in vitro conditions that simulate the physiological environment. Due to the demanding requirements for blood vessel substitutes, they have been extensively deployed in the culture and conditioning experiments of novel tissue-engineered vascular grafts (TEVGs) and have been often used to study haemodynamic mechanic stimuli, including the cyclic vessel expansion and wall shear stress. However, a key limitation of the currently available TEVG perfusion bioreactors is their often complex design and operation and the lack of standardisation of the mechanical characterisation.

In this study, the goal was to design, characterise, and construct a TEVG perfusion bioreactor that is foremost simpler to operate and extends the capabilities of particular currently available set-ups. A modular bioreactor design is presented that allows for the toolless mounting of the graft with a diameter up to 6 mm and features completely separated circuits for the intraand extraluminal side of the scaffold wall. The culture chamber encloses a removable graft frame, mainly machined out of polyether ether ketone (PEEK). In silico simulations have been used to assess local fluid dynamics within the scaffold, to predict the reliability of the simulated culture conditions. The presented design allows the exertion of a broad range of physiologically relevant shear stresses on cultured TEVGs, including arterial shear stresses. A test for the in vitro cytotoxicity showed that the medium extracts of the constructed graft frame did not show any cytotoxic potential. Finally, an assessment method for the estimation of the radial compliance is proposed, which aims to adhere to the relevant international standards on the mechanical characterisation of vascular substitutes.

Table of contents

Acknow	vledgements	3
Abstrac	ct	5
Table o	f contents	7
List of	Symbols	9
List of	figures	11
List of	tables	17
1 In	troduction	19
1.1	Blood vessels	19
1.1.1	Blood vessel anatomy	19
1.1.2	Biomechanics	20
1.2	Tissue Engineering	22
1.2.1	Scaffold mechanics	22
1.2.2	Biologic interaction	23
1.3	Bioreactor systems	24
1.3.1	Bioreactors in tissue engineering	24
1.3.2	Bioreactors for vascular tissue engineering	25
1.3.3	Computational fluid dynamics	28
1.3.4	Mechanical testing standard	29
1.4	Aim of this study	30
2 M	aterials	33
3 M	ethods	37
3.1	Design	37
3.1.1	Culture chamber	37
3.2	In silico simulation	39
3.2.1	Meshing	39
3.2.2	Physical setup	40
3.2.3	CFD validation	42
3.3	Chamber construction	42
3.4	Cytotoxicity test	43
3.5	Pressure monitoring	45
3.5.1	Sensor calibration	45
3.5.2	Readout	46
3.6	Compliance estimation	46

3.7	Leakage test	48
4	Results	49
4.1	Design of the bioreactor system	49
4.1.1	Overview	49
4.1.2	Graft frame and culturing chamber	52
4.2	Characterisation of the bioreactor system	55
4.2.1	Calibration	55
4.2.2	Pressure losses	57
4.2.3	Wall shear stress	60
4.2.4	Cytotoxicity test	64
4.2.5	Leakage test	65
4.3	Compliance estimation	66
5	Discussion	69
5.1	Culture chamber design	69
5.1.1	Design novelty	69
5.1.2	Medium consumption	70
5.2	Characterisation	.70
5.2.1	Fluid mechanics	. 71
5.2.2	Cytotoxicity and sterility	. 73
5.3	Compliance estimation	.73
6	Conclusion	75
7	Outlook	. 77
Biblio	ography	. 78
Appe	ndix	83
A.	Norms	83
I.	ISO 7198:2016	83
II.	EN ISO 10993-5:2009	84
B.	CAD Drawings	85
C.	Code	93
l.	Vessel dilation measurement (Algorithm 1: Real-time Hough Transform)	93
II.	Vessel dilation measurement (Algorithm 2: Width measurement by thresholding)	97
III.	Read wall shear stress from CFD data	98
D.	MTS raw data	. 99

List of Symbols

Symbol	Unit	Property
C	% / 100 mmHg	radial compliance
D	m, mm	diameter
$D_{ m i}$	m, mm	internal diameter
F	N	force (vector)
μ	Pa s, mPa s	kinematic viscosity
<i>p, P</i>	Pa	pressure
Q	ml min ⁻¹	volumetric flow rate
r	m, mm	radius
ρ	kg m ⁻³	density
Re	-	Reynolds number
t	S	time
τ	Pa	shear stress tensor
v, u	m s-1	velocity magnitude
V	m³, mL, L	volume
v	m s-1	velocity (vector)
x	m, mm	x-position
â		unit vector, x-direction
y	m, mm	y-position
z	m, mm	z-position

List of figures

Figure	e 1 Generalised structure of an artery indicating the three blood vessel layers (tunicae). Adapted from Marieb and Hoehn (2015)	. 20
Figure	e 2 A simplified drawing showing the effects of fluid flow in hollow bodies, such as blood vessels. The flowing fluid exerts a shear stress on the wall, which in turn can elicit a cascade of biologic reactions, resulting in the production of e.g. structural fibres	. 21
Figure	e 3 A bioreactor setup that has been specifically designed to exert a well-defined shear stress on a flat scaffold. Left: schematic cross section view of the bioreactor setup. Right: results of an in silico simulation show the expected flow rate and shear stress on the substrate. Figure from Hinderer et al. (2015). Image licensed under CC-BY 3.0.	. 25
Figure	e 4 A flow chamber of a perfusion bioreactor for vascular tissue engineering as developed by Diamantouros (2011). The TEVG is clamped in the flow chamber with its luminal side connected to the bioreactor system tubing. The red inlets (not connected to bioreactor system tubing) allow for a perfusion of the outer surface of the TEVG.	. 26
Figure	e 5 From left to right: Schematic representation of a centrifugal pump; a peristaltic or roller pump; and actuator mechanisms to induce a pulsatile flow, such as a piston-driven pulse chamber; a tubular constriction. Adapted from Wright (1997)	. 26
Figure	e 6 Pressure readout of a vascular bioreactor system that was set to mimic either fetal pulse conditions at 120 bpm (left) or adult pulse conditions at 60 bpm (right) (Hahn et al. 2007)	. 27
Figure	e 7 Left: Schematic illustration of the working principle of a laser- or LED-based optical micrometre that is often used to non-invasively measure the diameter of cultured TEVGs, which is used for the estimation of the radial compliance. The schematic illustration has been adapted from (Laterreur et al. 2014). Right: A pulsatile perfusion bioreactor system featuring optical micrometre (G) to measure the compliance of the vascular graft in a transparent graft chamber (F) inside an incubator to perform the experiment at physiological temperatures. (Diamantouros et al. 2013)	. 30
Figure	e 8 A schematic illustration of the principle of the ring tensile test. This test can be used to determine the circumferential tensile strength and as an indirect test for the burst pressure of a vascular graft.	. 30
Figure	e 9 Cross section of a structured three-dimensional mesh, showing the concentrically inflation layers and the use of hexahedronal cells near the wall.	. 39
Figure	e 10 Visualisation of the imposed velocity distribution on the inlet (equation 8). The inlet is positioned in the yz-plane. The inlet has a diameter of 3 mm and $vmax$ is 0.236 m/s	. 40
Figure	been designed such, that they possess all machining steps, which the actual bioreactor parts undergo as well. The surface area was used in the calculation of the required extraction medium volume.	. 44

performed with 6 technical replicates. For every group, 6 wells are filled with cells (solid colour) and 6 wells without cells (striped pattern). The latter are used as background correction in the evaluation of the MTS absorption	. 45
Figure 13 Summary of the diameter measurement workflow. A : A grayscale image is acquired. B : The contrast is adjusted to increase the difference between the foreground and background. A Gaussian filter is applied to remove noise. C : The Canny edge detection algorithm is used to create a binary image that only shows detected edges. However, this includes all edges and can also include curly edges due to unremoved noise or shadows. D : To quantify the location (and rotation) of straight edges in the pictures, the Hough transform is applied to the binary image. The bright areas around $\rho=200$, 470 and $\theta=0^{\circ}$ indicate that the image contains two vertical lines with a distance of 270 pixels from each other. E : The found distance between the left and right edge are displayed on an overlay image. F : The measurement is outputted for further analysis in e.g. Matlab.	
Figure 14 Summary of the rewritten diameter extraction algorithm. A: a grayscale image is acquired. B: the acquired video frames are converted to binary images. Consecutively, the number of pixels below the binary threshold (in black) are summed for every row. C: the mean of extracted widths is calculated per frame.	. 48
Figure 15 Schematic representation of the circulation of the bioreactor system, when the system is used for tissue culture. The shaded part of the bioreactor is placed inside an incubator. The orange colour indicates the intraluminal circulation that passes through the lumen of the vascular scaffold. The purple colour indicates the extraluminal circulation that passes through the exterior parts in the culture chamber. Dashed lines indicate arms of the circulation that can be closed off with three-way stopcocks	. 49
Figure 16 This schematic diagram shows the pressure regulating effect of the tube clamps. The pump delivers the total pressure head, which can be regarded as the potential for the fluid to flow through the circulation. The tube clamps introduce resistances to the intraluminal circulation, which raise the pressure upstream with respect to the clamps. This allows the pressure to be kept around 100 mmHg within the scaffold and at gauge pressure at the medium bottle, where the gas exchange takes place.	. 50
 Figure 17 Overview of the bioreactor set-up. The intraluminal circulation is coloured red by perfusing it with a red dye with the exception of the pulse chamber connection line. The extraluminal circulation is perfused with water and, thus, is shown by transparent tubing. In this set-up, only one pressure transducer has been connected. A: pump. B: pressure buffer. C: tube clamp. D: culture chamber. E: pressure transducer (not visible in the bottom picture). F: pulse chamber. G: intraluminal medium reservoir with sterile filter attached. H: extraluminal medium reservoir with sterile filter attached. 	. 51
Figure 18 Cross-sectional view of the culture chamber. In the wireframe model, the black parts show the scaffold frame, whereas the purple parts show the scaffold and its adapters. The frame is brought into the culture chamber in its entirety (light blue) and closed off with a bottle cap with a large bore hole (blue)	. 52

Figure 19 Photo of the graft frame without a scaffold. The Luer adapters with rotating collars are the graft mounting points. The red sealing o ring ensures the closing of the interior of the culture chamber and is pressed into place by the bottle cap
Figure 20 The graft frame can accommodate vascular graft with different diameters, as it uses standard Luer adapters as graft mounting points. The rotating collars of the Luer adapters prevent torqueing of the scaffold itself.
Figure 21 The sensitivity of the B. Braun pressure transducers per volt as function of the pressure. The pressure has been referenced to the output of the WIKA pressure sensor
Figure 22 Measured flow rates of the open-loop calibration of the flow rate as function of the Ismatec pump head rotation speed. The pressure was kept constant at 100 mmHg by regulating the tube clamp downstream of the culture chamber.
Figure 23 The intraluminal pressure in mmHg with respect to the pressure at the outlet, which has been set as the gauge pressure. In this depicted in silico case, a scaffold diameter of 5 mm and the rheological properties of water at 20 °C have been used. The imposed flow rate was 20 ml/min.
Figure 24 A comparison between the predicted (in silico) pressure loss from the in silico simulations and the measured pressure loss in mmHg. The pressure loss is defined as the pressure difference between the average pressure at the inlet and at the outlet
Figure 25 Pressure profiles as function of time for three different pump head rotation speeds, corresponding to flow rates of 1.9, 10.9 and 32.6 ml/min. The dotted lines indicate the root mean square deviation from the pressure mean.
Figure 26 A comparison between the predicted (in silico) pressure loss from the in silico simulations and the measured pressure loss in mmHg after implanting the pressure buffer. The pressure loss is defined as the pressure difference between the average pressure at the inlet and at the outlet.
Figure 27 The pressure was stabilised by the introduction of a pressure buffer. These pressure readings show the difference between the unstabilised pressure and the stabilised pressure. The pressure buffer has allowed for much higher flow rates
Figure 28 Colour plot of the velocity distribution within the intraluminal circulation in the culture chamber
Figure 29 This plot shows a subset of Figure 28 , namely the beginning of the scaffold, and the influence of flow profiles on the wall shear stress. The colour plot and the arrows in the bottom half display the velocity distribution within the scaffold up to 30 mm from the beginning of the scaffold. The streamlines show a recirculation zone at the entrance and redevelopment of a steady pipe flow in more downstream regions. The line plot in the upper half of the image shows the wall shear stress at the corresponding positions. The lowest shear stress occurs at the reattachment site of the recirculation zone (approximately at x = 4 mm). Further downstream, the wall shear stress returns to the Poiseuille value

Figure 30 Normalised wall shear stress profiles along the scaffold wall for different flow rates. The wall shear stress profiles have been normalised to the Poiseuille value, implying that the wall shear stress approaches 1 when the flow redevelops.	. 61
Figure 31 The length it takes for the flow to redevelop itself and to reach a stable wall shear stress as function of the imposed flow rate. Four in silico cases have been considered, where the scaffold diameter and the fluid properties of water were changed.	. 62
Figure 32 The achievable shear forces in the bioreactor compared to physiologically occurring shear forces in veins and arteries based on in vivo measurements (Ford et al. 2005; Rittgers et al. 1978; Wu et al. 2004). SFA: superficial femoral artery, ITA: internal thoracic artery, CCA: common carotid artery, BA: brachial artery. For the shear stress ranges of the bioreactor, the solid lines include the range up to 50 ml/min, which has been included in the CFD simulations. The dashed lines include the range up to 140 ml/min, which has only practically been tested without CFD simulations.	. 63
Figure 33 The Poiseuille values (developed wall shear stress value) within the scaffold for different flow rates. This plot compares the observed Poiseuille values to those of the analytical solution.	. 63
Figure 34 Results of the cytotoxicity test, assessed by means of a MTS assay. The results have been corrected for the background and have been normalised to the negative control (NC). PC: positive control. AI: Aluminium extract.	. 64
Figure 35 Any possible leakage within the culture chamber was assessed after one day and two days. Foreground: culture chamber. Background: extraluminal medium reservoir. No colouring of the extraluminal medium was seen.	65
Figure 36 A comparison of the performance of the diameter extraction algorithms. The extracted diameter has been plotted against the time and compared to the pressure that had been simultaneously recorded with the pressure transducer. On the top: the diameter has been extracted using the Hough transform. The 'stair casing effect' indicates that the diameter measurements are rounded to the nearest pixel. Bottom: the diameter has been extracted using the rewritten algorithm.	. 66
Figure 37 Left: the recorded pressure has been plotted against the correlated inner diameter, which have been acquired by slow pressurisation of the dummy scaffold. Right: The radial expansion has been analysed for three ranges: 50 – 90 mmHg, 80 – 120 mmHg, and 110 – 150 mmHg. The radial expansion is expressed in % per 100 mmHg. Error bars show the 95% confidence interval.	. 67
Figure 38 Analysis of the dynamic radial compliance estimation, where a scaffold is pressurised with a pulsatively at a physiological frequency of 1 Hz. A subset of 7 seconds of the recording of the pressure and the calculated internal diameter have been plotted against the time. On the left: the dummy scaffold has been pressurised over the range of 50 – 90 mmHg. On the right: the dummy scaffold has been pressurised over the range of 110 – 150 mmHg.	. 68
Figure 39 Left: the recorded pressure has been plotted against the correlated inner diameter, which	

have been acquired by oscillating pressurisation of the dummy scaffold at a frequency of 1

Hz over three ranges: 50 – 90 mmHg, 80 – 120 mmHg, and 110 – 150 mmHg. Right: The radial expansion has been analysed and expressed in % per 100 mmHg. Error bars show the 95% confidence interval	68
Figure 40 The achievable shear forces in the bioreactor compared to physiologically occurring	
shear forces in veins and arteries based on in vivo measurements (Ford et al. 2005; Rittgers	
et al. 1978; Wu et al. 2004) and studies on the influence of shear stress on cell behaviour.	
For the shear stress ranges of the bioreactor, the solid lines include the ranges up to 50	
ml/min, which were included in the CFD simulations. The dashed lines include the range up	
to 140 ml/min, which was only practically been tested without CFD simulations.	
Abbreviations: SFA: superficial femoral artery, ITA: internal thoracic artery, CCA: common	
carotid artery, BA: brachial artery.	72

List of tables

Table	1 Chemicals and raw construction materials, which were used in this study, are listed in the table below
Table	2 Components that have been used in the assembly of the bioreactor, are listed in the table below
Table	3 Used culture medium and supplements for culture of microvascular endothelial cells
Table	4 Used cells in the cytotoxicity test
Table	5 Non-exhausting overview of used equipment. This table includes the tools that have been used to machine the graft frame and assemble the AD circuit. However, some tools might not have been included in the list, as not all tools in the workshop were inventarised. Furthermore, this table includes all equipment that has been used during cell culture
Table	6 Overview of used cell culture disposables
Table	7 Overview of used software
Table	8 Overview of the bottles that have been considered as casing for the culturing chamber
Table	9 Overview of the used fluid properties in the numerical simulations. The properties have been taken from the physical properties of water at 20° C and at 37° C. The diameter of the inlet, d inlet, has been taken from the inner diameter of the first Luer adapter. The maximum velocities, v max, have been calculated based on the inlet diameter and the chosen flow rates Q , which have been varied between 0.2 and 50 ml/min
Table	10 Overview of the ANSYS CFD solver settings that have been used in this study
Table	11 Linear least squares fit of the calibration of the B. Braun pressure transducer readout. The fitted value for $x0$ can be regarded as the zero shift and the value for $x1$ as the sensitivity of the sensor. $R2$ gives the coefficient of determination (ordinary) of the fitted values
Table	12 Linear least squares fit of the intraluminal flow rate with respect to the applied pump head rotation speed

1 Introduction

Circulatory diseases and ischaemia are among the leading causes of death in western countries (WHO 2015). As these diseases become more prevalent in ageing societies, it is foreseen that they will remain a burden in the foreseeable future in developed countries. Despite efforts to prevent cardiovascular diseases (CVDs) by risk-reducing strategies, the World Health Organisation estimated that about 31% of all deaths could be related CVDs in 2015 and this is expected to rise even further in the future (Nichols et al. 2014; WHO 2015). Besides a better understanding of the development and prevention of these circulatory diseases, it is important to improve the currently available medical treatment of acute ischaemia. Since effective therapies to fully restore cardiovascular organs are lacking, regenerative medicine currently focusses on novel implants and treatment techniques and implants that have the potential to replace the use of autologous and homologous grafts.

1.1 Blood vessels

1.1.1 Blood vessel anatomy

Blood vessels form a circulatory and highly dynamic delivery system that pulsates, constricts, relaxes and proliferates. The walls of blood vessels can be subdivided into three distinct layers, the tunicae, that enclose the central blood-containing space, the lumen or intraluminal space, and separate it from the surrounding extraluminal space (Figure 1) (Marieb and Hoehn 2015). The innermost layer, the tunica intima, contains endothelial cells (ECs) that form the endothelium, which is critical for the proper functioning of a blood vessel and the prevention of thrombus formation (Isenberg et al. 2006). The lack or the inability by the body to form a functional endothelium on the inner side of vascular implants is often the primary cause of the implant's failure. The middle layer, the tunica media, is mostly circularly aligned and contains smooth muscle cells (SMCs) and elastin fibres. It contributes to the mechanical strength of the blood vessel wall and is responsible for maintaining the blood pressure by regulating vasoconstriction and vasodilatation (Marieb and Hoehn 2015). The outer layer of the blood vessel, the tunica adventitia, is primarily populated by fibroblasts, residing in a loosely woven collagen network, which anchors the vessel to its surroundings (Pugsley and Tabrizchi 2000).

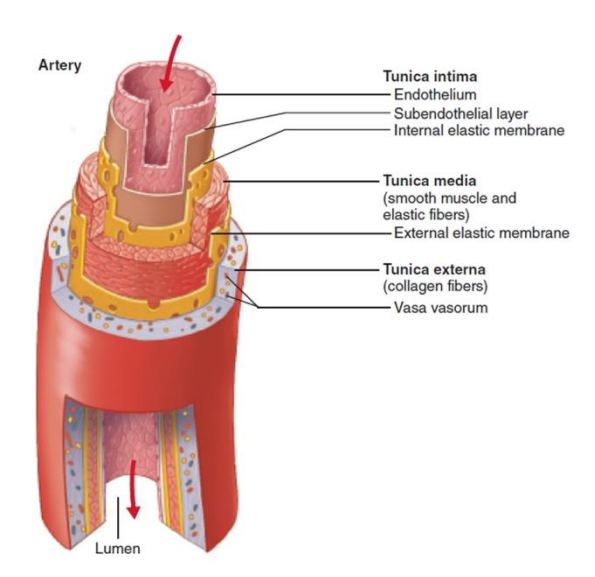


Figure 1 Generalised structure of an artery indicating the three blood vessel layers (tunicae). Adapted from Marieb and Hoehn (2015).

1.1.2 Biomechanics

To understand the physiology of circulation, it is necessary to remember that the entire circulatory system starts and ends at the heart, acting as a pulsatile pump that drives the entire system (Marieb and Hoehn 2015). Blood consecutively flows through the blood vessels from its starting point with high pressure to its end point at the right atrium with low pressure, driven by the pressure gradient. At the same time, it encounters an opposing resistance force as blood flows along the vessel walls. This resistance force depends on the viscosity of the blood, vessel length, and vessel diameter (Marieb and Hoehn 2015). Since the viscosity of blood and total vessel length remain fairly constant, the local blood flow is mainly affected by the diameter of the blood vessels and their ability to expand under pressure. Due to the pulsatile nature of blood flow, blood vessels are continuously subjected to a repeated loading. The elastin fibres allow the blood vessel wall to expand and relax under systolic and diastolic pressure and act as a pressure reservoir to maintain the pressure gradient during the heart's diastole (Opie and Paterson 2004). Lack of functional elastin fibres and endothelial dysfunction can lead to arterial stiffness, which is often accompanied by an increased systemic blood pressure. Inversely, any lack of stiffness has been associated with the development of aneurisms (Kielty 2006). The extent to which a blood vessel is expanded with increased transmural pressure is an important quantifiable mechanical property, which is referred to as the compliance (Kelly and Chowienczyk 2002). The compliance is defined as the ratio of the change in volume ΔV of a hollow body with respect to the change in pressure Δp :

$$C = \frac{\Delta V}{\Delta p} \tag{1}$$

Since the volume of a hollow body, in this case a blood vessel, is mainly affected by its diameter d, this relation can be expanded to:

$$C = \frac{\Delta d/d_{p_1}}{\Delta p} = \frac{d_{p_2} - d_{p_1}}{d_{p_1} (p_2 - p_1)}$$
 (2)

where d_{p_1} and d_{p_2} refer to the diameter at pressure p_1 and p_2 respectively. In physiology, the circumferential compliance is often expressed as a percentage per 100 mmHg. It is important to note, that the mechanical properties of a blood vessel wall are non-linearly elastic (Vito and Dixon 2003). Therefore, to be able to compare the compliance between vascular grafts, the compliance has to be measured in the same pressure range, commonly between 80 and 120 mmHg. Blood vessels also express viscoelastic mechanical properties, which means that the compliance does not only depend on the strain, but also on the strain rate (Maxwell and Anliker 1968). In vivo measurements of the compliance of blood vessels are possible with highresolution ultrasound analysis or with magnetic resonance imaging (MRI) (Arndt et al. 1968; Hokanson et al. 1972; Leeson et al. 2006). Ex vivo or in vitro conditions enable the implementation of much easier methods to measure the compliance of blood vessels (Langewouters et al. 1984). The pulsatile nature of the blood flow through the arterial system results in a number of haemodynamic forces, to which blood vessel walls are subjected. These forces include tensile stress due to circumferential deformations, hydrostatic pressure stress, and shear stress acting longitudinally due to blood flow (Marieb and Hoehn 2015). In turn, the exertion of these forces on the blood vessel wall results in varying responses, such as protein expression, protein secretion, and morphological changes. It has been shown that the shear stress plays an important role in the expression of structural proteins (Hinderer et al. 2015). To understand the idea of shear forces, it is helpful to look at an idealised laminar flow profile in a blood vessel, as displayed in figure x. The fluid velocity will take a parabolic velocity profile, which in turn results in linear velocity gradient that peaks near the walls. Multiplying this gradient with the viscosity μ of the fluid, yields the shear force:

$$\tau = \mu \frac{\partial u}{\partial y} \tag{3}$$

The highest shear force is found near the walls, which will be referred to as the wall shear stress.

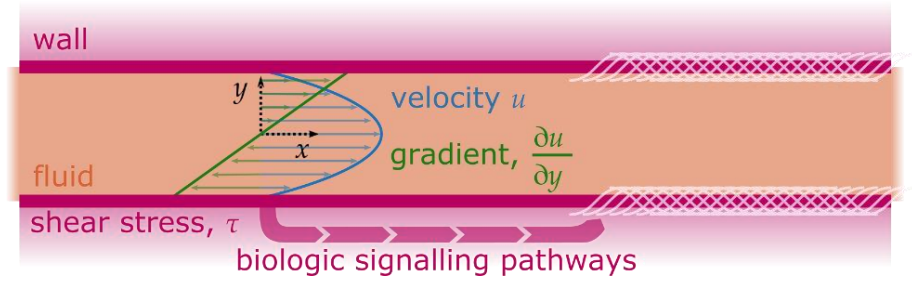


Figure 2 A simplified drawing showing the effects of fluid flow in hollow bodies, such as blood vessels. The flowing fluid exerts a shear stress on the wall, which in turn can elicit a cascade of biologic reactions, resulting in the production of e.g. structural fibres.

1.2 Tissue Engineering

The high mechanical demands and active and critical functions of the endothelium, make blood vessels a challenging organ to substitute. Since effective therapies to fully restore organs is lacking, the emerging field of tissue engineering has focussed on the creation and improvement of functional biomaterials to create scaffolds that have the potential to partially or fully replace diseased organs (Kelleher and Vacanti 2010). The biomaterials that are used in tissue engineering, should meet some basic requirements, which are generally referred to as the biocompatibility (Williams 2008). They should foremost not evoke unwanted responses in the host, they have to be sterilisable, and they should possess the mechanical properties that match those of the native tissue. The precise definition of the term has been subject to constant change. As of today, there is still no single definition. An attempt to construct an elaborate, yet precise definition has been done by Williams (2008) and reads:

"Biocompatibility is the ability of a biomaterial to perform its desired function with respect to a medical therapy, without eliciting any undesirable local or systemic effects in the recipient or beneficiary of that therapy, but generating the most appropriate beneficial cellular or tissue response in that specific situation, and optimising the clinically relevant performance of that therapy."

Biomaterials come in a wide variety, including metals, ceramics, and polymers. Biomaterials can be biodegradable, acting solely as a temporary substitute, or they can be nondegradable, which means they will stay within the body after implantation (Rakhorst and Ploeg 2008). In the case of vascular tissue engineering, often used biomaterials to create blood vessel scaffolds are polyesters, such as: PCL, polylactic acid (PLA), and polylactic-co-glycolic acid (PLGA). Other polymers include polyethylene oxide (PEO) and polyurethanes (PUs) (Khorshidi et al. 2016; Zhang et al. 2009). Scaffolds can be adapted to host cells and promote tissue restoration, which can be achieved by modifying the microstructural properties or by making the material functional, so it can contain proteins, growth factors and extracellular matrix (ECM) components. Highly promising are the so-called biomimetic scaffolds, which imitate the native ECM architecture and provide an in vivo-like microenvironment that is tailored to specific cells and allow for the generation of high levels of cellular complexity (Kelleher and Vacanti 2010). Scaffold architecture affects cell attachment, proliferation, migration, and differentiation (Kim et al. 2012).

1.2.1 Scaffold mechanics

The success of a tissue-engineered scaffold is to a large extent determined by its resilience and elasticity, as it will continuously be subjected to mechanical stresses, when implanted in vivo. Grafts must be able to withstand supraphysiologic loading conditions and at the least match the mechanical properties of native tissues (Stylianopoulos et al. 2008). For tissue-engineered vascular grafts (TEVGs), important mechanical properties comprise the stiffness of the material, compliance of the vessel and the burst pressure. The exemplary case for a smalldiameter blood vessel is the internal thoracic artery (ITA), which has an elastic modulus of

around 20 MPa and a burst pressure of around 3000 mmHg, largely depending on factors including age, sex and/or cardiovascular diseases (Konig et al. 2009). The stiffness of the material is usually taken as the first indicator of the mechanical capability of a material and is specific for the structure of the material. It can be drastically different from the elastic modulus of the raw material in its extruded form (Chow 1980; Coble and Kingery 1956). A good example is given by the use of poly-ε-caprolactone (PCL) in tissue engineering. Although PCL has often been used in biomedical engineering as biomaterial, the polymer shows poor mechanical properties for application in TEVGs. Typical stress-strain curves of fibrous PCL mats show a very high stiffness and signs of early onset of plastic deformation (Huang et al. 2003; Li et al. 2002). However, fine tuning of the elastic modulus has been made possible by exploiting the electrospinning technique to precisely control the fibre diameter (Khorshidi et al. 2016; Rnjak-Kovacina and Weiss 2011; Wong et al. 2008). In previous studies, it has been shown that the elastic modulus of fibrous PCL blend scaffolds can be varied over a range from 0.26 MPa to 32.94 MPa by controlling the diameter of PCL fibres (Drilling et al. 2009; Ju et al. 2010). Other techniques to control the elastic properties of fibrous mats, include controlling the fibre orientation (Ayres et al. 2006; Matthews et al. 2002). This has enabled researchers to even more closely mimic the overall structure of a native blood vessel, whose elastic properties are largely determined by the alignment of ECM fibres in the laminae (McClure et al. 2009; Pauly et al. 2016; Wu et al. 2018). In the long term, mechanical properties should not change after repetitive loading or under oxidative environments. The stability of the mechanical properties are important indicators of the durability of a TEVG and is a key requirement of a graft's acceptance to the clinical practice.

1.2.2 Biologic interaction

The most complete way to evaluate whether the implanted graft fulfils its role, is to test the graft in vivo in an animal trial. The main material of the scaffold, remnants of the production process, and incorporated bioactive components, can trigger adverse effects in the recipient, ranging from local tissue remodelling to a systemic auto-immune response (Rakhorst and Ploeg 2008). A TEVG should enable cell infiltration, promote native tissue ingrowth, and consequently result in the production of ECM components (Kennedy et al. 2017; Khorshidi et al. 2016). The design of the scaffold can also be adapted to promote these specific responses in the host. The cellmatrix interaction is highly dependent on the scaffold structure, the mechanical properties, and biochemical signals that are sensed by the infiltrating cells (Kennedy et al. 2017). An important condition for the ability of cells to grow into the scaffold is a high porosity and interconnectivity of the cavities inside the fibrous mats. These two material parameters form a large surface to volume ratio, which contributes to the cellular adhesion and growth (Khorshidi et al. 2016; Rnjak-Kovacina and Weiss 2011). Fine-tuning of the fibre diameter of ECM-mimicking porous scaffolds in the submicron range has shown to accelerate early cell attachment kinetics and to contribute to a more developed cytoskeletal organisation (Ju et al. 2010). Another way of controlling the biologic responses is achieved by biofunctionalisation of the scaffolds. As

synthetic polymers lack cell recognition sites or do not always possess the most optimal surface properties for cell adhesion, a growing number of studies have looked into various strategies for the chemical (Cao et al. 2004; Tallawi et al. 2015) and biological (Braghirolli et al. 2017; Hinderer et al. 2018) functionalisation of scaffolds to make the materials more attractive to cells.

1.3 Bioreactor systems

1.3.1 Bioreactors in tissue engineering

To evaluate whether the TEVG will be able to uphold its biocompatibility and to study the biologic interaction, it is necessary to reproduce the conditions to which the graft will be exposed after implantation. Bioreactor systems are important tools in the emulation of these in vivo conditions. Bioreactors have traditionally been associated with large cylindrical vessels, also called stirred-tank reactors that were specifically used in the area of biochemistry or chemical engineering. Tissue engineering stimulated an interest in specifically designed bioreactor systems, as the research area created a need for highly controlled tissue culture, which cannot be achieved using established culture techniques. Bioreactor systems for tissue engineering should "simulate physiological environments for the creation, physical conditioning, and testing of cells, tissue, precursors, support structures, and organs in vitro" (Barron et al. 2003). The design of modern tissue engineering bioreactors is more closely related to clinical artificial perfusion systems than to the 'classic bioreactors'. Artificial perfusion systems originated from the pioneering work by Carrel and Lindbergh in the 1930s (Carrel and Lindbergh 1938). These systems formed the foundation of heart-lung systems, which made their clinical introduction in the 1950s. With respect to its predecessors, the core of the design principle of the tissue engineering bioreactor has remained largely unchanged (Kasyanov et al. 2005). It should provide the tissue with sufficient nutrients and simultaneously ensure an adequate removal of metabolic waste products, while controlling the environmental variables of the tissue (Martin et al. 2004). Tissue engineering has extended the requirements, including the possibility to expose the tissue-engineered constructs to precisely defined physical stimuli and closely monitor tissue during culture to an extent that was not possible using standard culturing techniques. Pörtner et al. (2005) and Barron et al. (2003) listed the functions and tasks a bioreactor can perform:

- a) provide sufficient fresh medium and nutrients, whilst simultaneously removing waste products
- **b)** control concentration of gases in the culture medium and the environmental variables of the tissue, such as temperature, oxygen, carbon dioxide and pH
- c) monitor tissue and culture parameters
- d) exert physical stimuli on the cultured tissue
- e) enable uniform cell seeding
- f) promote cell proliferation and migration

Since bioreactors enable a very precise control of the in vitro environment, they provide an optimal solution for simulating in vivo culturing conditions. To investigate the biologic interaction,

multiple research groups have adapted computer-controlled perfusion bioreactors to perform tissue conditioning experiments (Diamantouros et al. 2013; Engbers-Buijtenhuijs et al. 2006; Hahn et al. 2007; Ju et al. 2017; Maschhoff et al. 2017; Song et al. 2012; Wang et al. 2010; Wolf et al. 2018). These bioreactors can impart mechanical and biochemical stimuli, which in turn promotes cell differentiation, ECM protein production, and tissue remodelling. Physiologically accurate stimuli are crucial for the development of functional tissues. Deviations in the pressure and frequency from normal physiological values are known to significantly influence the development of engineered tissues (Stock and Vacanti 2001). A study by Hinderer et al. (2015) focussed on the creation of developed and functional elastic fibres as function of the applied shear forces on the scaffold. Smooth muscle cells seeded on electrospun polyethylene glycol dimethacrylate (PEGdma) were subjected to a defined shear stress in a perfusion bioreactor (Figure 3). This shear stress had been first calculated using an in silico simulation of the bioreactor, which simulated the shear stress on the substrate as function of the defined medium flow rate at the inlet. As a result, a positive effect on elastin expression and deposition was observed, as well as new functional fibre formation.

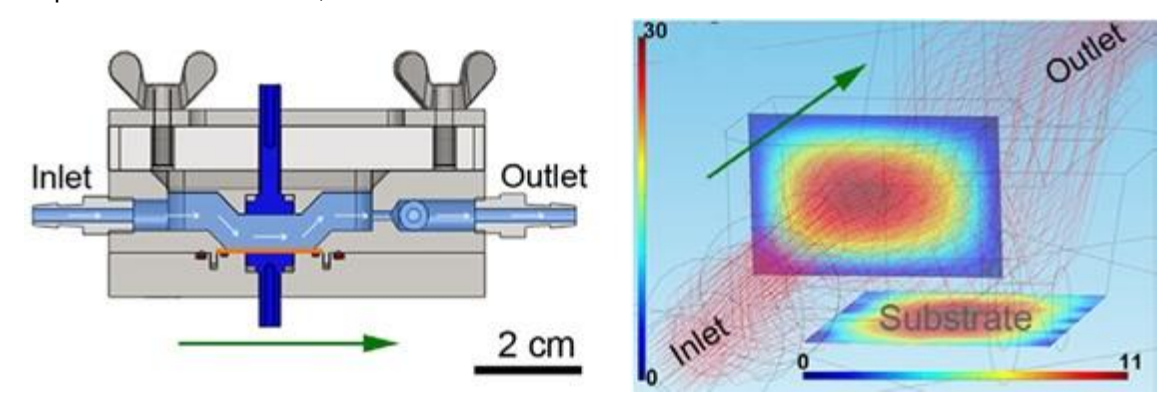


Figure 3 A bioreactor setup that has been specifically designed to exert a well-defined shear stress on a flat scaffold. Left: schematic cross section view of the bioreactor setup. Right: results of an in silico simulation show the expected flow rate and shear stress on the substrate. Figure from Hinderer et al. (2015). Image licensed under CC-BY 3.0.

Bioreactors for vascular tissue engineering 1.3.2

An interesting subclass of bioreactors for use in the creation of TEVGs are perfusion bioreactors, which can be deployed for mechanical testing, cell seeding, and mechanical cell preconditioning (Martin et al. 2004). The characteristic components of vascular perfusion systems are a pump, tubing, a medium reservoir, and a flow chamber, in which the TEVG is clamped (Figure 4). The flow chamber is used to perfuse the luminal side and the outer surface of the TEVG with culture medium. When the lumen and the exterior flow chamber compartment outside of the vessel (extralumen) are connected to different tubing circuits and different cell medium reservoirs, a fully separated perfusion of the lumen and the outer part of the vessel with different culturing media is possible (Maschhoff et al. 2017; Tosun and McFetridge 2013). This way, different cells can be independently cultured on the lumen and ablumen. Most vascular bioreactor systems, however, feature a non-separated flow circuits that are both connected to

the same medium reservoir (Diamantouros et al. 2013; Engbers-Buijtenhuijs et al. 2006; Hahn et al. 2007; Melchiorri et al. 2016; Piola et al. 2013; Song et al. 2012; Wolf et al. 2018).

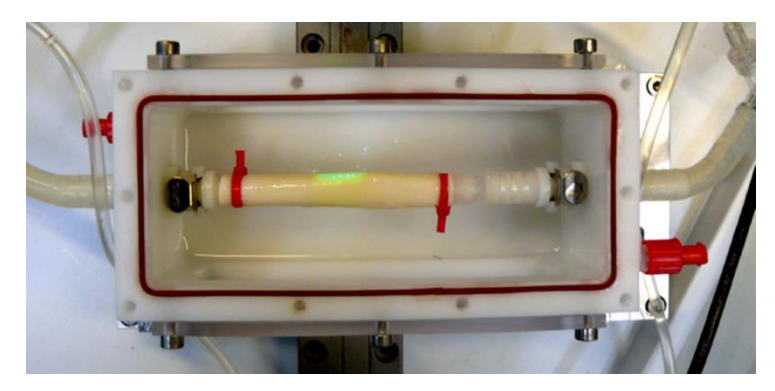


Figure 4 A flow chamber of a perfusion bioreactor for vascular tissue engineering as developed by Diamantouros (2011). The TEVG is clamped in the flow chamber with its luminal side connected to the bioreactor system tubing. The red inlets (not connected to bioreactor system tubing) allow for a perfusion of the outer surface of the TEVG.

The scaffold is usually fixed onto simple Luer-type tapers in combination with specially designed cuffs or simple universal disposables, such as tie wraps, to ensure a water-tight connection between the scaffold and the chamber inlets. The exact procedure to clamp the vascular scaffold into the flow chamber is, however, often poorly described. Diamantouros has written an elaborate description of the bioreactor assembly procedure, including steps to attach the vascular scaffold in the flow chamber (Diamantouros 2011). It states that the assembly of the entire bioreactor requires the operation by two persons to assure a sterile assembly. The majority of the set-up, including the flow chamber, silicone tubing, pump, pulse chamber, and reservoir, has to be assembled inside a sterile work bench, before it is transferred in its entirety to an incubator.

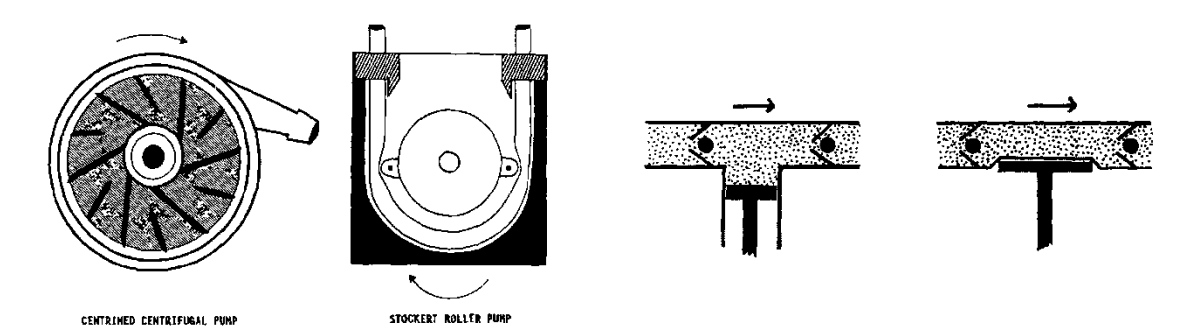


Figure 5 From left to right: Schematic representation of a centrifugal pump; a peristaltic or roller pump; and actuator mechanisms to induce a pulsatile flow, such as a piston-driven pulse chamber; a tubular constriction. Adapted from Wright (1997).

The pump is the driving force behind the circulation of the culture medium in a bioreactor system. Peristaltic pumps, also known as roller pumps, mimic the principle of peristalsis of the gastrointestinal tract by compressing a flexible tube by lobes fixed on a rotor (**Figure 5**). As the rotor lobes do not come in contact with the fluid, peristaltic pumps do not pose any risk of

contamination and require little maintenance. This has favoured the use of peristaltic pumps in medical applications. Centrifugal pumps can be costlier in maintenance, as the interior of the pump comes in contact with the fluid and therefore should be thoroughly sterilised after use. Wolf et al. (2018) focussed on the low price and disposability of bioreactors in a clinical application and opted to use a low-cost disposable centrifugal pump. A specific design aspect of many vascular perfusion reactors is the ability to perfuse the construct with a pulsatile flow (as opposed to a continuous flow), which mimics the natural blood flow. However, peristaltic pumps are not suited for the creation of high-amplitude pulsatile flow, which necessitates the use of external actuating mechanisms to induce pulses by means of additional pulsatile pumps, pulse chambers or the constriction of tube walls (Wright 1997). These simple mechanisms can induce high-amplitude pulses with completely independent control of stroke volume and pulse frequency, which allows for flow waveforms that closely resemble cardiac output. Pulsatile pumps and pulse chambers enable a precise control of the pressure and can create pulses with a steep peak (Figure 6) and have been often applied in vascular perfusion reactors (Diamantouros 2011; El-Kurdi et al. 2009; Hahn et al. 2007; Maschhoff et al. 2017).

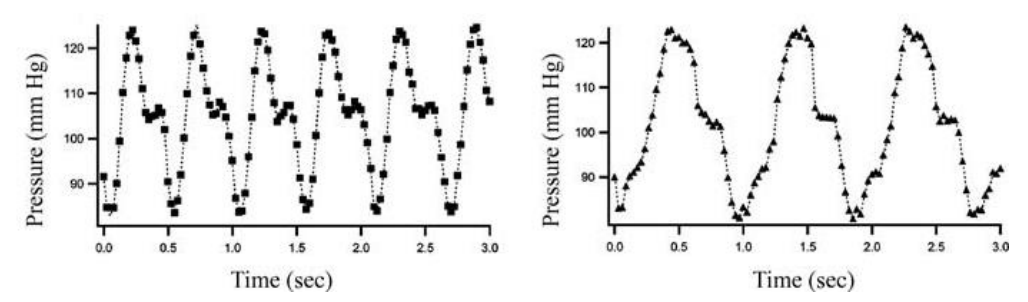


Figure 6 Pressure readout of a vascular bioreactor system that was set to mimic either fetal pulse conditions at 120 bpm (left) or adult pulse conditions at 60 bpm (right) (Hahn et al. 2007).

Wolf and colleagues used a centrifugal pump in combination with variable resistance to induce a pulsatile flow by constricting flexible tubing (Wolf et al. 2018). A more bio-inspired design approach was taken by Thompson, who created a vascular perfusion bioreactor without the use of rotary pumps and, instead, used the propulsion principle of a heart as reference (Thompson et al. 2002). A combination of one-way valves and pressure pulses applied by an air pump through a silicone membrane sufficed for the creation of a physiologically reasonably accurate flow profile. Some research groups have completely omitted a complete circulation and the use of any pump in their bioreactor design (Laterreur et al. 2014; Levesque et al. 2011). Instead in these cases, a syringe driven by a stepper motor was connected through a tube to the interior of the TEVG. Depending on the specific purpose of the bioreactor, the set-up can be equipped with additional components to control or monitor the cultured tissue. The standard approach to control the tissue environment is to place the bioreactor, or only the flow chamber, in an incubator, which maintains desired temperature and CO2 level. Perfusion bioreactors can be further equipped with sensors and feedback systems in order to continuously control the environment and flow conditions. Sensor readout and actuator control is usually facilitated by an

analogue-to-digital converter (ADC) and a serial connection to a computer running a software platform such as LabView. Another approach is to omit the use of a desktop computer and deploy programmable microcontrollers for the control of the bioreactor (Wolf et al. 2018). Vascular perfusion systems can also be designed to mimic a physiologically accurate shear force. This aspect is, however, often underexposed or left unmentioned in published designs of such systems. A number of research groups have presented vascular bioreactors that were specifically designed to investigate the effects of the shear force on the cell morphology and protein expression on cellularised vascular grafts (Hahn et al. 2007; Inoguchi et al. 2007). Melchiorri et al. showed a simplified design of a single-circulation vascular perfusion bioreactor that imparted a physiologically relevant venous wall shear stress on endothelial progenitor cells (EPCs) (Melchiorri et al. 2016). The dynamically cultured grafts showed increased expression of markers for mature endothelial tissues with respect to statically cultured grafts. Such responses of EPCs have been shown before by cell culture in flow chambers without scaffolds (Egorova et al. 2012; Obi et al. 2012). The study by Melchiorri et al. shows that relatively simple bioreactors can be used to reproduce this effect on cellularised three-dimensional vascular scaffolds. The recent increase in use of in silico simulations with computational fluid dynamics (CFD) software has enabled further optimisation of the flow conditions in bioreactors and can, if available computational power permits, even be used to adjust flow conditions during cultivation (Martin et al. 2004; Maschhoff et al. 2017). Maschhoff et al. used an in silico model of the vascular graft that was updated by an ultrasound measurement of the tissue on the graft during culture (Maschhoff et al. 2017). This way, the flow rate could be adjusted to keep a stable shear force on the wall of the graft, as it grew during tissue culture.

1.3.3 Computational fluid dynamics

To determine whether the bioreactor suits the demands for the specific tissue engineering application, it is necessary to know the rheology within the bioreactor. However, characterisation of rheological features by physical testing is often insufficient and analytical expressions are limited to idealised shapes. Computational fluid dynamics (CFD) is an in silico technique, where numerical simulations are exploited to provide a much more elaborate insight in local flow-related phenomena in complex structures, such as flow profiles, flow regimes, and shear forces. Fluid simulations can predict the regions in the bioreactor that fulfil the shear stress requirements for cell culturing and conditioning, prior to the construction of the bioreactor. This section briefly covers the physics on which numerical computations are based. The first principle that has to be satisfied is the conservation of mass, which dictates that for any closed system, mass can neither be spontaneously created nor destroyed. Any mass accumulation or loss must be due to mass either entering or leaving this control volume:

$$\frac{\partial \rho}{\partial t} = -\nabla \cdot (\rho \mathbf{v}) \tag{4}$$

where ρ denotes the density and ${\bf v}$ is the fluid velocity vector. The left-hand side of the equation gives the change in mass density over time, due to amount of mass accumulation on the right-

hand side of the equation. Since blood, just like water, is assumed to be incompressible, the density can be considered constant. Therefore, equation (4) can be simplified to

$$(\nabla \cdot \mathbf{v}) = 0 \tag{5}$$

essentially stating, that the mass accumulation should be zero. Another conservation law that has to be satisfied, is the conservation of momentum. Similarly to the conservation of momentum, it is possible to formulate an expression for the rate of inflowing and outflowing momentum: $\nabla \cdot \rho \mathbf{vv}$. However, momentum can also be lost or gained by viscous transfer and external forces acting on the system. The equation that takes these additional factors into account, also called the equation of motion is given by

$$\frac{\partial}{\partial t} \rho \mathbf{v} = -\left[\nabla \cdot \rho \mathbf{v} \mathbf{v}\right] - \nabla p - \left[\nabla \cdot \boldsymbol{\tau}\right] + \mathbf{F}$$
(6)

where p is the pressure, τ is the shear stress tensor, and F is the sum of all external forces acting on the system. Knowing that our control volumes are incompressible (5), the Navier-Stokes equation is acquired:

$$\rho\left(\frac{\partial \mathbf{v}}{\partial t} + \mathbf{v} \cdot \nabla \mathbf{v}\right) = -\nabla p - [\nabla \cdot \boldsymbol{\tau}] + \mathbf{F}$$
(7)

CFD software is essentially written to iteratively solve explicit formulations of the Navier-Stokes equation. Three-dimensional computer models are subdivided into a large number of cells that act as small control volumes. This process is called meshing. The conservation law problem is rewritten to a differential equation and solved for every cell face. Boundary conditions for these differential equations are imposed by for example stating, that certain cell faces are impermeable (the model's walls) or certain locations have a defined pressure or velocity profile (the model's inlet and outlet).

1.3.4 Mechanical testing standard

To conserve comparability between studies of artificial vascular grafts, the international standard ISO 7198:2016 has been specified, of which a large portion is dedicated to the mechanical evaluation of vascular prostheses. This standard supersedes the older ISO 7198:1998 standard (ISO 2016). Relevant test procedures in the norm regarding the mechanical characterisation are the measurement of the dynamic radial compliance (Figure 7), circumferential tensile strength (Figure 8), and pressurised burst strength. In the dynamic radial compliance test, the vascular graft is pressurised with a gas or fluid in a cyclic fashion with the intention to determine the radial compliance of the vascular graft. The length of the tested prosthesis should have a length of more than 10 times its diameter, fixated with a longitudinal preload between 0.294 and 0.588 N (ISO 2016). For permeable and porous vascular grafts, the use of a non-permeable liner is prescribed, which needs to have a compliance that is significantly higher than the compliance of the vascular graft to be measured. Three pressure ranges have to be considered to account for nonlinear elastic properties: 50 - 90 mmHg, 80 -120 mmHg, and 110 - 150 mmHg. Moreover, the standard requires, that the transducer should be able to measure the pressure to an accuracy of 2 mmHg and that the error in the

measurement of the diameter should not exceed 0.02 mm. The compliance is subsequently determined according to equation (2). The test conditions should approximate the in vivo environment. The determination of the compliance has to be carried out at 37 ± 2 °C and with a pulsatile frequency of 60 ± 10 bpm (ISO 2016). A more elaborate overview of the standards can be found in the appendices of this report.

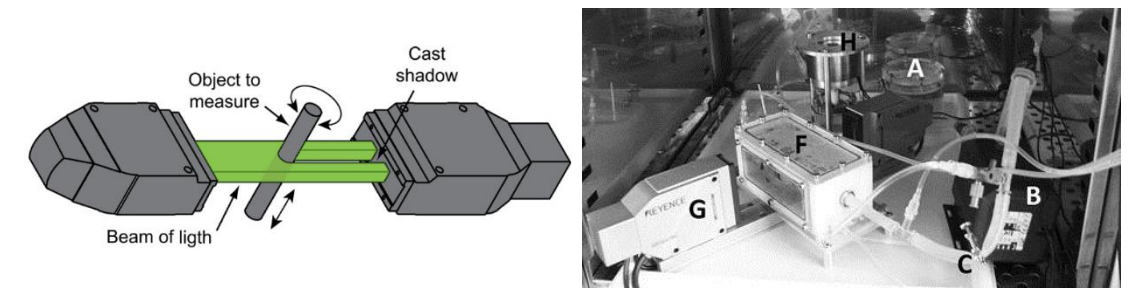


Figure 7 Left: Schematic illustration of the working principle of a laser- or LED-based optical micrometre that is often used to non-invasively measure the diameter of cultured TEVGs, which is used for the estimation of the radial compliance. The schematic illustration has been adapted from (Laterreur et al. 2014). Right: A pulsatile perfusion bioreactor system featuring optical micrometre (G) to measure the compliance of the vascular graft in a transparent graft chamber (F) inside an incubator to perform the experiment at physiological temperatures. (Diamantouros et al. 2013)

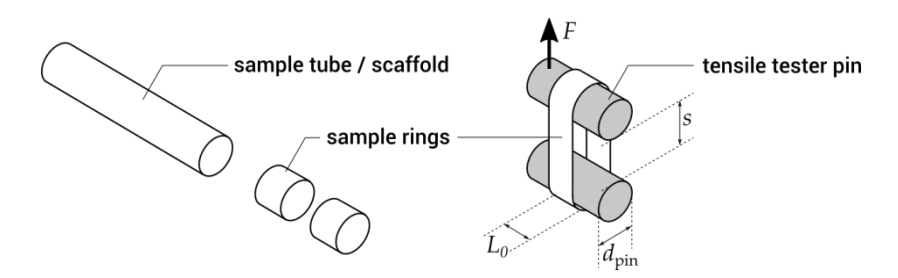


Figure 8 A schematic illustration of the principle of the ring tensile test. This test can be used to determine the circumferential tensile strength and as an indirect test for the burst pressure of a vascular graft.

1.4 Aim of this study

A number of research groups have looked into adapting computer-controlled perfusion bioreactors to perform dynamic tissue culture experiments on vascular grafts. A lot of bioreactors, however, require tedious handling under sterile conditions or are otherwise imparted by the gradually increasing number of measurement modalities. Furthermore, not all bioreactors focus on the reproduction of physiologically accurate shear forces. Recent studies have shown that these forces play an important role in protein expression and the development of engineered tissues. In this study, the aim is to present a design and develop a bioreactor that is both simpler to use and addresses some of the shortcomings of the currently available tissue-engineering bioreactors in literature. A novel bioreactor for vascular tissue engineering should

have a simpler operation and method to clamp and detach vascular scaffolds. An important aspect in the design of the bioreactor is the ability to mimic physiologically relevant shear stresses on the cultured tissue. In silico simulations shall indicate whether the design is able to reproduce these shear stresses on the scaffold wall. In addition to that, the focus lies on a design that has the potential to parallelise the tissue culture, so multiple scaffolds can be assessed in long-term culture experiments simultaneously. Lastly, it is important to perform the mechanical characterisation in compliance with international standards to improve comparability between studies. Therefore, this study will also present an approach towards a mechanical test of the cultured tissue in accordance with the ISO standard on the mechanical characterisation of vascular grafts.

2 **Materials**

Table 1 Chemicals and raw construction materials, which were used in this study, are listed in the table below.

Chemical	Company		Ref. no.	LOT no.
CellTiter 96 Aqueous One	Promega GmbH	Mannheim, Germany	G3580	0000246915
Endothelial Cell Growth Medium MV	PromoCell GmbH	Heidelberg, Germany	C-22020	431M369
Endothelial Cell MV Supplement Mix	PromoCell GmbH	Heidelberg, Germany	C-39225	429M083
Ethanol 70%	Carl Roth GmbH & Co KG	Karlsruhe, Germany		
Isopropanol 70%	Carl Roth GmbH & Co KG	Karlsruhe, Germany		
Polyether ether ketone (PEEK)	ADS Kunststofftechnik	Ahaus, Germany	111780	
Polyoximethylene (POM)	Reiff TP	Reutlingen, Germany	178120	
Polytetrafluorethylene (PTFE)	Reiff TP	Reutlingen, Germany		
Ponceau S / Acid Red 112	Carl Roth GmbH & Co KG	Karlsruhe, Germany	5938.2	462193737
Trypan blue solution (0.4%)	Sigma-Aldrich	Darmstadt, Germany	T8154	RNBC1670
CellTiter 96 Aqueous One	Promega GmbH	Mannheim, Germany	G3580	0000246915

Table 2 Components that have been used in the assembly of the bioreactor, are listed in the table below.

Туре	Name	Company		Product no.
Bottle	DURAN Youtility Clear GL45 250ML	Schott	Mitterteich, German	y21 881 36 53
Сар	DURAN GL45 Blue Cap PP	Schott	Mitterteich, German	y 29 239 28
Сар	DURAN Youtility GL45 Cap PP	Schott	Mitterteich, German	y 29 229 28 02
Connectors	Adapter Luer F to 1/4"-28 UNF	GoNano Dosiertechnik	Breitstetten, Germany	VPABSML-6005-1
Connectors	Rotating Luer M to 1/4"-28 UNF	GoNano Dosiertechnik	Breitstetten, Germany	VPSFTLL-1
Connectors	M6 to 3mm Barb Connector	Cole-Parmer	Vernon Hills (IL), United States	
Connectors	Fitting Luer F to 1/4" PC	Cole-Parmer	Vernon Hills (IL), United States	45501-20
Connectors	Fitting Luer F to 1/8" PC	Cole-Parmer	Vernon Hills (IL), United States	45501-04
Connectors	Fitting Luer M to 1/8" PC	Cole-Parmer	Vernon Hills (IL), United States	45504-04
Connectors	Plug Barbed 1/8" Nylon	Cole-Parmer	Vernon Hills (IL), United States	31220-13
Electronics	ADS1115	Texas Instruments	Dallas (TX), United States	ADS1115
Electronics	Arduino Nano ATmega328	Open-source hardware		

Frame	Alu 4mm rod	Toom	Köln, Germany	1704197
O Ring	MVQ 26mm x 2mm	Reiff TP	Reutlingen, Germany	4365680
O Ring	FPM 14mm x 1mm	Reiff TP	Reutlingen, Germany	1007960
Pump	ISMATEC ISM404	Cole-Parmer	Vernon Hills (IL), United States	10704
Sensor	Combitrans Exadyn Pressure Transmitte	er B. Braun	Melsungen, Germany	8913536
Sensor	S-10 01 bar	WIKA	Klingenberg am Main, Germany	36306215
Tubing	Ismatec Pharmed 2-Stop SC0746	Cole-Parmer	Vernon Hills (IL), United States	95692-48
Tubing	Ismatec Tygon LMT-55 SC0048T	Cole-Parmer	Vernon Hills (IL), United States	05502-48
Tubing	Rotilab Silicone	Carl Roth	Karlsruhe, Germany	9562.1
Tubing	Rotilab Silicone	Carl Roth	Karlsruhe, Germany	9569.1
Valve	4-way stopcock	Cole-Parmer	Vernon Hills (IL), United States	30600-04
Valve	Discofix 3-way stopcock	B. Braun	Melsungen, Germany	1710500

Table 3 Used culture medium and supplements for culture of microvascular endothelial cells.

Component	Company		Ref. no.	LOT no.
Endothelial Growth Cell Medium MV	PromoCell GmbH	Heidelberg, Germany	C-22020	431M369
Endothelial MV Supplement Mix:	PromoCell GmbH	Heidelberg, Germany	C-39225	429M083
5.0% FCS				
0.4% EC growth supplement				
10 ng/ml Epidermal growth factor				
90 μg/ml Heparin				
1 μg/ml Hydrocortisone				
Antibiotics supplements:				
Penicillin-Streptomycin				

Table 4 Used cells in the cytotoxicity test.

Cell type	Origin	Donor	LOT
Human microvascular endothelial cells	Primary isolation	F, 48 years, upper arm	AZb, 23.08.17, P1

Table 5 Non-exhausting overview of used equipment. This table includes the tools that have been used to machine the graft frame and assemble the AD circuit. However, some tools might not have been included in the list, as not all tools in the workshop were inventarised. Furthermore, this table includes all equipment that has been used during cell culture.

Туре	Name	Company	
Bioreactor fabrication			
Benchtop power supply	Triple Power Supply HM8040-3	Hameg	Mainhausen, Germany
CNC Milling Machine	2-Axis Flatbed	Isel	Eichenzell, Germany
Drill press	AB3/ESV	Alzmetall	Altenmarkt an der Alz, Germany
Milling cutters	1 mm Carbide Micro End – 668.507-0106	μSPPW	Lich, Germany
Milling cutters	3 mm Carbide Extra Long – 662.640-0300	μSPPW	Lich, Germany
Milling cutters	4 mm Carbide Extra Long – 662.640-0400	μSPPW	Lich, Germany
Milling cutters	5 mm Micro Radius – 668.529-0500	μSPPW	Lich, Germany
Milling cutters	8 mm 4-Flute Carbide – 664.640-0800	μSPPW	Lich, Germany
Multimeter	70 III	Fluke	Everett (WA), United States
Syringe pump	2-syringe pump	Cole Parmer	Vernon Hills (IL), United States
Thread dies	M4 Die 6G Garant	Hoffmann Group	München, Germany
Thread taps	1/4"-28 UNF	μSPPW	Lich, Germany
Thread taps	M5 Hand tap 132200	Precitool	Neuenstein, Germany
Thread taps	M6 Hand Tap 132200	Precitool	Neuenstein, Germany
Cell culture			
Centrifuge	Rotofix 32	Hettich	Tuttlingen, Germany
Freezer	öko	Privileg	Stuttgart, Germany
Fridge	öko Energiesparer	Privileg	Stuttgart, Germany
Incubator	BBD 6220	Binder GmbH	Tuttlingen, Germany
Microscope	Eclipse TS100	Nikon	Tokyo, Japan
Pipette controller	Pipetboy	Integra	Zizers, Switzerland
Microplate reader	EnVision 2105 Multimode Plate Reader	PerkinElmer	Waltham, MA (USA)
Hemocytometer	Blaubrand Neubauer Improved	Brand	Wertheim, Germany
Precision pipette	Multipette Plus	Eppendorf	Hamburg, Germany
Precision pipette	Single 10 μl, Research Plus	Eppendorf	Hamburg, Germany
Precision pipette	Single 1000 μl, Research Plus	Eppendorf	Hamburg, Germany
Precision pipette	Single 200 µl, Research Plus	Eppendorf	Hamburg, Germany
Sterile bench	S 1800	BDK Luft- und Reinraumtechnik	Sonnenbühl, Germany
Compliance estimation			
Dummy scaffold	Clear silicone sleeve ID6 / 0.5	Hilltop	Warrington, United Kingdom
Microscope	SteREO Discovery.V12	Carl Zeiss	Oberkochen, Germany

Table 6 Overview of used cell culture disposables.

Туре	Name	Company		Product no.
Aspirating pipettes				
Cell culturing flasks	CellStar T75 Cell Culture Flask (TC-treated)	Greiner	Kremsmünster, Austria	C7231
Cell culturing flasks				
Centrifuge tubes	15 mL centrifuge tube	Greiner	Kremsmünster, Austria	T1943
Centrifuge tubes	50 mL centrifuge tube	Greiner	Kremsmünster, Austria	T2318
Centrifuge tubes	CentriStar Self-standing 50 mL Centrifuge Tubes	Corning		430921
Microplate	Cell Culture Plate, 96-well (TC-treated) Eppendorf		0030 730.119
Pipette tips	10 μl, TipOne	Starlab	Hamburg, Germany	
Pipette tips	1000 μL, TipOne	Starlab	Hamburg, Germany	,
Pipette tips	200 μL, Research Plus	Starlab	Hamburg, Germany	,
Pipette tips	Pipette tips (1000 μl)	Eppendorf		0030 077.571
Serological pipette	10 ml, Cellstar	Greiner	Kremsmünster, Austria	
Serological pipette	5 ml, Cellstar	Greiner	Kremsmünster, Austria	

Table 7 Overview of used software.

Name	Publisher	Version	Application
ANSYS Fluent	ANSYS Inc.	19.0	CFD simulations
Arduino IDE	Open Source Software	1.8.5	C coding for Arduino
Endnote	Clarivate Analytics	X8	Reference management
Inkscape	Open Source Software	0.92.3	Thesis illustrations
IsyCAM	Isel	2.9.0	CNC motor control
Matlab	Mathworks	2016a, 2018b	Data acquisition and analysis
Office	Microsoft	2010	Text processing
OpenCV	Open Source Software	3.4.2	Video processing library
Solidworks	Dassault Systèmes	2017	CAD modelling
Tecplot 360	Tecplot Inc.	2014 R1	Post CFD data visualisation
Visual Studio	Microsoft	2017	C++ coding, compiling
Wallac EnVision Manager	PerkinElmer	1.12	Multiplate reading

3 **Methods**

3.1 Design

3.1.1 Culture chamber

The culturing chamber has been an important aspect in the design of the bioreactor, as it forms the largest obstacle in the culturing preparation. This study will present a bioreactor system, including an optimised design of the culture chamber, while also taking the ISO standard requirements into consideration. To eliminate the steps that complicate culture preparation, the approach in designing the culture chamber included a number of design principles, which are listed below:

- a) The assembly of the culture chamber should be toolless. Not only does the use of tools increase the chance of introducing insterilities to the system, it also greatly increases the number of parts that has to be sterilised prior to culturing. A possible drawback, however, is that the assembly should be made water-tight using only muscle power, which can complicate the design.
- b) The culture chamber should be leak-free. First of all, it must be closed off when it is placed in an incubator to ensure sterile conditions inside the culture chamber. Secondly, the intraluminal and extraluminal circulation should be separated.
- c) The culture chamber should enable sensor read out, enabling the monitoring of the culture conditions.
- d) Testing of the scaffold should not damage the scaffold.

In this study, the idea was to use a transparent casing with a single opening. This reduces the chance of leakage, as the chamber has to be closed off at a single location. The scaffold itself, would be attached onto a graft frame, which would be brought in its entirety into the culturing chamber through the single opening. A difficulty in the design process arose, when a suiting object had to be found that could serve as the transparent casing of the culturing chamber, as a number of requirements should be taken into consideration, which are listed below:

- a) The casing should be autoclavable or a relatively cheap disposable, which can be obtained in sterile packaging.
- b) The casing should be clear.
- c) The dimensions of the casing should be able to accommodate a vascular graft, while minimising the amount of needed medium. Generally, this means, that oblong shapes are preferred.
- d) In case real-time optical measurements of the vascular graft are performed, the casing should have flat and parallel faces. Any other face shapes will refract light entering and

- leaving the casing, which will complicate the optical assessment methods, such as measurement of the diameter.
- e) The opening should be big enough to enable the insertion of the graft frame.
- f) The material of the casing should, especially at the inlet, be able to withstand forces that are exerted on the casing, when the graft frame is inserted and is enclosed water-tight.

In the search for a suitable casing, two possible approaches were evaluated.

Self-milled chamber

One possible approach was to mill the chamber from a single block of transparent polymer. This would theoretically enable a fully customisable culturing chamber design, fulfilling all requirements that have been listed above. Transparent polymers that are suited for CNC machining and are often as a transparent layer of a bioreactor include polycarbonate and polysulfone (PSU). However, the geometry requirements would likely prove this approach to be very challenging, as it is difficult to mill deep and narrow pockets with a conventional milling setup. Furthermore, a milled surface of a transparent material needs post-processing treatments to smoothen the surface and achieve the best transparency. Due to the extreme concave form of the interior of the culturing chamber, this would most likely not have been possible with the available equipment in the workshop of the institute.

Using laboratory utensils

Another approach was to look for lab utilities that could be repurposed as casing for the culturing chamber. Bottles proved to be the most promising lab ware. The search was narrowed down to square bottles, as their square shapes could minimise light refraction and, therefore, enable optical measurement during cultivation. At first, square wide-mouth bottles from ThermoFisher, Bürkle, Corning, Schott, and Simax were considered (figure x). Since the datasheets that were available online only provided limited details on the bottle dimensions, product samples have been requested to assess the usability of the bottles. All glass bottles were already available in the lab.

Table 8 Overview of the bottles that have been considered as casing for the culturing chamber.

Company	Product	Material	Volume	Sample obtained
ThermoFisher	Nalgene Dilution Bottle	Polysulfone	220 ml	no (not in stock)
Buerkle	Square PC Lab Bottle	Polycarbonate	250 ml	no (exceeded max. sample value)
Buerkle	Square PET Lab Bottle	Polyethyleentereftalaat	250 ml	yes
Corning	Square PC Storage Bottle	Polycarbonate	250 ml	yes
Schott	Duran Square Lab Bottle	Borosilicate glass	250 ml	
Schott	Duran Square Lab Bottle	Borosilicate glass	500 ml	
Simax	Square Lab Bottle	Borosilicate glass	500 ml	

The 500 ml bottles were considered to be unsuitable, since extraluminal perfusion would require large amounts of cell culture medium. The square 250 ml bottles, however, bore another dimensional problem. Their height was insufficient for the graft frame, if the recommendation of the ISO standard on minimum graft length was taken into consideration, which states that the length of a cultured and tested vascular graft should be at least 10 times its diameter. Although the height of the Schott Duran square bottle would suffice, the glass has an irregular thickness. Therefore, the idea of a square culturing chamber that enables optical compliance measurement during culturing was abandoned, in favour of round bottles that come in longer sizes.

3.2 In silico simulation

The bioreactor model was designed in Solidworks. Unfortunately, ready-to-use CAD models and dimensional information of lab ware, such as flasks and measuring cylinders, were often lacking and models had to be measured and made by hand, after requesting sample products from the respective companies.

3.2.1 Meshing

The CAD models were consequently prepared for numerical fluid simulations. The three-dimensional surfaces of the bioreactor culture chamber model that are in contact with the intraluminal medium, have been imported into ANSYS Mesher as a SLDPRT file, whilst omitting other irrelevant parts of the culturing chamber. The result practically resembled a 'pipe model' of the intraluminal circulation. To assure a quicker convergence and stable results, the thee-dimensional pipe model has been mostly meshed with a hexahedronal (six-sided) mesh structure. The walls of the pipe model have been *inflated* to create a structured smooth transition along the wall of the model (**Figure 9**), which is important for a stable simulation of the wall shear stress. The resulting cell count in the meshed models was around 500.000 cells.

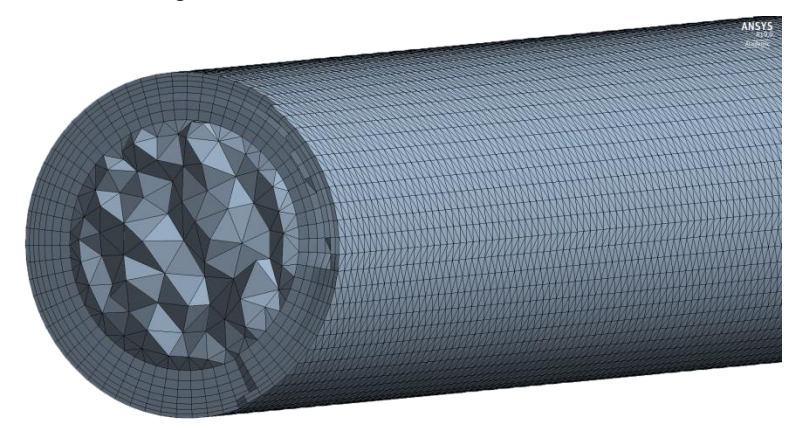


Figure 9 Cross section of a structured three-dimensional mesh, showing the concentrically inflation layers and the use of hexahedronal cells near the wall.

3.2.2 Physical setup

The meshes were imported in Fluent 19, executed in the three-dimensional double precision mode and appointed all eight logical CPU cores on the computer. The simulation was carried out with a rigid model of the scaffold wall. A paraboloid velocity distribution was imposed on the inlet, representing an already fully developed flow profile at the entrance of the culture chamber, given by the following equation:

$$\mathbf{v} = v_{max} \left(1 - \frac{y^2 + z^2}{r^2} \right) \cdot \hat{\mathbf{x}}$$
 (8)

where v_{max} is the maximal velocity at the entrance and r refers to the radius of the inlet. Since the inlet is positioned in the yz-plane, the velocity vector has only a non-zero component in the $\hat{\mathbf{x}}$ -direction. The velocity distribution at the inlet is visualised in **Figure 10**. Furthermore, a noslip velocity boundary condition was imposed on the walls.

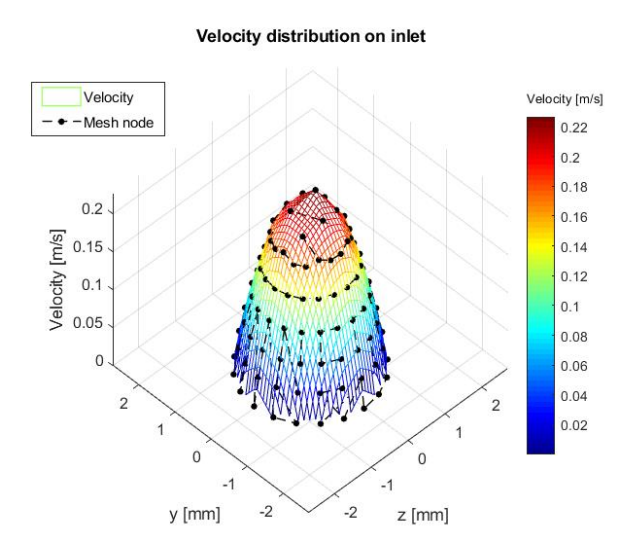


Figure 10 Visualisation of the imposed velocity distribution on the inlet (equation 8). The inlet is positioned in the yz-plane. The inlet has a diameter of 3 mm and v_{max} is 0.236 m/s.

Three cases have been considered (**Table 9**). Since cell medium is an aqueous solution and is only marginally affected by serum concentration up to 10 %, cell medium has been approximated by the physical properties of water at 20 °C and at 37 °C (Hinderliter et al. 2010). A blood-approximating medium was considered as well, to assess the shear stresses on the scaffold in case the medium viscosity is increased by the addition of viscosity-modifying components, such as polysaccharides. Dextran is an often used cell medium additive in studies on the effects of shear stress on cell differentiation and protein expression (Gusic et al. 2005; Obi et al. 2012). Dextran solutions feature a mostly constant viscosity for all relevant shear rates (up to 1000 /s) Although whole blood shows extreme shear thinning properties, implying that the viscosity increases for lower shear rates, dextran solutions have a fairly constant viscosity for all

relevant shear rates up to 1000 s⁻¹ (Chien 1970; Tirtaatmadja et al. 2001). Therefore, a steady flow with solely Newtonian rheology was considered in all cases, implying that the media were given a constant viscosity for all shear rates. The rheological properties of the bloodapproximating medium are analogous to the Newtonian approximation of whole blood with an haematocrit level of 45% at a shear rate of 100 s⁻¹, at which the dynamic viscosity is 3.7 mPa·s (Chien 1970).

Table 9 Overview of the used fluid properties in the numerical simulations. The properties have been taken from the physical properties of water at 20°C and at 37°C. The diameter of the inlet, $d_{\rm inlet}$, has been taken from the inner diameter of the first Luer adapter. The maximum velocities, v_{\max} , have been calculated based on the inlet diameter and the chosen flow rates Q, which have been varied between 0.2 and 50 ml/min.

Quantity	Evaluated values			
-	water, T = 20°C	water, T = 37°C	blood approx. medium	
μ [mPa s]	1.002	0.691	3.700	
ho [kg m ⁻³]	997.0	993.0	1060.0	
d _{inlet} [mm]		3.0		
$d_{ m scaffold}$ [mm]		3.0, 5.0, 6.0		
Q [ml min ⁻¹]		0.2 - 50.0		
v_{max} [m s ⁻¹]		0.0009 - 0.2358		

The numerical simulations in ANSYS Fluent have been performed using the built-in pressurebased solver. An overview of the solver-related solution methods are given in Table 10.

Table 10 Overview of the ANSYS CFD solver settings that have been used in this study.

Solver property	Used setting	
Solver type	Pressure based	
Pressure-velocity coupling	SIMPLE	
Gradient discretisation	Least squares cell based	
Pressure discretisation	Second order	
Momentum discretisation	Second order upwind	
Pressure under-relaxation factor	0.2	
Momentum under-relaxation factor	0.6	
Initialization method	Hybrid, 12 steps	

The solution was considered to be converged, when the residuals had reached 10⁻⁷ or 3000 iteration cycles were completed and no significant decrease in residual value was observed. The results from the numerical simulations were exported in a comma-separated file format and imported into MATLAB for data analysis and plotting. The Matlab code for the extraction of the wall shear stress is given in Appendix C.III.

3.2.3 CFD validation

The results of the CFD simulations have been validated by rerunning the simulation using different meshes to assess whether the simulation was mesh-independent. Consecutively, extracted values have been compared to analytical approximations at certain locations of the bioreactor. The wall shear stress for a laminar flow in straight circular pipes can be found analytically with the Hagen-Poiseuille equation, given by

$$\Delta P = \frac{8\mu LQ}{\pi r^4} \tag{9}$$

where Q denotes the flow rate, L the total pipe length, ΔP the pressure head loss, μ is the dynamic viscosity, and r the internal pipe radius. A derived formulation of the Hagen-Poiseuille equation gives the wall shear stress τ , when the fluid viscosity, flow rate and pipe diameter are known:

$$\tau = \frac{4\mu Q}{\pi r^3} \tag{10}$$

3.3 Chamber construction

From the available manufacturing techniques, milling was considered to be the most suited machining process for the creation of the culture chamber parts. Milling allows for the use of wider range of materials and a larger accuracy compared to most additive manufacturing techniques. All milled parts have been milled using a 2.5-axis flatbed milling setup from Isel with computer numerical control (CNC). This 2.5D setup required that all designed parts should be made by means of pocket or contour milling. Raw extruded polymers have been cut to their approximate dimensions before milling. The raw material fixed by using double-sided bonding tape onto an underlay, protecting the flatbed underneath the raw material. The underlays were consecutively tightly fixated to the flatbed with screws. The CNC milling procedures were set using the IsyCAM software, after importing two-dimensional drawings from Solidworks in the DXF format. The translation speed of the milling cutter was chosen depending on the used cutter diameter and the milled material and ranged between 5 and 20 mm/s. Generally, softer materials, such as polymers, and larger cutter diameters allowed for a higher translational velocity. First try-outs were constructed out of polytetrafluorethylene (PTFE, Teflon) and polyoxymethylene (POM), due to their low price and ease-of-use in machine milling. The final model was constructed out of biocompatible and heat-resistant polyether ether ketone (PEEK), after a definitive design had been chosen. After milling, the parts were removed from their underlay and residual adhesive was dissolved in isopropanol. Additional bore holes on the lateral sides of the models, which could not be reached with the flatbed milling setup, were

drilled using a drill press. Consecutively, threads were tapped to accommodate the Luer adapters and other parts of the frame. The constructed parts were rinsed with isopropanol again, to remove leftover cutting lubricant. Bore holes were cleaned using pressurised air to clear remaining chips from tapping.

3.4 Cytotoxicity test

A cytotoxicity test according to EN ISO 10993-5 has been performed using a MTS assay on human microvascular endothelial cells (mVECs), which had been obtained through primary isolation. Only the modified parts of the bioreactor system have been subjected to a cytotoxicity assay. The biocompatibility of the tubing and glass bottle is already guaranteed by the suppliers, Cole Parmer and Schott respectively, in accordance with ISO 10993. Similarly, comparable Luer adapters have been used in previous bioreactor projects and, therefore, have been excluded from the cytotoxicity test as well. Instead, machined parts of the bioreactor, such as milled PEEK and aluminium, have been used for the cytotoxicity test.

Cell culture

mVECs were cultured according to a previously established protocol. The mVECs that had been stored in liquid nitrogen, were thawed and added to a centrifuge tube containing 5 mL endothelial cell growth medium. After centrifuging, the supernatant medium was removed and the cell pellet was resuspended in fresh medium and transferred to a T75 cell culture flask and left for culture in an incubator (37°C, 5% CO2, 92% relative humidity). Consecutively, the growth medium was changed every second day.

Sample preparation and extraction

Each sample has been prepared in triplet and the extraction has been defined according to part surface to extraction medium volume ratio. In this case, an extraction ratio of 3 cm²/ml was chosen. Since the actual geometry of the bioreactor parts would require a rather large amount of extraction medium, smaller machined parts have been used for the extraction (Figure 11). These smaller parts still possessed all machining steps of the actual bioreactor parts, to test the cytotoxicity influence of both the material and the machining steps. The small machined PEEK samples have a total surface of 9 cm², thus requiring 3 ml extraction medium each. After construction of these test parts, the samples have been steam sterilised at 121°C for 20 minutes. The three samples were consecutively transferred to centrifuge tubes, to which 3 ml of endothelial growth medium with neither FCS nor antibiotics was added. A fourth tube without any sample was filled with 3 mL of medium, acting as a blind test to check for systematic cell seeding errors. All four tubes were incubated at 37°C for 72 hours.

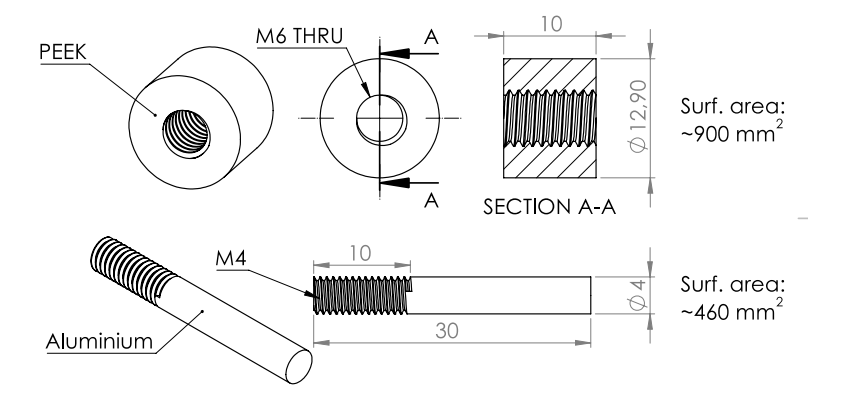


Figure 11 Prepared samples that have been used for the cytotoxicity assay. Both samples have been designed such, that they possess all machining steps, which the actual bioreactor parts undergo as well. The surface area was used in the calculation of the required extraction medium volume.

Cell seeding and test

A cell solution was prepared with a concentration of 100.000 cells/ml in endothelial cell growth medium containing 5% FCS, but no antibiotics. The cell concentration was determined by counting the cells using a Neubauer chamber with a trypan blue staining. A 96-well plate has been used for the cell seeding and the following cell test. Six test groups have been defined: three samples, a blind test, a negative control, and a positive control (**Figure 12**). For every test group, six wells were filled with 200 µl of cell solution each, resulting in 20.000 cells per well. The plate was left for 24 hours of incubation at 37°C. After incubation, the medium in the wells was aspirated and replaced by the extraction and control media, after the addition of 5% FCS. The medium of the positive control was supplemented by 1% sodium dodecyl sulphate (SDS). Medium was also added to empty wells, acting as a background for the MTS assay. The microplate was left for another 24 hours at 37°C to incubate.

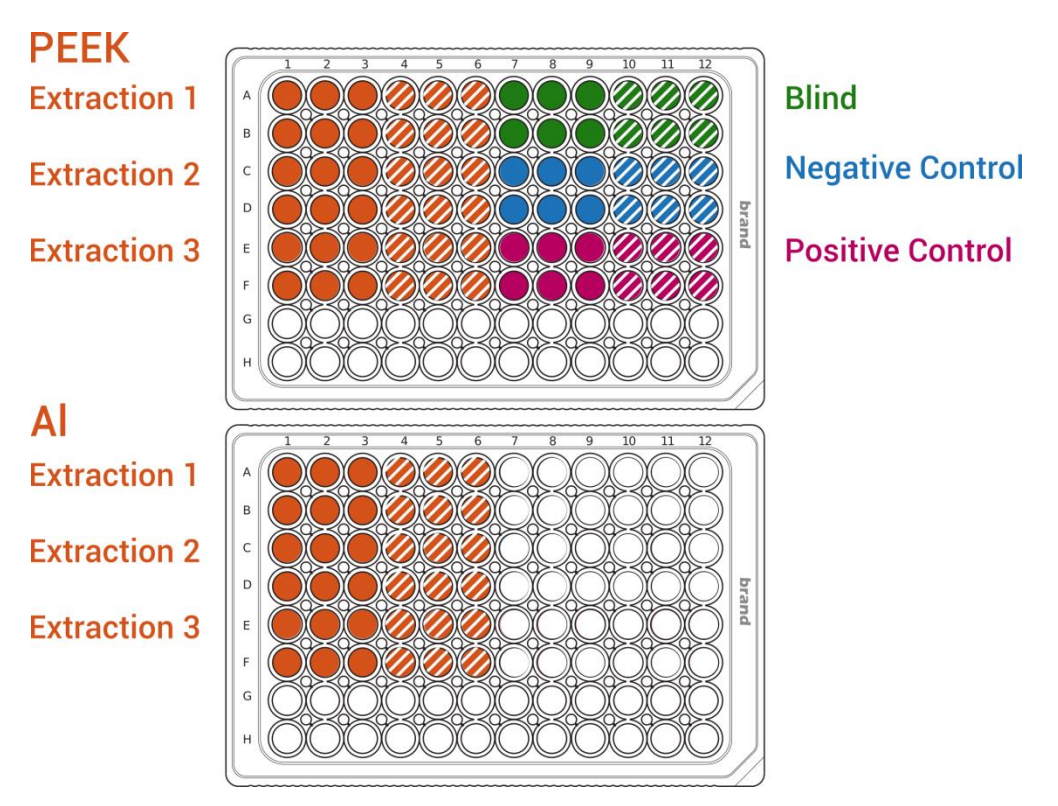


Figure 12 Overview of the extraction and control groups for the MTS assay. Every group has been performed with 6 technical replicates. For every group, 6 wells are filled with cells (solid colour) and 6 wells without cells (striped pattern). The latter are used as background correction in the evaluation of the MTS absorption.

Consecutively, the medium was removed and replaced by 20 μ l of MTS reagent solution and 100 μ l of unsupplemented growth medium per well. The 96-well plate was incubated for 30 minutes in the dark. Finally, the light absorbance at 492 nm was measured using a microplate photometer. The proliferation in the wells is calculated according to the relative absorbance of the individual wells, from which the background is subtracted, with respect to the absorbance of the negative control.

3.5 Pressure monitoring

3.5.1 Sensor calibration

The B.Braun clinical invasive blood pressure transducers have been calibrated with an accredited pressure transducer from WIKA. The WIKA pressure transducer had been tested according to EN 10204-2.2, to have a conformity error of not greater than 0.25% of the full span. To calibrate the B. Braun pressure transducers, one port was connected to the WIKA sensor through flexible tubing and another port was connected to syringe, clamped into a syringe pump to gradually increase the pressure. An input voltage of 18.0 V was applied to the WIKA pressure transducer by a bench power supply and the output (0 - 5V) was read with a digital multimeter. Since the output of the B. Braun pressure transducer is much smaller, the output has to be amplified. The output of the B. Braun pressure transducer was fed through an ADS1115 16-bits

analogue-to-digital (AD) converter, whose internal Programmable Gain Amplifier (PGA) was set to 16 times. According to the datasheet of the AD converter, the effective input range is 256 mV, when the PGA is set to x16. This means that one bit corresponds to:

$$1 \text{ bit} = \frac{256 \text{ mV}}{2^{15}} = 0.0078125 \text{ mV}$$
 (11)

where a scale of 2¹⁵ instead of 2¹⁶ has been used, as the 16th bit is used for the sign of the voltage. An ATmega328P-based microcontroller and a small OLED display have been used to display the output of the AD converter. Fitting the output of the AD converter to the pressures, as measured by the WIKA sensor, gives the sensitivity of the B. Braun pressure transducer.

3.5.2 Readout

The calibrated pressure transducers have consecutively been used in the measurement of the pressure in the bioreactor set-up. The aforementioned AD converter has been used to convert the analogue signal into a digital signal. Since the working principle of the pressure transducers is based on a *Wheatstone bridge*, it takes a differential voltage measurement to measure the pressure. Although the used AD converter can take up only two differential inputs simultaneously, multiple AD converters can be hooked up to a single microcontroller in serial, if more inputs are required. The microcontroller has been programmed to output the voltage readings to a computer over USB at a rate of 25 measurements per second.

3.6 Compliance estimation

To measure the diameter for the compliance estimation, a camera setup is used in this study, which will function as a proof-of-concept prior to the acquisition of a more expensive optical micrometer. First, a small integrated USB microscope was used to acquire a live image, which was positioned directly over the graft frame. The video feed was processed by a programme written in C++, utilising the OpenCV image processing library, because of the speed advantage of the compiled code and the possibility to run this in real-time. The code is given in its entirety in Appendix C.I. The main purpose of the programme is to detect the edges of the scaffold and to measure the distance between these edges, which yields the width of the scaffold in pixels. It is not necessary to know the diameter in actual units, as only the relative diameter dilatation is required for the calculation of the compliance, as is seen from equation (2). The algorithms that have been used in this programme are the Canny edge detection algorithm (Canny 1986) and the Hough transform (Duda and Hart 1972), which have been included in the workflow summary (Figure 13). The Hough transform is a feature extraction technique in digital image processing, that is used in combination with an edge detection algorithm to detect and position straight lines in an image. However, the quality of the acquired imagery from the USB microscope proved to be insufficient and another set-up had to be used instead. Furthermore, the algorithm did not optimally utilise all available information, as the width could be only extracted rounded to the nearest pixel, resulting in a very coarse estimation of the diameter.

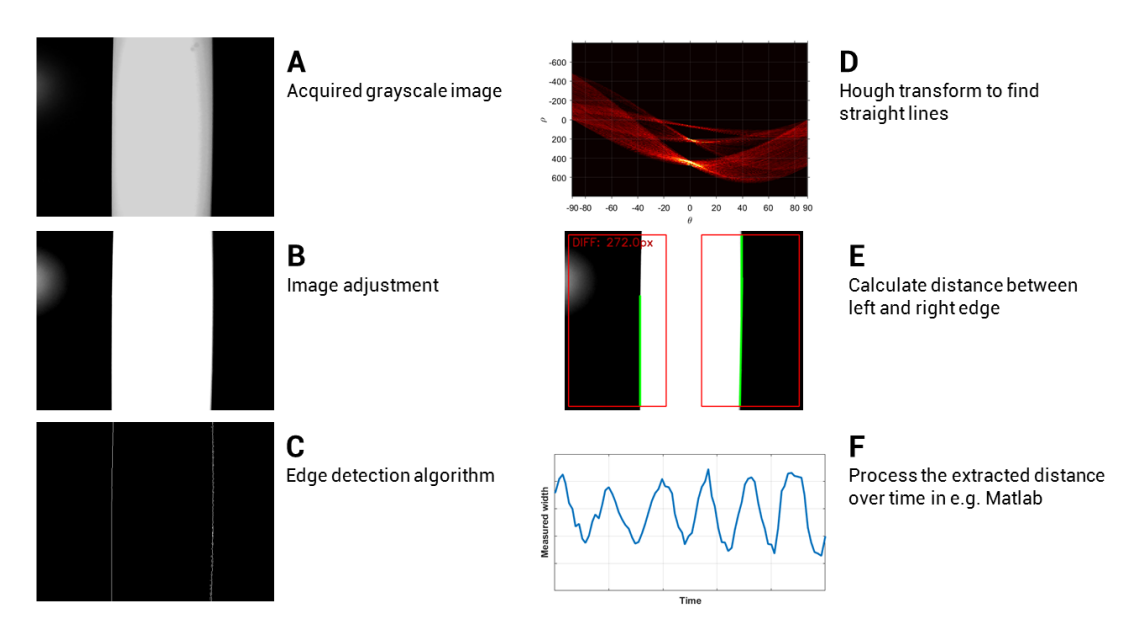


Figure 13 Summary of the diameter measurement workflow. **A**: A grayscale image is acquired. **B**: The contrast is adjusted to increase the difference between the foreground and background. A Gaussian filter is applied to remove noise. **C**: The Canny edge detection algorithm is used to create a binary image that only shows detected edges. However, this includes all edges and can also include curly edges due to unremoved noise or shadows. **D**: To quantify the location (and rotation) of straight edges in the pictures, the Hough transform is applied to the binary image. The bright areas around $\rho = 200$, 470 and $\theta = 0^{\circ}$ indicate that the image contains two vertical lines with a distance of 270 pixels from each other. **E**: The found distance between the left and right edge are displayed on an overlay image. **F**: The measurement is outputted for further analysis in e.g. Matlab.

The integrated USB microscope was replaced by a stereo microscope with a digital microscope camera attached. The camera was connected to a computer over FireWire and a video was recorded in ZEN Lite and processed afterwards. Since the requirement to process video in real-time was dropped, the algorithm was adapted to be run in Matlab. In Matlab, the video frames were converted to binary images with a set threshold and the width was extracted for every horizontal video line (**Figure 14**). For a video resolution of 1388x1040, this results in 1040 width measurements. After taking the average of these individual widths, a much more refined estimation of the width was extracted for every video frame. To test the set-up, a thin-walled silicone tube with an outer diameter of 7 mm and inner diameter of 6 mm was used as a dummy scaffold. The dummy scaffold was attached onto the graft frame and a pulsatile pressure was imposed by hand, using a pulse chamber with a silicone membrane spanned over the top in the ranges 50 – 90 mmHg, 80 – 120 mmHg, and 110 – 150 mmHg. The graft frame was placed under the microscope to measure the expansion of the dummy scaffold. The pressure was simultaneously recorded with a clinical pressure transducer as described in section 3.5.2. After extracting the outer diameter over time, the internal diameter was calculated:

$$D_i = D - 2t \tag{12}$$

where t is the unloaded thickness of the tube. Since the deformation of the tube is relatively small, the internal diameter can be calculated with the unloaded thickness according to ISO

7198:2016. The inner diameter was consecutively correlated to the pressure readings from the pressure transducer. The code of the algorithm has been given in Appendix C.II.

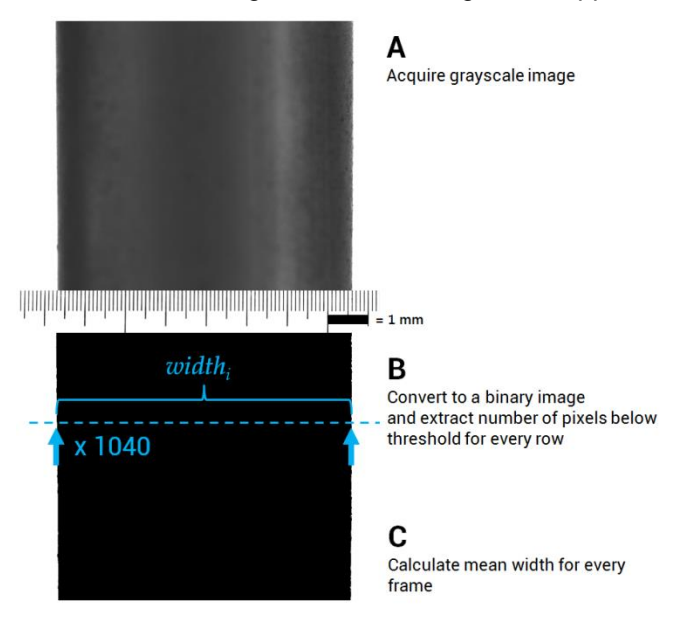


Figure 14 Summary of the rewritten diameter extraction algorithm. **A**: a grayscale image is acquired. **B**: the acquired video frames are converted to binary images. Consecutively, the number of pixels below the binary threshold (in black) are summed for every row. **C**: the mean of extracted widths is calculated per frame.

3.7 Leakage test

The bioreactor should maintain a physiological pressure in the intraluminal circulation and be operable under sterile conditions. Two different media were used, to test whether the set-up has leak-free separation between the intraluminal and extraluminal circulation. For the intraluminal circulation, a strongly coloured aqueous solution of Ponceau S, also known as Acid Red 112, at a concentration of 1 mg/ml was created. For the extraluminal circulation, undyed water was used. The intraluminal space was perfused at a constant rate and maintained at an overpressure of around 160 mmHg. The clinical pressure transducers were used to measure any possible pressure loss over 48 hours of continuous perfusion at overpressure.

4 Results

4.1 Design of the bioreactor system

4.1.1 Overview

A schematic representation of the definitive bioreactor system is displayed in Figure 15.

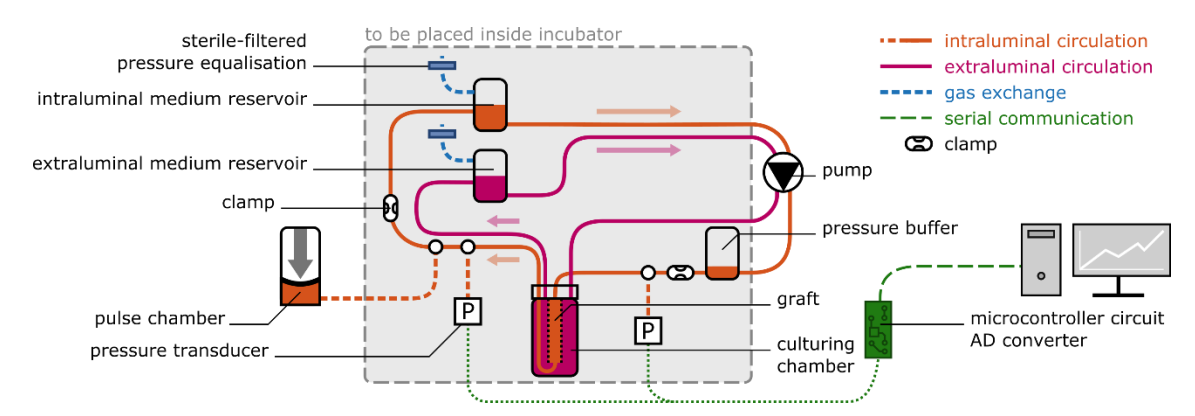


Figure 15 Schematic representation of the circulation of the bioreactor system, when the system is used for tissue culture. The shaded part of the bioreactor is placed inside an incubator. The orange colour indicates the intraluminal circulation that passes through the lumen of the vascular scaffold. The purple colour indicates the extraluminal circulation that passes through the exterior parts in the culture chamber. Dashed lines indicate arms of the circulation that can be closed off with three-way stopcocks.

As can be seen from the distinctive colours in the schematic representation (Figure 15), the bioreactor system features, depending on the permeability of the vascular graft, two completely separated circulation loops. The first one, referred to as the intraluminal circulation, passes through the lumen of the vascular graft in the culturing chamber. This circuit is also connected to a pulse chamber that superimposes a pulsatile pressure profile on the main pressure. The second one, referred to as the extraluminal circulation, is pulse-free and perfuses the exterior of the vascular graft in the culture chamber. Both circuits have their own medium reservoir, which allows for the culture of different cell types on the inner and outer surface of the vascular graft. Secondly, it enables to assess the intraluminal and extraluminal cell culture independently, as signalling molecules and other influencing factors are kept separated. Both circuits are driven by a single ISMATEC peristaltic pump with a rotating head that can accommodate 8 channels. Utilising one channel for the intraluminal circulation and another one for the extraluminal circulation, this means, that a total of 4 systems can be driven by this pump. Since the rotor heads of the pump do not come in contact with the medium, maintenance is made significantly easier. To ensure sterility, PharMed autoclavable peristaltic pump tubing has been selected with an inner diameter of 2.79 mm. The rest of the circuit has been connected with autoclavable Rotilabo silicone tubing with an inner diameter of 3 mm. Sections that contain tube clamps were connected with Tygon R 3603 tubing, since they allow for a finer regulation of the compression by the tube clamps. It was found, that simple silicone tubing could almost exclusively be either

fully compressed or uncompressed. The tube clamps are used to regulate the intraluminal pressure in the scaffold. Simply adding fluid to achieve a static intraluminal overpressure would not permit the use of a gas exchange filter, since the gas exchange would be limited by the pressure gradient at the sterile filter. Therefore, the tube clamps are used to increase the pressure head in the circuit when the pump is running, as depicted by the pressure diagram in **Figure 16**. The pump at the start of the circulation, delivers the total pressure head. The tube clamps act as resistances in the flow and thereby introduce pressure losses to the system. By varying the tube clamps, the pressure can be kept around 100 mmHg at the position of the vascular graft, but at a much lower pressure in the medium reservoir, where the sterile filter is located and the gas exchange takes place. The clamps have to be regulated to keep a constant pressure at the scaffold, when the flow rate is adjusted.

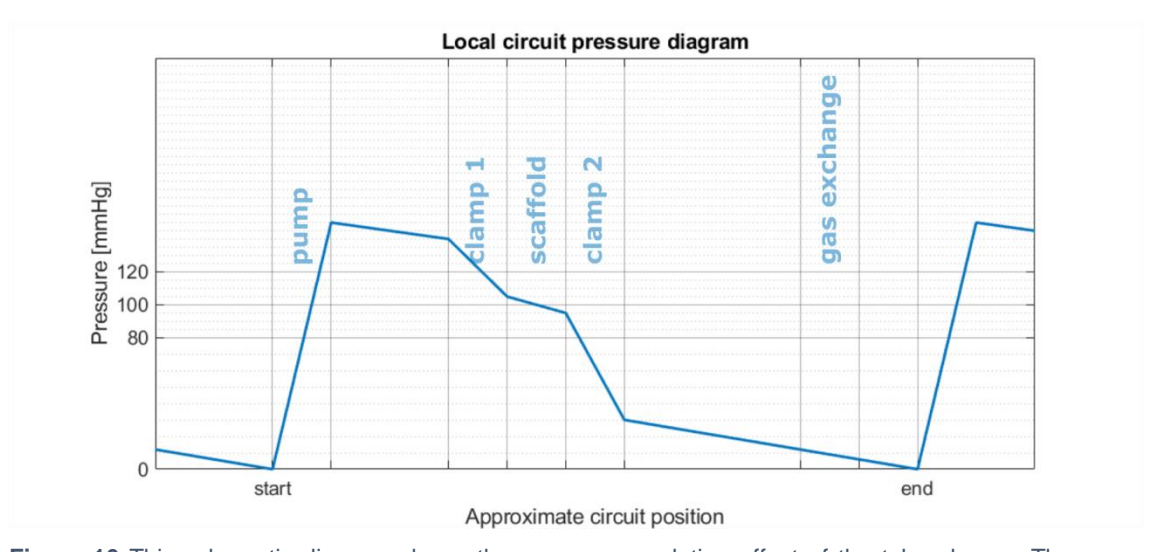


Figure 16 This schematic diagram shows the pressure regulating effect of the tube clamps. The pump delivers the total pressure head, which can be regarded as the potential for the fluid to flow through the circulation. The tube clamps introduce resistances to the intraluminal circulation, which raise the pressure upstream with respect to the clamps. This allows the pressure to be kept around 100 mmHg within the scaffold and at gauge pressure at the medium bottle, where the gas exchange takes place.

A pulsatile pressure chamber is connected to the circuit to enable the superposition of well-defined pressure pulses. The pressure chamber consists of a milled PEEK chamber with silicone membrane spanned over the top. This silicone membrane is clamped onto the chamber with an aluminium ring, which is tightened with six hex screws. On the side of the membrane, there is a threaded opening, where a tube connector connects the interior of the pulsatile pressure chamber with a silicone tube. A photograph of the entire set-up can be seen in **Figure 17**.

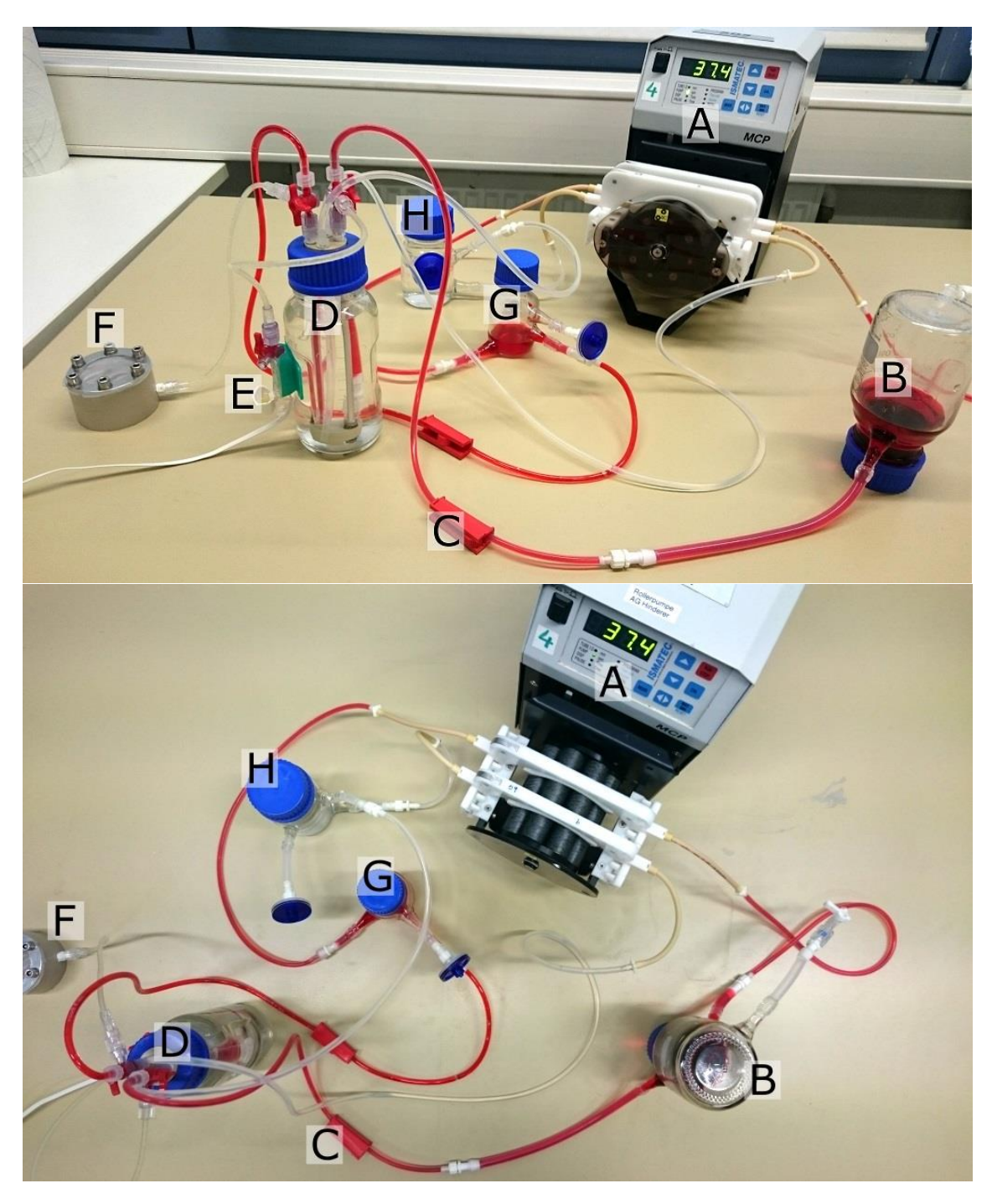


Figure 17 Overview of the bioreactor set-up. The intraluminal circulation is coloured red by perfusing it with a red dye with the exception of the pulse chamber connection line. The extraluminal circulation is perfused with water and, thus, is shown by transparent tubing. In this set-up, only one pressure transducer has been connected. A: pump. B: pressure buffer. C: tube clamp. D: culture chamber. E: pressure transducer (not visible in the bottom picture). **F**: pulse chamber. **G**: intraluminal medium reservoir with sterile filter attached. **H**: extraluminal medium reservoir with sterile filter attached.

4.1.2 Graft frame and culturing chamber

Figure 18 shows a computer-generated cross-sectional view of the graft frame and the culturing chamber in their assembled configuration. The graft frame serves as a construct that holds the vascular graft in place and accommodates the inlets and outlets, through which the culture medium is perfused. The graft frame is brought in its entirety into a Schott Duran Youtility bottle, acting as the casing of the culturing chamber and sealed using a bottle cap, which presses the upper part of the graft frame (the port cap) onto a sealing o ring. On the right-hand side, the wireframe view displays the components of the assembly that are handled separately: the graft frame (black lines), the bottle cap (blue lines), the scaffold (purple lines), and the bottle that serves as the casing of the culturing chamber (light-blue lines).

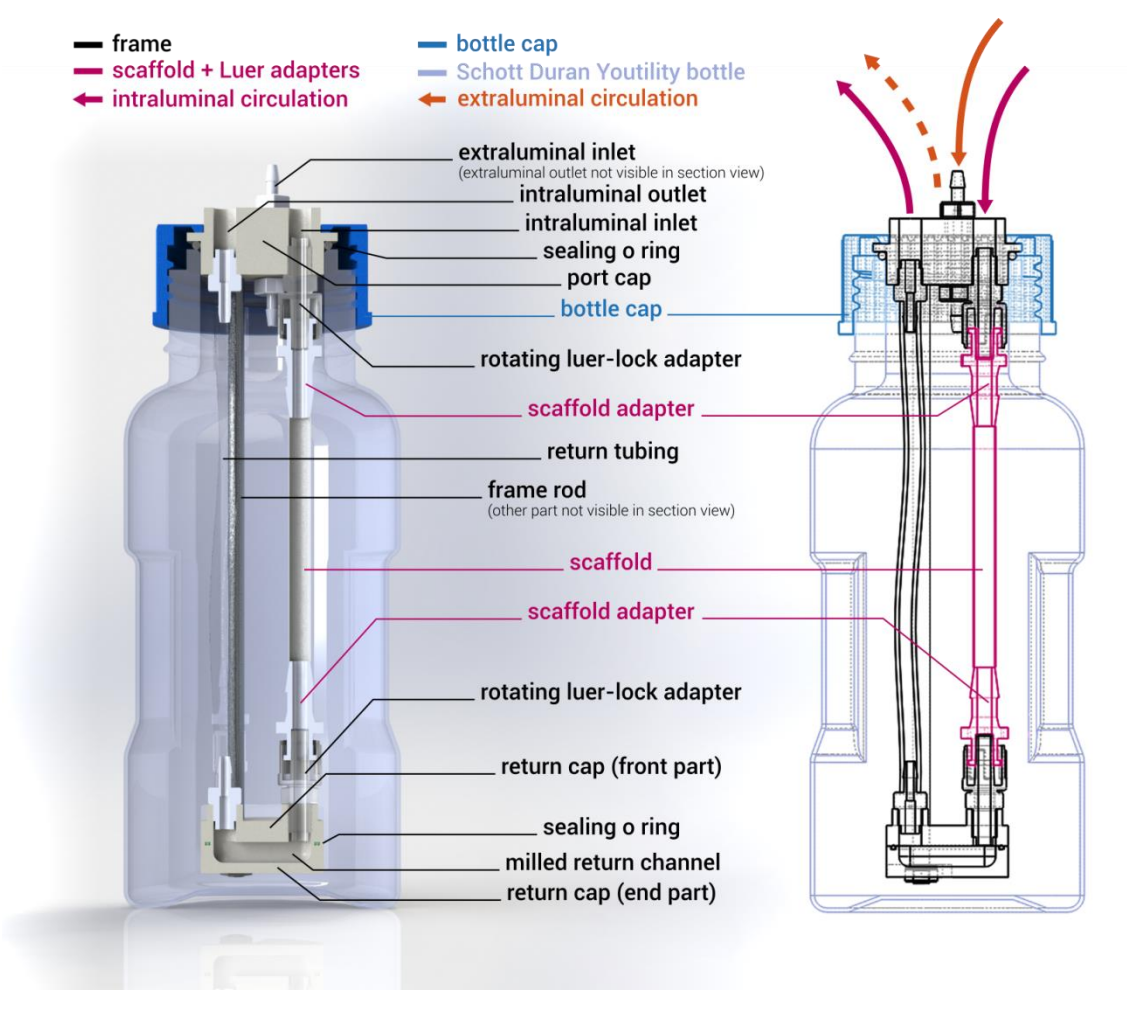


Figure 18 Cross-sectional view of the culture chamber. In the wireframe model, the black parts show the scaffold frame, whereas the purple parts show the scaffold and its adapters. The frame is brought into the culture chamber in its entirety (light blue) and closed off with a bottle cap with a large bore hole (blue).

The graft frame (Figure 19 and Figure 20) can be used for a wide range of vascular grafts, due to the standard sized Luer adapters that are used for mounting the vascular graft onto the graft frame. The vascular graft itself has to be slipped onto scaffold adapters, which are essentially tube-to-Luer F adapters. These adapters come in many sizes to hold flexible tubes of varying inner diameters. The Luer connector, on the other hand, has standardised dimensions, while still ensuring a leak-free process connection. Luer tapers require a turning motion for connection. To prevent torqueing of the scaffold itself, Luer adapters with a rotating collar are used to fasten the scaffold adapters. The diameter of the graft that can be mounted onto the graft frame is only limited by the ISO requirement on the length/diameter ratio of vascular grafts, which states that the vascular graft shall have a length of no smaller than 10 times its diameter. Since the construction allows for a maximum distance between two scaffold adapters of 65 mm, this means that vascular grafts with a diameter of up to 6.5 mm can be cultured in this bioreactor.

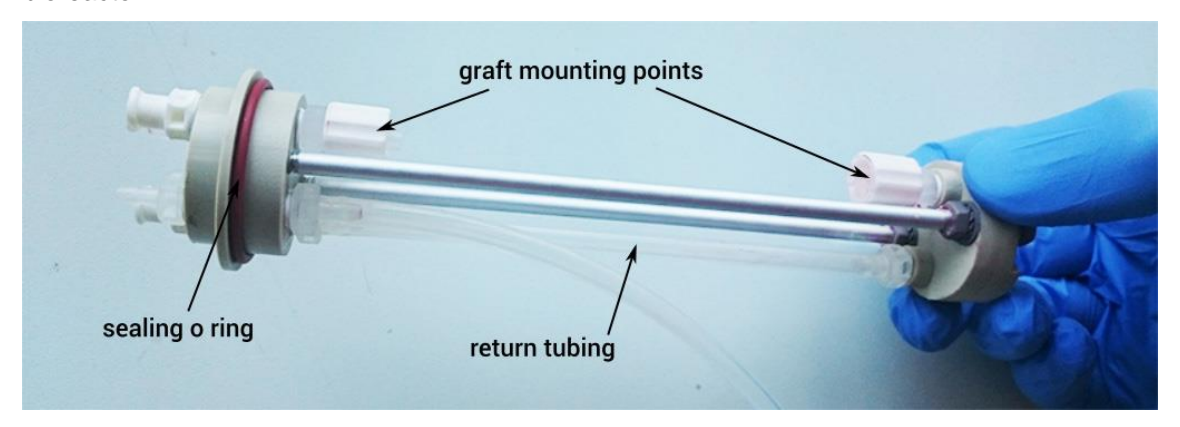


Figure 19 Photo of the graft frame without a scaffold. The Luer adapters with rotating collars are the graft mounting points. The red sealing o ring ensures the closing of the interior of the culture chamber and is pressed into place by the bottle cap.

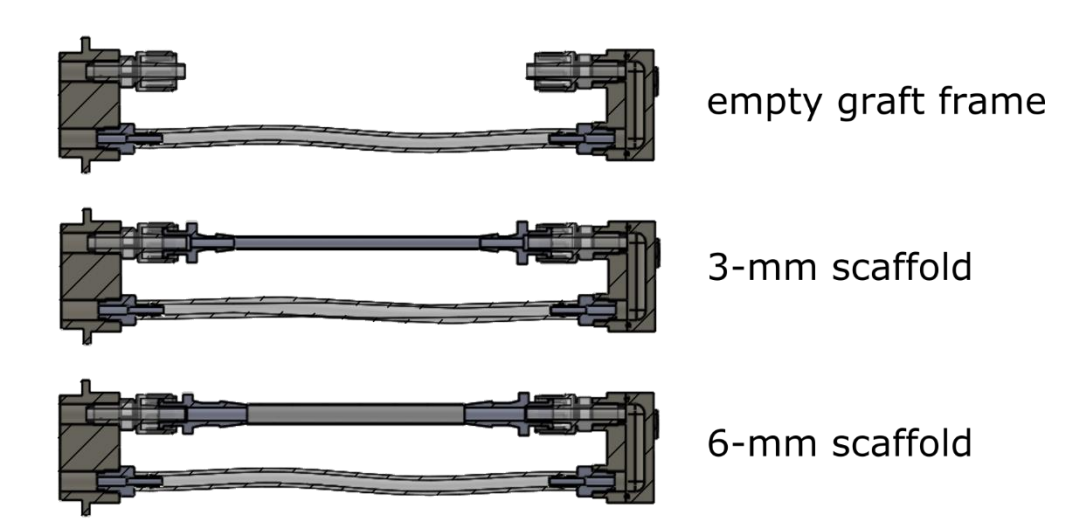


Figure 20 The graft frame can accommodate vascular graft with different diameters, as it uses standard Luer adapters as graft mounting points. The rotating collars of the Luer adapters prevent torqueing of the scaffold itself.

4.2 Characterisation of the bioreactor system

Calibration 4.2.1

The first calibration that was performed, was the calibration of the pressure transducers. The results are plotted as the transducer sensitivity per volt in Figure 21. The pressure calibration was performed with a supply voltage of 5 volts to the pressure transducers, which means the readings have been divided by 5. The linear least squares fit yielded a sensitivity of 36 and 37 μV/V/mmHg for the first and second sensor respectively, as shown in Table 11. One remarkable observation is that the obtained sensitivities are drastically different from the provided value in the datasheet of the sensors, where a sensitivity of 5 µV/V/mmHg was stated. This might be explained by the setup that is used in this study. It has to be noted, that these sensors are meant for use with proprietary hardware, such as clinical heart beat and pressure monitors. Therefore, not all specifications in the datasheet have to correspond with the observed values in this calibration. Furthermore, the error of the WIKA pressure sensor has to be taken into account, which has been calibrated to an error of 0.25% of the full span, corresponding to 1.8 mmHg.

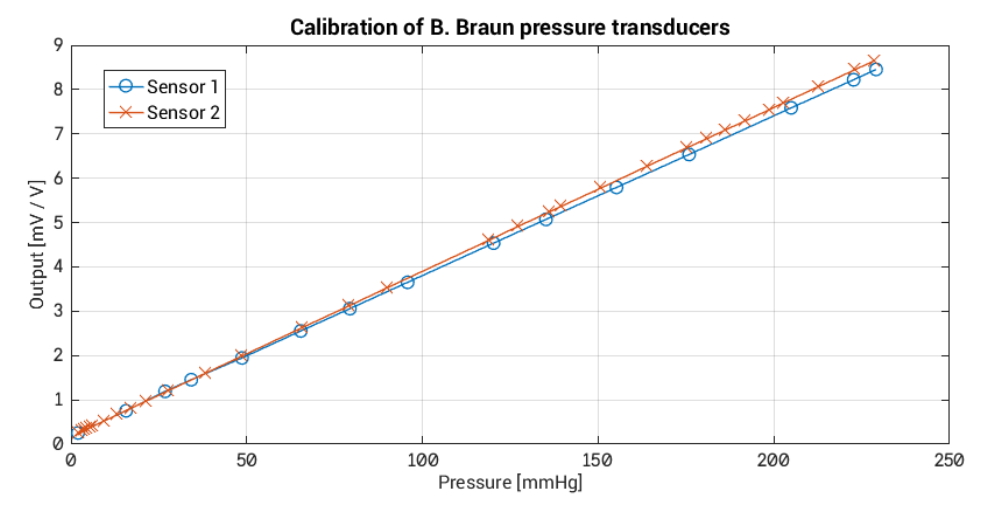


Figure 21 The sensitivity of the B. Braun pressure transducers per volt as function of the pressure. The pressure has been referenced to the output of the WIKA pressure sensor.

Table 11 Linear least squares fit of the calibration of the B. Braun pressure transducer readout. The fitted value for x_0 can be regarded as the zero shift and the value for x_1 as the sensitivity of the sensor. R^2 gives the coefficient of determination (ordinary) of the fitted values.

Fitted par.	Value
Sensor 1:	
x_0	$0.20326 \pm 0.00535 \text{ mV/V}$
x_1	$0.03603 \pm 0.00004 \; \mathrm{mV/V/mmHg}$
R^2	0.999983
Sensor 2:	
x_0	$0.18017 \pm 0.00201 \text{ mV/V}$
x_1	$0.03712 \pm 0.00002 \; \mathrm{mV/V/mmHg}$
R^2	0.999995
Datasheet:	
<i>x</i> ₁	0.005 mV/V/mmHg

The results of the calibration of the flow speed is shown in **Figure 22**, with the linear least squares fit of the data given in **Table 12**. For this fit, the x_0 parameter was fixed at 0, as no flow is expected when the pump is not running.

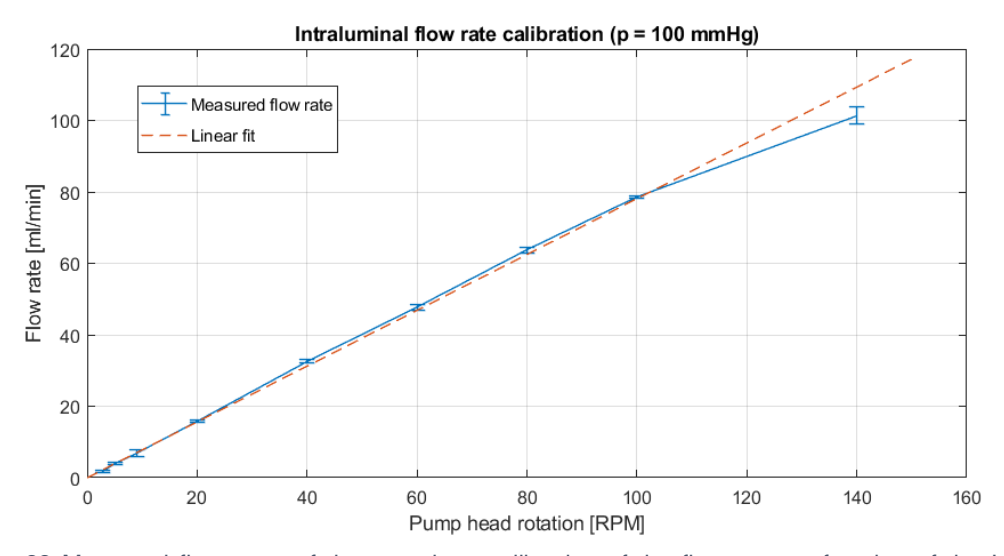


Figure 22 Measured flow rates of the open-loop calibration of the flow rate as function of the Ismatec pump head rotation speed. The pressure was kept constant at 100 mmHg by regulating the tube clamp downstream of the culture chamber.

Table 12 Linear least squares fit of the intraluminal flow rate with respect to the applied pump head rotation speed.

Fitted par.	Value
$\overline{x_1}$	0.6895 ± 0.0280
R^2	0.9953

4.2.2 **Pressure losses**

A plot of the intraluminal pressures with respect to the outlet are displayed in Figure 23. In this figure, the case at 20 °C with a scaffold diameter of 5 mm has been and a flow rate of 20 ml/min has been chosen as an exemplary case. The total pressure loss in this case was predicted to be 0.67 mmHq. The pressure slowly decreases over the path length in the beginning of the circulation until the return channel. About 15% of the total pressure loss can be attributed to the first half of the circulation. The majority of the pressure loss can be attributed to the second half of the circulation, where the pressure drops over the remaining 0.55 mmHg. This can be ascribed to the tube connectors in this half that have a relatively small inner diameter. This insight is useful for the location of the pressure transducer to measure the intraluminal pressure at the scaffold. Connecting the pressure transducer line directly at the inlet will yield a more representative pressure reading than at the outlet.

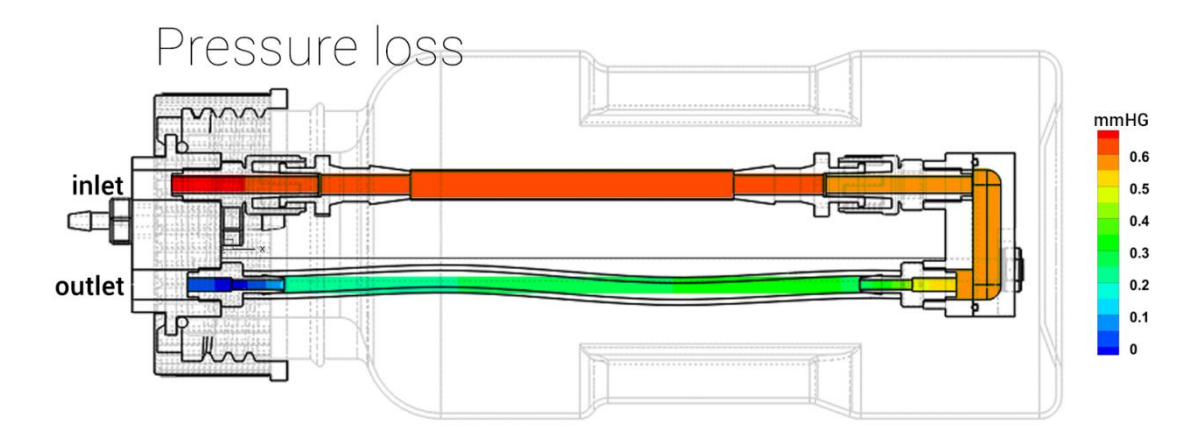


Figure 23 The intraluminal pressure in mmHg with respect to the pressure at the outlet, which has been set as the gauge pressure. In this depicted in silico case, a scaffold diameter of 5 mm and the rheological properties of water at 20 °C have been used. The imposed flow rate was 20 ml/min.

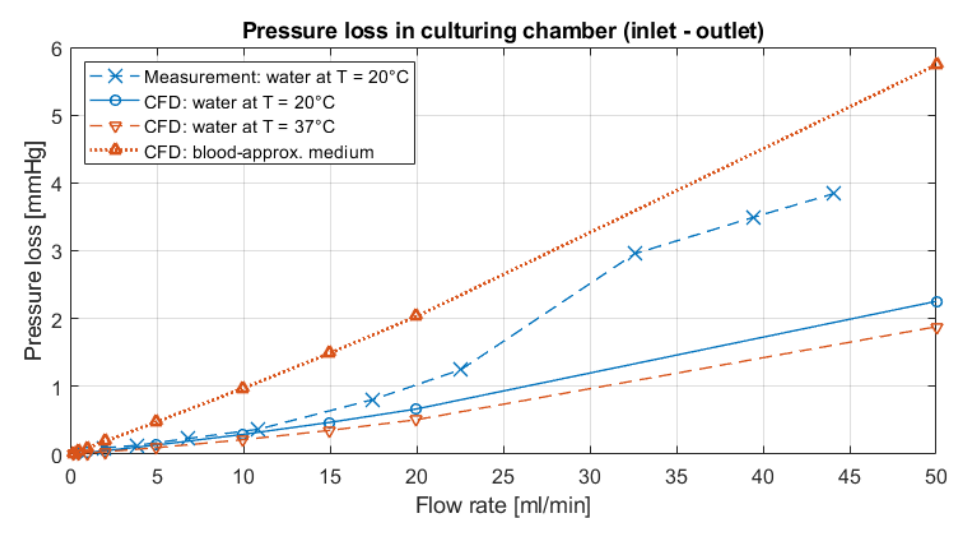


Figure 24 A comparison between the predicted (in silico) pressure loss from the in silico simulations and the measured pressure loss in mmHg. The pressure loss is defined as the pressure difference between the average pressure at the inlet and at the outlet.

The in silico simulations predict a merely linearly increasing pressure loss as function of the intraluminal flow rate (Figure 24). Since the majority (except for the return channel) of the circulation consists of straight pipe-like geometry, this can be explained by the pressure loss in a pipe flow given by the Hagen-Poiseuille law (equation 9) in section 3.2.3 on the validation of CFD simulations. The Hagen-Poiseuille law states that the pressure loss ΔP is linearly dependent on the flow rate Q, given a laminar flow regime. This last condition is satisfied, as the in silico simulation predicts a laminar flow regime in the bioreactor for all considered flow rates. Even for the highest flow rate of 50 ml/min, the Reynolds number peaks around Re = 920 at the entrance of the scaffold and is on around Re = 500 for the rest of the scaffold. Only small regions in the return tubing see a Reynolds number of Re = 1500 at this flow rate. The measured pressure loss compares very well with the in silico values at 20 °C (both shown in blue) up to a flow rate of 10 ml/min. However, this does not hold for all flow rates. At 20 ml/min a difference of about 0.5 mmHg is seen between the measured and the simulated pressure loss. At even higher flow rates, this difference becomes significantly larger and the linear relation seems to be lost. The maximum observed pressure loss in the measurements is 3.9 mmHg at a flow rate of 44 ml/min, whereas a maximum pressure loss of only 2.3 mmHg at 50 ml/min is seen in the silico simulation. A look at the pressure profile plotted against the time reveals a possible explanation (Figure 25). It was found, that the head rollers of the peristaltic pump induced pressure vibrations at higher flow rates. These vibrations have not been accounted for in the fluid simulations. The pump-induced vibrations do not represent a physiological pulsatile pressure profile, which actually should be created with the pulse chamber.

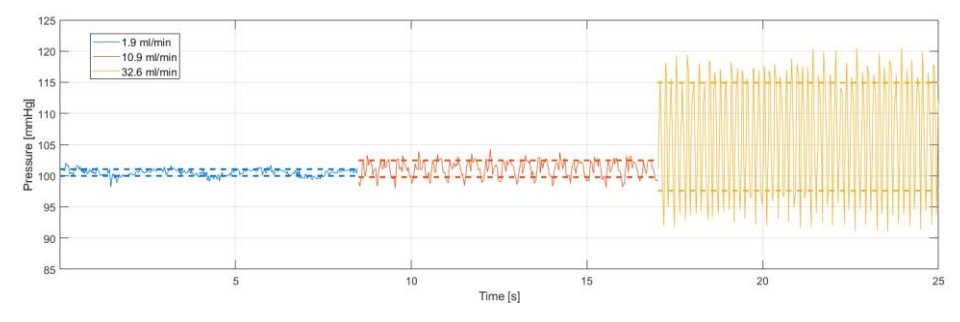


Figure 25 Pressure profiles as function of time for three different pump head rotation speeds, corresponding to flow rates of 1.9, 10.9 and 32.6 ml/min. The dotted lines indicate the root mean square deviation from the pressure mean.

The problem was solved by introducing a buffer between the pump and the culture chamber (**Figure 26**). This consisted out of an armed Schott bottle, which is mostly filled with air during culture. Since air has a much higher compliance than the liquid-phase medium, it absorbs the pulsating pressure from the roller pump (**Figure 27**) and additionally acts as a bubble trap to keep the scaffold's lumen free of bubbles.

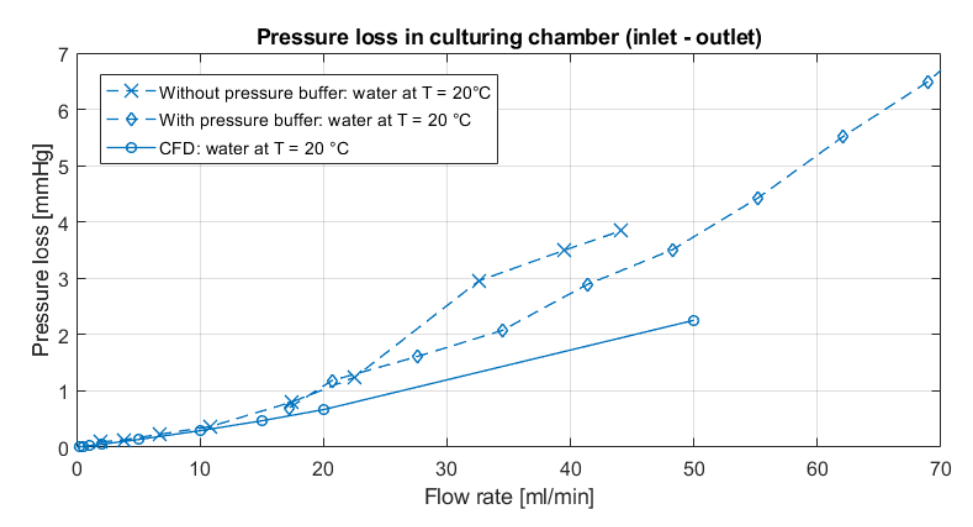


Figure 26 A comparison between the predicted (in silico) pressure loss from the in silico simulations and the measured pressure loss in mmHg after implanting the pressure buffer. The pressure loss is defined as the pressure difference between the average pressure at the inlet and at the outlet.

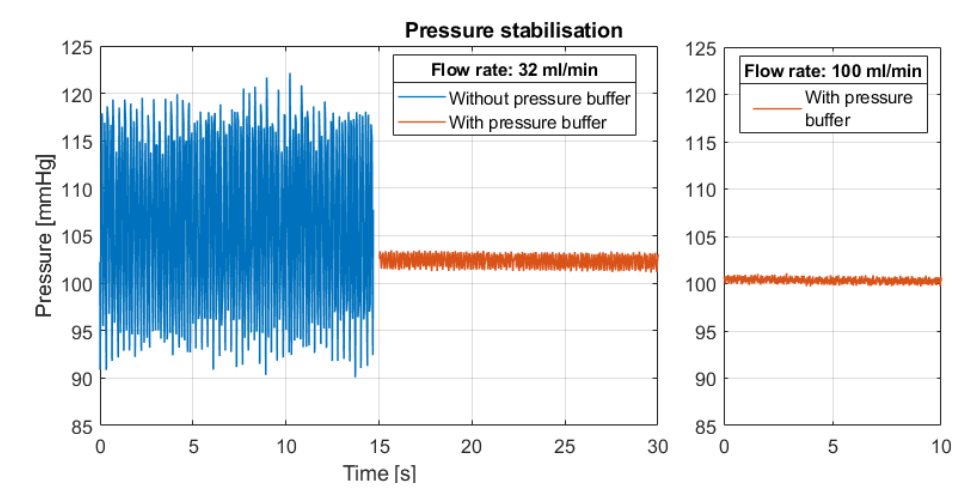


Figure 27 The pressure was stabilised by the introduction of a pressure buffer. These pressure readings show the difference between the unstabilised pressure and the stabilised pressure. The pressure buffer has allowed for much higher flow rates.

4.2.3 Wall shear stress

In **Figure 28** the flow velocity of the case with T = 20 °C, d = 5 mm, and Q = 20 ml/min is taken as an exemplary case to explain the relevant flow phenomena. The highest flow velocities are seen in regions of stenosis, whereas the fluid flows slower in regions with a larger diameter.

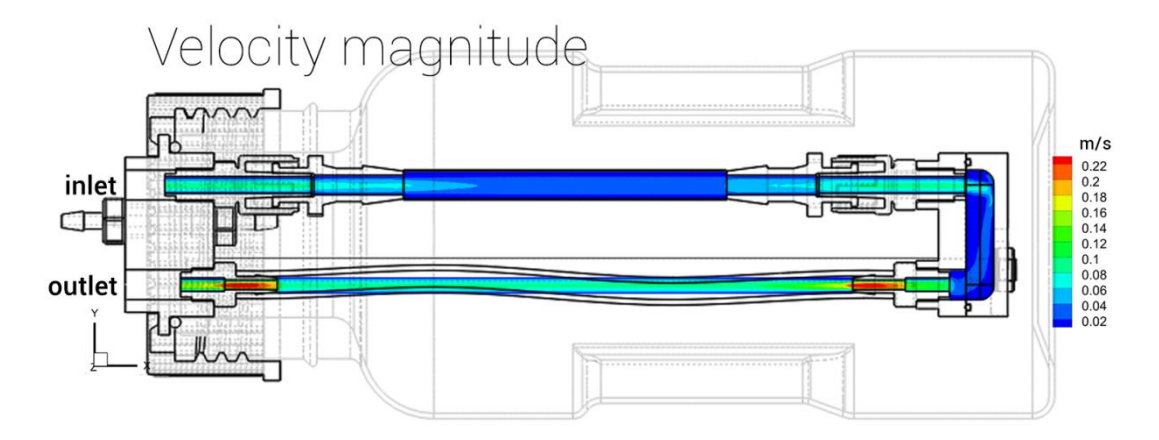


Figure 28 Colour plot of the velocity distribution within the intraluminal circulation in the culture chamber.

The transition of the flow rate does not happen instantly. To illustrate the flow in regions, where the diameter of the circulation suddenly widens, the entrance region of the scaffold has been plotted enlarged in **Figure 29**. Although the high flow velocity at the scaffold entrance results in a high velocity gradient around the scaffold's axis, the wall shear stress is actually relatively lower due to a recirculation zone near the wall. The lowest wall shear stress is found at the reattachment site of the recirculation zone. Further downstream, the wall shear stress slowly restores to the expected analytical wall shear stress for straight pipes, which is referred to as the Poiseuille value.

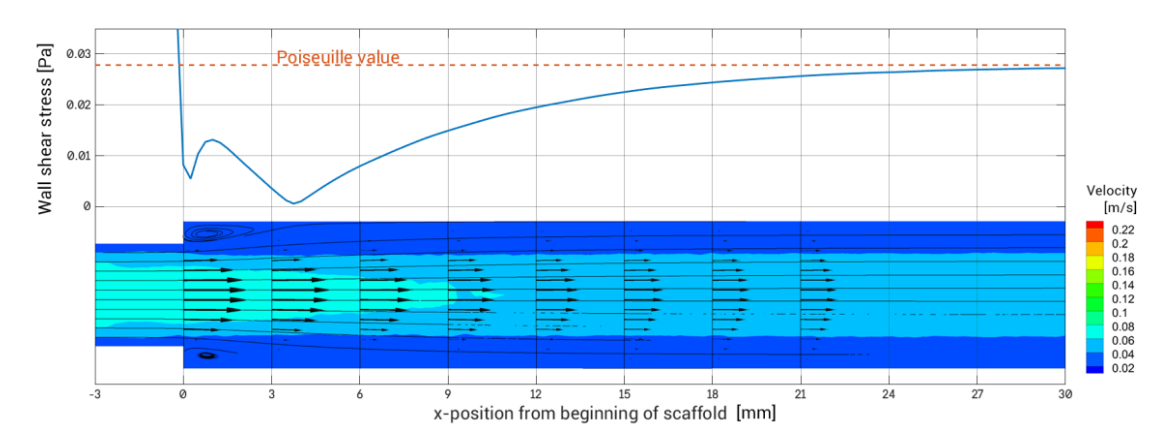


Figure 29 This plot shows a subset of **Figure 28**, namely the beginning of the scaffold, and the influence of flow profiles on the wall shear stress. The colour plot and the arrows in the bottom half display the velocity distribution within the scaffold up to 30 mm from the beginning of the scaffold. The streamlines show a recirculation zone at the entrance and redevelopment of a steady pipe flow in more downstream regions. The line plot in the upper half of the image shows the wall shear stress at the corresponding positions. The lowest shear stress occurs at the reattachment site of the recirculation zone (approximately at x = 4 mm). Further downstream, the wall shear stress returns to the Poiseuille value.

The length of the recirculation zone and the low shear stress region is dependent on the flow conditions. In the case of Figure 29 (water at T = 20 °C, d = 5 mm, and Q = 20 ml/min), the length of the recirculation zone is about 4 mm. It takes another 20 mm for the wall shear stress to regain the steady Poiseuille value. This implies that the first 24 mm of cultured tissue on the scaffold's inner wall is not subjected to the desired shear stress and will not yield representative tissue culture results. To see what length it takes to re-establish a fully developed flow within the scaffold, the normalised wall shear stress has been considered for different flow rates, which means that the steady wall shear stress has been indexed at 1 for all flow rates. Figure 30 shows the normalised wall shear stress for two of the simulated cases (water at T = 20 °C and the blood-approximating medium, scaffold d = 5 mm). It can be seen that higher flow rates cause a larger region of low wall shear stress.

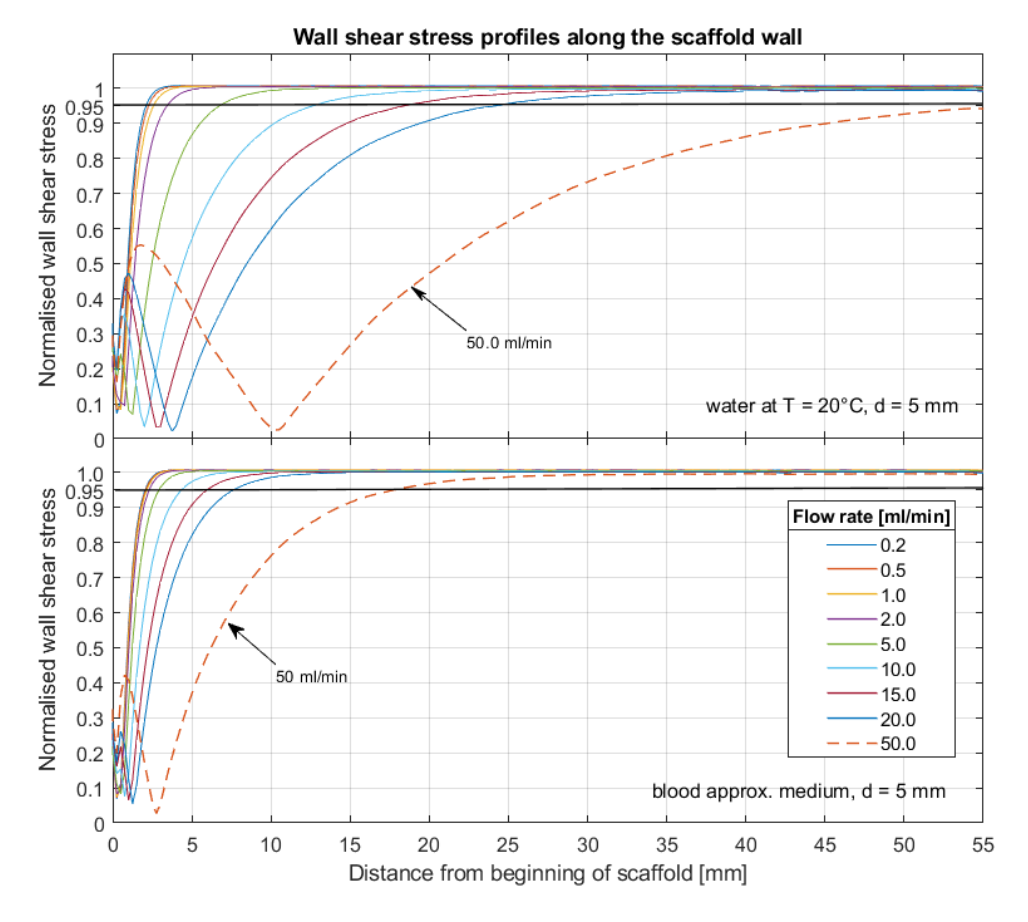


Figure 30 Normalised wall shear stress profiles along the scaffold wall for different flow rates. The wall shear stress profiles have been normalised to the Poiseuille value, implying that the wall shear stress approaches 1 when the flow redevelops.

To enable a quantitative comparison for different flow rates and cases, the length it takes to reach 95% of the Poiseuille value is named the *flow redevelopment length* and is compared and plotted against the flow rate in **Figure 31**. Both the flow rates and the fluid properties are found to influence the length for the flow to redevelop itself. Generally, a higher flow rate and a lower viscosity contribute to a larger portion of the cultured scaffold to be unusable. In three in silico cases, a steady wall shear stress was not reached within the length of the scaffold at the highest simulated flow rate of 50 ml/min with aqueous medium. These cases are marked by the lines that terminate prematurely at 20 ml/min. The viscous blood-approximating medium was found to ensure the fastest redevelopment of a steady wall shear stress. Even at the highest simulated flow rate of 50 ml/min, 11.5, 17.5, and 24.0 mm of the scaffold wall is affected by the recirculation zone, subjecting the majority of the scaffold wall to a steady shear stress.

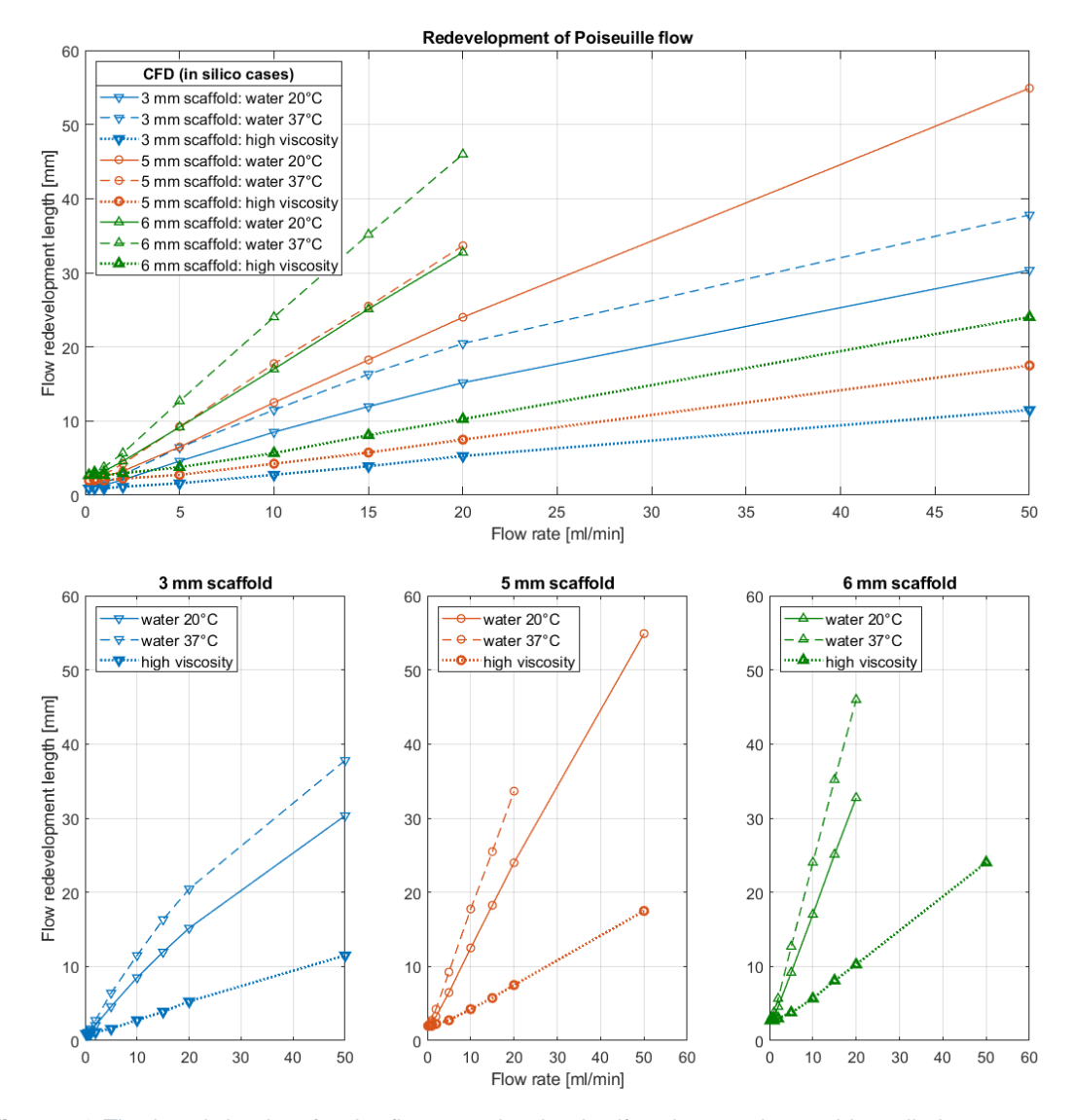


Figure 31 The length it takes for the flow to redevelop itself and to reach a stable wall shear stress as function of the imposed flow rate. Four in silico cases have been considered, where the scaffold diameter and the fluid properties of water were changed.

Increasing the viscosity of the medium has another advantage. The use of the blood-approximating medium would make the bioreactor suitable for applying both venous and arterial physiological shear forces, as seen in **Figure 32**. Using aqueous media with the viscosity of water at 20°C, arterial shear stress would only be achieved at flow rates of over 50 ml/min in 3 mm scaffolds. Using a medium with a dynamic viscosity of 3.7 mPa s, a large range of arterial shear stresses can be achieved with 3 mm scaffolds. The arterial shear stress of the femoral, thoracic artery, and common carotid artery can be achieved at flow rates, which have been validated in the CFD simulations.

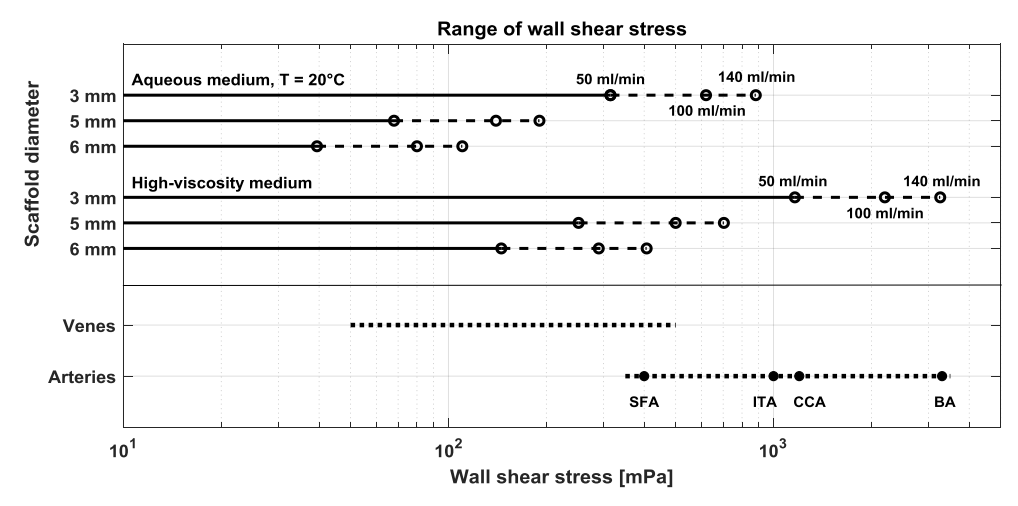


Figure 32 The achievable shear forces in the bioreactor compared to physiologically occurring shear forces in veins and arteries based on in vivo measurements (Ford et al. 2005; Rittgers et al. 1978; Wu et al. 2004). SFA: superficial femoral artery, ITA: internal thoracic artery, CCA: common carotid artery, BA: brachial artery. For the shear stress ranges of the bioreactor, the solid lines include the range up to 50 ml/min, which has been included in the CFD simulations. The dashed lines include the range up to 140 ml/min, which has only practically been tested without CFD simulations.

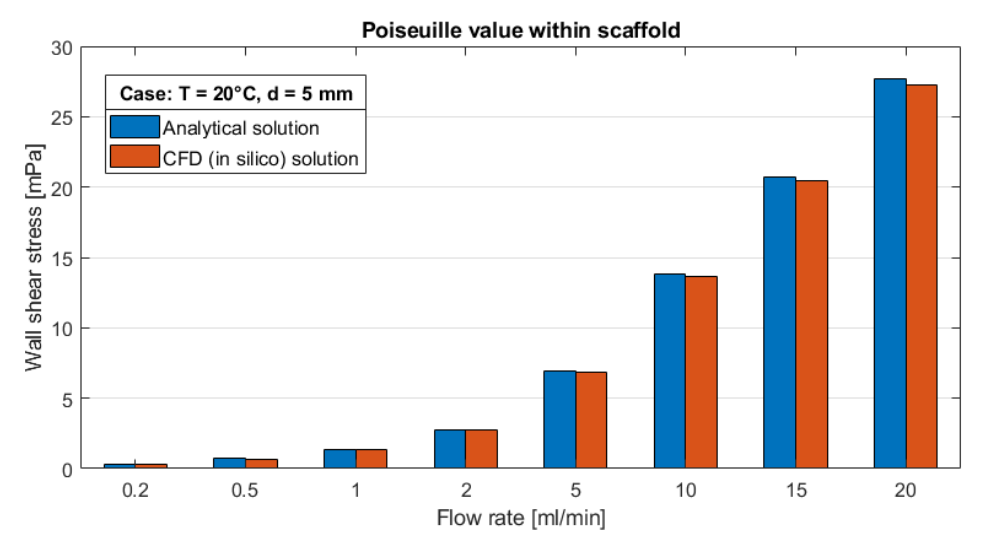


Figure 33 The Poiseuille values (developed wall shear stress value) within the scaffold for different flow rates. This plot compares the observed Poiseuille values to those of the analytical solution.

The actual wall shear stress values at the inner scaffold wall for different flow rates are plotted in **Figure 33**. The observed Poiseuille values in the CFD simulations correspond well to the analytical solution for the wall shear stress for all flow rates between 0.2 and 20 ml/min.

4.2.4 Cytotoxicity test

The results of the cytotoxicity test (**Figure 34**) does not show any negative impact of the extracts on the metabolic activity of the mVECs with respect to the negative control (NC), which has been set to 100%. On the contrary, the mVECs in the extract groups show a higher metabolic activity with the PEEK group having a relative metabolic activity of 139%. The positive control (PC) and a blind group had a metabolic activity of 1% and 88% respectively. According to ISO 10993-5:2009, the extract does not have a cytotoxic potential if the relative viability is not reduced below 70%. This condition is satisfied in this cytotoxicity test.

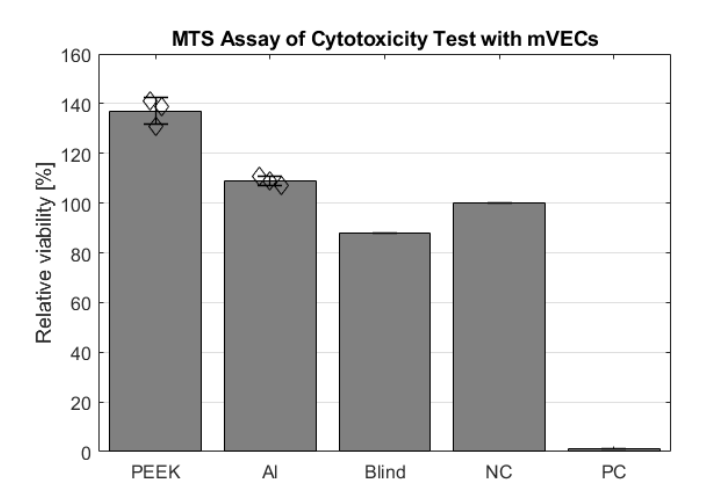


Figure 34 Results of the cytotoxicity test, assessed by means of a MTS assay. The results have been corrected for the background and have been normalised to the negative control (NC). **PC**: positive control. **Al**: Aluminium extract.

4.2.5 Leakage test

The pressure averaging at 159.8 ± 3.8 mmHg over the course of the leakage test. The colouring of the extraluminal compartment was assessed after 24 and 48 hours (Figure 35). No colouring of the extraluminal medium was seen in the culture chamber, nor in the medium reservoir.

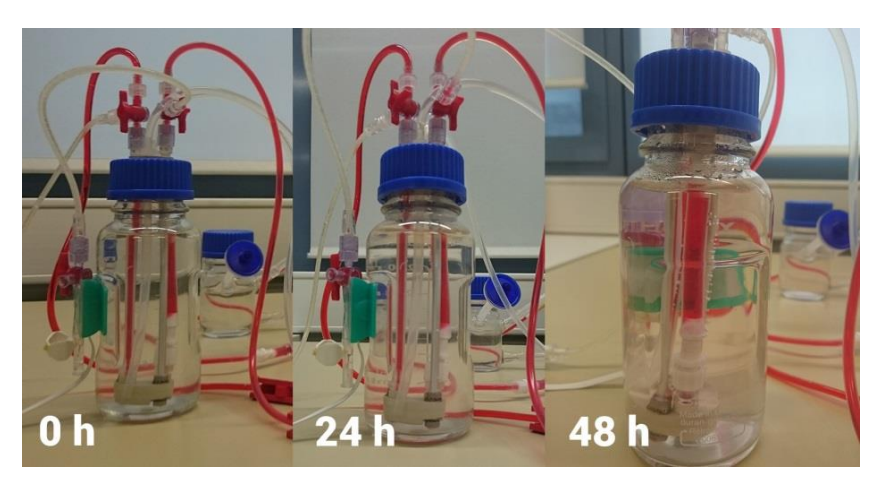


Figure 35 Any possible leakage within the culture chamber was assessed after one day and two days. Foreground: culture chamber. Background: extraluminal medium reservoir. No colouring of the extraluminal medium was seen.

4.3 Compliance estimation

A comparison between the results of the two diameter extraction algorithms have been plotted against the time in **Figure 36**. On the top, the results of the diameter extraction algorithm based on the Hough algorithm are plotted against the time together with the applied pressure. A magnification of 15.6x was used with a resolution of 1388x1040 and a pixel size of 6.3 μ m/pixel. In this example, the pressure was slowly ramped to 200 mmHg and then reduced, while superimposing a pulsatile pressure. The 'stair casing effect' in the diameter plot shows a major limitation of this algorithm, as it indicates that the algorithm is only able to extract the diameter rounded to the nearest pixel and small deviations in the diameter are not recorded.

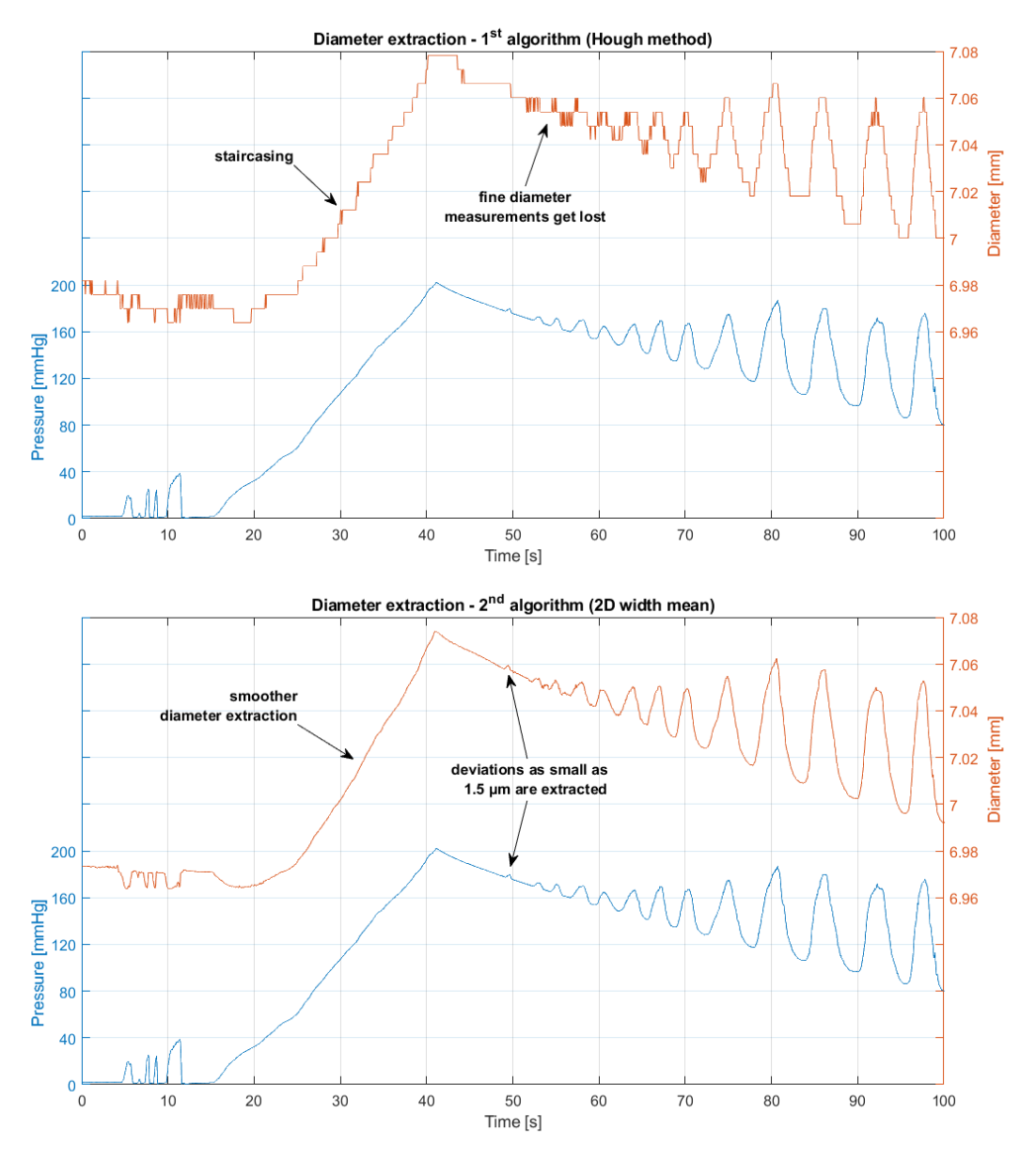
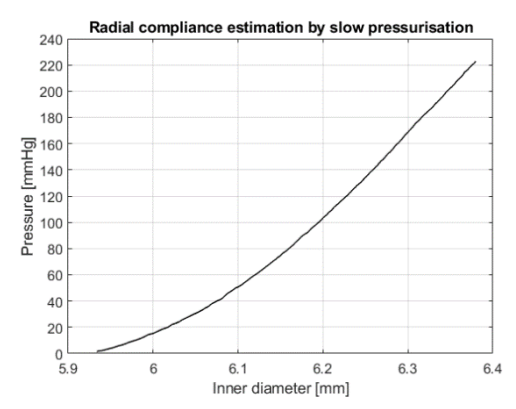


Figure 36 A comparison of the performance of the diameter extraction algorithms. The extracted diameter has been plotted against the time and compared to the pressure that had been simultaneously recorded with the pressure transducer. On the top: the diameter has been extracted using the Hough transform. The 'stair casing effect' indicates that the diameter measurements are rounded to the nearest pixel. Bottom: the diameter has been extracted using the rewritten algorithm.

The same microscope video recording was then reanalysed with the new algorithm that takes a width measurement of every horizontal line and combines those measurements for every frame. The extracted diameter has been plotted against the time in comparison to the applied pressure on the bottom of Figure 36. Small dilations that were not previously measurable, have been made visible with the rewritten algorithm. The smallest recognisable dilation was measured to be 1.5 µm, which lies below the pixel size of the video and is at least a tenfold smaller than the required resolution size prescribed in the ISO standard. The recorded pressure and extracted diameter were consecutively correlated to acquire the pressure as function of the diameter for an estimation of the compliance and have been plotted in Figure 37. On the left, the analysis of a slowly increasing pressurisation is shown. The pressure and diameter readings in the time domain have been correlated with each other to acquire the pressure as function of the diameter. This has resulted in a radial expansion of 2.31, 2.02, and 1.83 % / 100 mmHg for the pressure ranges 50 – 90 mmHg, 80 – 120 mmHg, and 110 – 150 mmHg respectively.



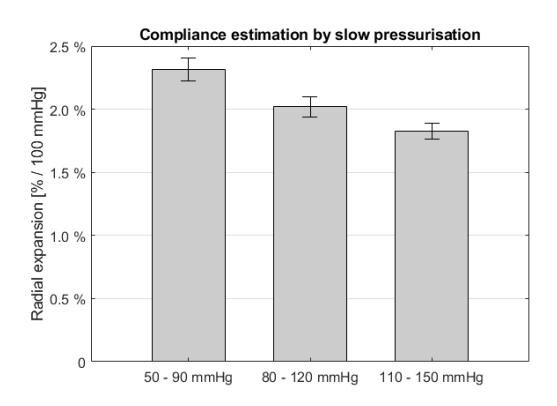


Figure 37 Left: the recorded pressure has been plotted against the correlated inner diameter, which have been acquired by slow pressurisation of the dummy scaffold. Right: The radial expansion has been analysed for three ranges: 50 - 90 mmHg, 80 - 120 mmHg, and 110 - 150 mmHg. The radial expansion is expressed in % per 100 mmHg. Error bars show the 95% confidence interval.

The analysis of the dynamic radial expansion is shown in **Figure 38**. Here, individual measurements were made for the different pressure ranges, over which the dummy scaffolds were pressurised in a cyclic fashion for 30 seconds at a frequency of 1 Hz. The pressure and diameter readings in the time domain of the individual measurements have been correlated with each other to acquire the pressure as function of the diameter (**Figure 39**).

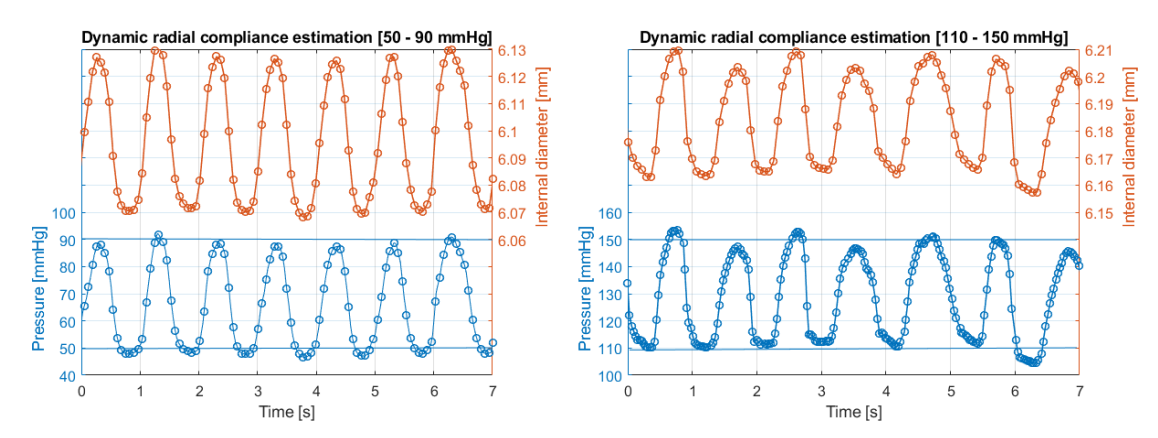


Figure 38 Analysis of the dynamic radial compliance estimation, where a scaffold is pressurised with a pulsatively at a physiological frequency of 1 Hz. A subset of 7 seconds of the recording of the pressure and the calculated internal diameter have been plotted against the time. On the left: the dummy scaffold has been pressurised over the range of 50 – 90 mmHg. On the right: the dummy scaffold has been pressurised over the range of 110 – 150 mmHg.

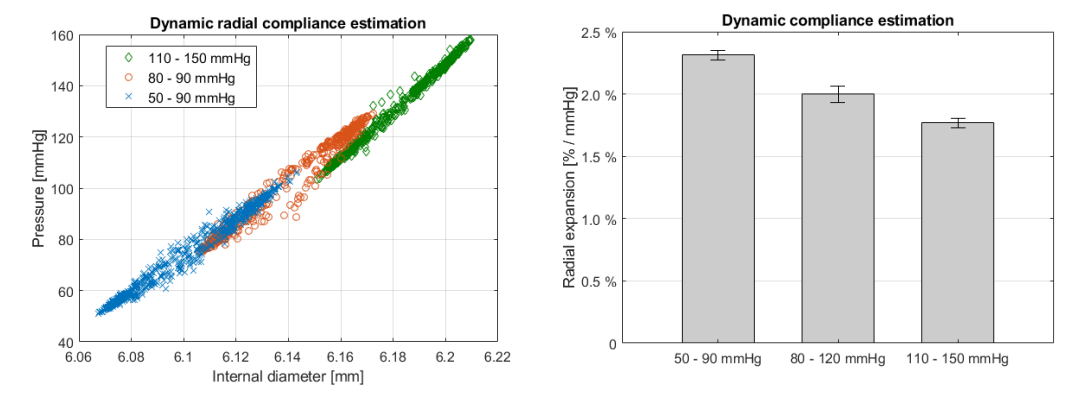


Figure 39 Left: the recorded pressure has been plotted against the correlated inner diameter, which have been acquired by oscillating pressurisation of the dummy scaffold at a frequency of 1 Hz over three ranges: 50 – 90 mmHg, 80 – 120 mmHg, and 110 – 150 mmHg. Right: The radial expansion has been analysed and expressed in % per 100 mmHg. Error bars show the 95% confidence interval.

5 **Discussion**

Previously published studies have shown the versatile uses of perfusion bioreactor set-ups to perform dynamic cell culture experiments on TEVGs. Most bioreactor systems have been designed to study cell behaviour and tissue remodelling under mimicked physiological flow conditions (Diamantouros et al. 2013; Engbers-Buijtenhuijs et al. 2006; Hahn et al. 2007; Hoenicka et al. 2010; Maschhoff et al. 2017; Melchiorri et al. 2016; Piola et al. 2013; Song et al. 2012; Wang et al. 2010). Some studies have tailored the bioreactor to more clinically oriented applications and have worked towards the creation of off-the-shelve vascular prostheses (Wolf et al. 2018). Here, the purpose was to present a design of a bioreactor for dynamic culture of TEVGs, which features a simplified set-up regarding both operation and modularity. It was required that the presented bioreactor set-up is able to reproduce the in vivo conditions with regards to the exerted shear forces on the scaffold. Furthermore, it should allow for a mechanical characterisation in compliance with relevant standards on the testing of vascular implants.

5.1 Culture chamber design

5.1.1 Design novelty

The final bioreactor design presented in this study features a culture chamber that is easier to handle and does not require any tools in the assembly. This greatly simplifies maintaining sterility during assembly. Most previously published bioreactor designs require tools to close the culture chamber. This has been circumvented in the present design, by repurposing standard laboratory utensils that are meant to provide sealable storage. The used Schott laboratory glass bottle proved to be a suitable culture chamber. The bottle is easy in maintenance, as it is autoclavable in its entirety, and is large enough to accommodate the presented graft frame design, which can be inserted and sealed off watertight without any tools. The separate graft frame, onto which the vascular graft is mounted, distinguishes the present vascular culture chamber design from most designs in literature, where the mounting points form an integral part of the entire culture chamber. The single-sided opening is a rather unconventional approach for a vascular culture chamber design. In two studies by the same research group, a similar approach was presented (Bono et al. 2017; Piola et al. 2013). Piola and colleagues created a compact vascular bioreactor, where a vascular grafts was mounted onto a separate graft frame, which was consecutively slid into a 50 mL Falcon tube that acted as the culture chamber and medium reservoir (Piola et al. 2013). A separation of the flow circuits was not foreseen. The graft frame could accommodate vascular grafts with a diameter of around 3 mm, which were secured using elastic tourniquets around barbed connectors. Most presented vascular bioreactor systems allow for the mounting of vascular scaffolds with only a fixed specific diameter. Here, the fixed-diameter mounting points have been replaced by more versatile LuerLock connectors with rotating collars. This enables the uncomplicated mounting of practically any small-diameter (< 6 mm) vascular graft without modifying the graft frame. Furthermore, depending on the used scaffolds, the culture chamber design enables a fully separated culturing of the intraluminal and extraluminal wall side. Unfortunately, due to the porous nature of electrospun scaffolds, it was not possible to test the leak-free separation of the circuits in the culture chamber with our own vascular scaffolds, neither was it possible to mechanically characterise our scaffolds by means of direct pressurisation. It is self-evident, that a leak-free separation of the circuits is only guaranteed, when the scaffold itself is non-permeable. This does not, however, prohibit the use of porous scaffolds in the bioreactor, as an impermeable tissue layer can be formed during cell culture. Regarding the mechanical characterisation, the ISO norm prescribes the use of an impermeable liner for porous vascular grafts. The liner should have a significantly higher diameter at 120 mmHg than the nominal diameter of the porous vascular graft, so the compliance estimation is not affected by the mechanical properties of the liner.

5.1.2 Medium consumption

Since the culture chamber is made out of repurposed existing lab ware, several compromises were unavoidable, as its design could be altered to a limited extent. The extraluminal compartment of the culture chamber is relatively large with respect to the surface area of the scaffold. Filling the 250 mL bottle with medium, results in a required medium volume of 20 mL per square centimetre of scaffold surface for a vascular graft with a diameter of 6 mm and around 38 mL per square centimetre for a vascular graft with a diameter of 3 mm. This vastly supersedes the required medium in static cell culture, considering that a T-75 usually gets filled with around 15 mL of medium and a single well in a 96-well plate with around 200 μL, corresponding to 0.2 mL and 0.6 mL per square centimetre of growth area respectively. This does not take around 100 mL of medium in the medium reservoir and dead spaces, such as tubes, into account. In static cell culture, the amount of cell medium is a trade-off between the nutrient depletion rate and gas exchange, as an excess column of medium results in reduced gas exchange by diffusion (Gstraunthaler et al. 1999). The latter, however, is not applicable to dynamic cell culture in bioreactors, as the continuous mass transport ensures a more reliable supply of oxygen and nutrients in large volumes, granted that the 3D tissue itself does not hinder the mass transport and the flow conditions are optimised for an adequate mix of the medium (Martin et al. 2004). It should be, however, taken into consideration, that anything produced by the cells under culture, such as signal molecules, will be diluted and, therefore, will be possibly harder to detect.

5.2 Characterisation

The bioreactor has been characterised in a number of steps. First, the reading of the pressure transducers and the flow rate as function of the pump head rotation speed were calibrated to enable successive measurements. The subsequent characterisation steps were aided by CFD

simulations to gain an insight in the fluid dynamics within the intraluminal circulation during culture.

5.2.1 Fluid mechanics

A total of 81 different in silico simulations were performed with three scaffold geometries, three fluid properties, and nine flow rates. The pressure loss was assessed to optimise the reading of the pressure within the scaffold, since the pressure can only be read at locations outside of the culture chamber. A noticeable pressure drop for higher flow rates was expected, because the intraluminal circulation in the culture chamber features two 90-degrees bends and the tube connectors introduce narrowings to the circulation. As the majority of the pressure loss (85%) occurs downstream of the scaffold, a pressure transducer at the intraluminal inlet yields a more accurate pressure reading. Another option is to use two pressure transducers and interpolate the pressure readings between the inlet and outlet (in this case at 15%). The same approach was used in the TEVG perfusion reactor of Diamantouros, although no CFD simulations were performed in this study, neither did the intraluminal flow encounter any sharp bends (Diamantouros 2011). It has to be noted, that the actual measured pressure loss is slightly higher than the predicted pressure loss by the fluid simulations at higher flow rates, especially above 20 ml/min. This might be partly explained by the extents of the three-dimensional model that has been used for the CFD simulations. The CFD model only included the graft frame components itself. The pressure line of the pressure transducer is connected to a three-way stopcock right before the intraluminal inlet, which has not been included in the CFD model. A second explanation follows from the pressure oscillations that were induced by the roller pump head at higher rotation speeds. The introduction of a pressure buffer between the roller pump and the intraluminal inlet of the culture chamber has almost completely eliminated the oscillations, which reduced the pressure loss and also greatly extended the functional operating range of the bioreactor set-up. Oscillation-free flows have been achieved and tested at a flow rate of 100 ml/min, enabling shear forces that are five times larger than at a flow of 20 ml/min, at which the flow was becoming too unstable without a pressure buffer. The operating limits of the roller pump are at 140 ml/min. This permits the simulation of a wide range of physiological arterial shear forces (Figure 40). Shear forces in the upper venous and lower arterial range, for example those found in the femoral artery (typical values are around 370 mPa), can be reproduced in grafts of any diameter between 3 and 6 mm (Wu et al. 2004). This range has often been used in studies, where explanted blood vessels were perfused ex vivo, such as the saphenous vein (Gusic et al. 2005; Hoenicka et al. 2010; Maschhoff et al. 2017). A large number of studies have been devoted to the study of EC responses to shear stress (Ando and Yamamoto 2009). Arterial shear stresses over the range between 500 and 2600 mPa are assumed to determine the morphology and the cytoskeletal organisation of ECs (Dewey et al. 1981; Wechezak et al. 1985). These shear stress have also been applied to study EC orientation and organisation on EC-seeded TEVGs in perfusion bioreactors (Inoguchi et al. 2007; Ju et al. 2017). Another interesting deployment area, is the investigation of the ESC and

EPC differentiation responses to culturing with mechanical stimuli (Egorova et al. 2012; Kutikhin et al. 2018; Obi et al. 2012; Yamamoto et al. 2003), as differentiation is influenced by whether the applied strain is continuous or cyclic (Shimizu et al. 2008). The findings have been used to observe maturation and endothelialisation of bioreactor-cultured EPC-seeded vascular graft (Melchiorri et al. 2016). A shear stress of 600 mPa has been shown to be sufficient, to produce vascular grafts with greatly increased neotissue formation and expression of EC-specific markers compared to static culture (Melchiorri et al. 2016). The culture chamber design presented in this study, allows the reproduction of these shear stresses with both aqueous media and high-viscosity media.

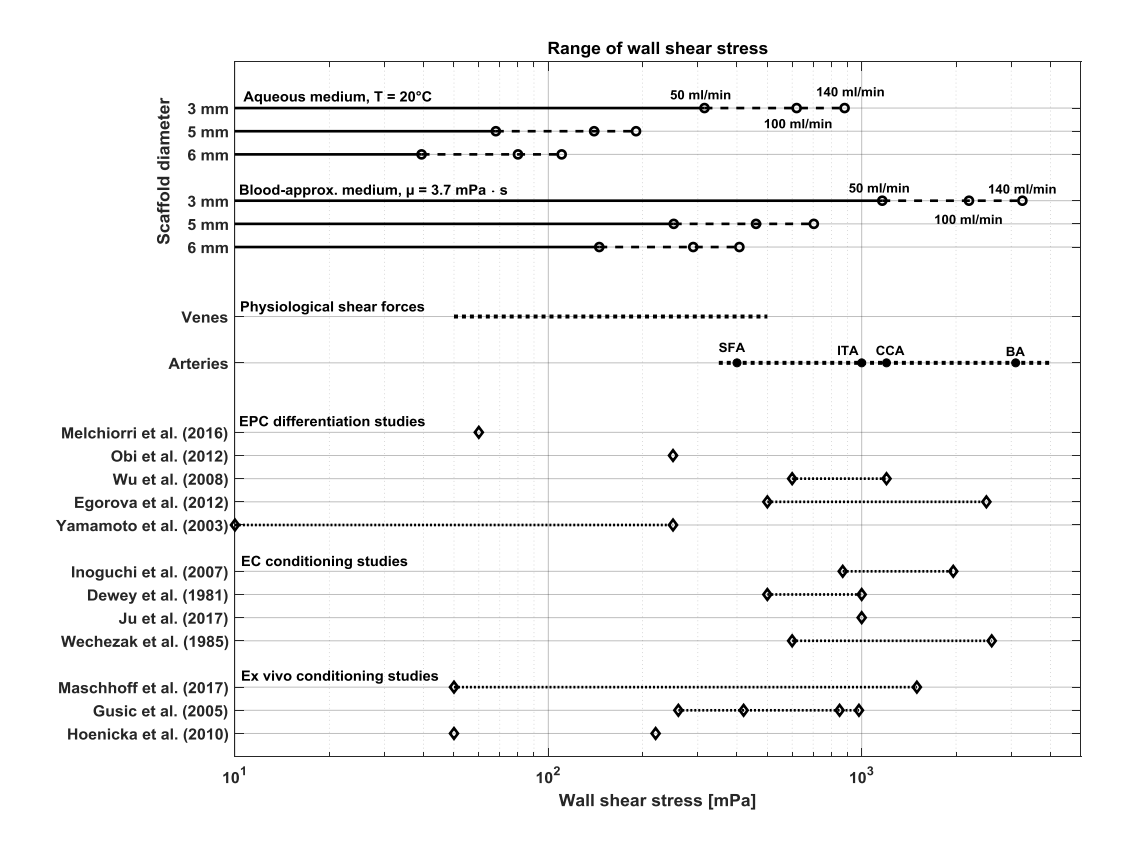


Figure 40 The achievable shear forces in the bioreactor compared to physiologically occurring shear forces in veins and arteries based on in vivo measurements (Ford et al. 2005; Rittgers et al. 1978; Wu et al. 2004) and studies on the influence of shear stress on cell behaviour. For the shear stress ranges of the bioreactor, the solid lines include the ranges up to 50 ml/min, which were included in the CFD simulations. The dashed lines include the range up to 140 ml/min, which was only practically been tested without CFD simulations. Abbreviations: SFA: superficial femoral artery, ITA: internal thoracic artery, CCA: common carotid artery, BA: brachial artery.

It has to be noted that the achievable shear stress values in the scaffold, refer to a steady pipe flow, which can be calculated analytically. The shear stress was further examined by CFD, to assess its distribution along the scaffold wall. At the entrance, when the culture medium exits the narrow interior of the tube connector, a recirculation zone is observed in the CFD simulations. The recirculation zone causes fluid to slowly flow in the opposite direction near the scaffold wall up to the reattachment zone. This region has a significantly reduced wall shear stress compared to the analytical Poiseuille value and its length is dependent on both the fluid

properties and the imposed flow rate. This revealed another advantage of the high-viscosity medium, as the low-shear stress zone was found to be the smallest in these cases and spanned less than half of the scaffold wall for all flow rates. Especially the combination of smaller sized scaffolds and the use of a high-viscosity medium will both make the bioreactor deployable for a larger shear stress range (Figure 40) and feature the largest region with a stable fully developed flow, which in turn contributes to reproducible results. In case an aqueous medium at 37 °C is used, the low-shear stress zone can span a considerable portion of the scaffold. Moreover, at flow rates of over 20 ml/min, a redevelopment of a steady Poiseuille flow is not guaranteed within the length of 5 and 6 mm-diameter scaffolds with aqueous medium, as the scaffold length is too short. The maximum length of the scaffold is, however, limited by the culture chamber, which presented a drawback of repurposing existing lab ware. Tissue that is cultured within the redevelopment region, will not be subjected to an evenly distributes shear stress that can be calculated analytically on forehand. The intraluminal flow has only been characterised by CFD simulations up to a flow rate of 50 ml/min. This has caused a flow regime with a Reynolds number around Re = 1500 with aqueous medium in small portions of the bioreactor, which is still within laminar range. The simulation of higher flow rates will require both a more refined meshing and models for turbulent flow, which have not been used in this study.

5.2.2 Cytotoxicity and sterility

The constructed bioreactor is composed mostly of autoclavable parts, including the medium reservoir bottles, culturing chamber, and the majority of the graft frame. The graft frame can be autoclaved in its entirety, with the exception of the silicone return tubing, which should be replaced after every use. The medium extracts that have been incubated with the machined PEEK and Aluminium parts did not show any cytotoxic potential on mVECs. In contrast, the PEEK group showed a relative viability of over 100 % with respect to the negative control that was cultured with fresh medium. It is known that PEEK has an excellent biocompatibility in vitro (Wang et al. 2015; Wenz et al. 1990). However, there is no solid evidence to explain why PEEK extracts would significantly outperform the negative control in an in vitro cytotoxicity test (Morrison et al. 1995; Wang et al. 2015). The increased viability observed in the present study, might be caused by a pipetting error in the last step of the cytotoxicity test, when the MTS reagent was added to the 96-well plate. This step was, in contrast to the previous steps, carried out with a single-channel pipette. The manual pipetting could have created an incubation time difference, as the colorimetric reaction already started while the last wells were still being filled (Appendix D).

5.3 Compliance estimation

Many research groups provide different strategies and definitions in the mechanical characterisation of vascular substitutes (Laterreur et al. 2014). In this study, the aim was to work towards a mechanical characterisation that adheres to requirements that are stated in ISO

7198:2016. The graft frame allows for the culture of grafts that are at least 10 times longer than their diameter and a direct pressurisation with a read out accuracy that complies with the standard's requirements. However, a solution has to be found for how the graft will be fixated for mechanical characterisation. Currently, the graft frame does not permit any longitudinal elongation nor contraction of the graft, as it is constrained by the rigid construction of the graft frame, whereas the standard requires the graft to be fixed with a longitudinal preload, corresponding to a suspended load between 30 g and 60 g (ISO 2016). The current strategy would therefore necessitate the use of a different frame that is solely used for the mechanical characterisation. It is noteworthy that the diameter analysis algorithm was able extract features of subpixel resolution. The smallest extracted dilatations measured 1.5 µm, whereas the pixel resolution was measured to be 6.3 µm at a magnification of 15.6x. Since the diameter extraction algorithm combines 1040 individual width measurements for every frame, a simple superresolution measurement is acquired. Theoretically, the minimum feature size can be reduced even further, as the used magnification was limited by the large diameter of the dummy scaffold. The achieved resolution far supersedes the accuracy requirement of ISO 7198:2016. The international standard states, that the diameter should be measured with a device capable of achieving an accuracy of ±20 µm. This places the method to measure the diameter in the compliance estimation used in this study at an advantage in respect to measuring the diameter by means of an optical micrometer. Although currently available optical micrometers that are capable of measuring objects that are larger than 6 mm, also surpass these requirements and offer an accuracy in the sub-micron range (Keyence Corp. 2006; Valiño et al. 2012), a microscope could serve multiple purposes. For example, labs specialising in microphysiological systems often already have a sterile bench with a microscope under the hood, which could be used to perform the compliance estimation under sterile conditions. Ideally, the graft should not have to be taken out of the culture chamber for a compliance measurement at all. TEVG perfusion bioreactors that enable diameter measurements during tissue culture have already been presented by various research groups (Bilodeau 2004; Diamantouros et al. 2013; Maschhoff et al. 2017). Maschhoff and colleagues presented a perfusion bioreactor capable of measuring the internal diameter during tissue culture directly by means of ultrasound. Not only did this provide a more detailed three-dimensional model for CFD calculations during culture, it also provided a better estimation of the compliance, as the wall thickness changed during tissue culture (Maschhoff et al. 2017). This has come at the cost of the simplicity of inserting and mounting the vascular graft in the culture chamber. Parallelisation and up-scaling of the tissue culture is hindered, as the measurement equipment either forms an integral part of the culture chamber (Maschhoff et al. 2017) or requires precise alignment of the culture chamber with the measuring apparatus (Bilodeau 2004; Diamantouros et al. 2013). Assessment of the compliance during tissue culture is not possible with the culture chamber design presented in this study, since the medium-filled round culture chamber would diffract the light.

6 **Conclusion**

The main purpose of this study was to design and construct a simplified perfusion bioreactor for tissue-engineered vascular grafts with the focus on the possibility to exert physiologically accurate mechanical stimuli on the cultured scaffolds. This has been accomplished by repurposing commercially available lab ware as the casing for the culture chamber and presenting a novel graft frame design that enables a toolless mounting of the vascular graft of different sizes. The use of existing lab ware also permits uncomplicated upscaling of the tissue culture. Pressure read out is modular and achieved with disposable clinical pressure transducers. The resulting design enables the in vitro culture of vascular grafts with a diameter up to 6 mm under sterile conditions after placing the culture chamber in an incubator, as its interior is completely sealed off from the exterior. The graft frame consists of autoclavable materials, of which the extracts show no sign of cytotoxicity. The design also allows for a separated perfusion of the intraluminal and extraluminal side of the scaffold wall, which permits the simultaneous cell culture with different cell media and a complete separation of signalling molecules released by the cultured cells. The subsequent in silico characterisation of the bioreactor has provided a more in-depth insight in the local fluid dynamics within the intraluminal circulation. The current design allows the exertion of a broad range of physiologically relevant shear stresses on cultured TEVGs. At the highest simulated flow rate of 50 ml/min, arterial shear stresses can be simulated in a laminar regime, when a cell medium with a viscosity of 3.7 mPa s is used. When using aqueous medium, it should be noted that a significant portion of the scaffold is not subjected to a constant wall shear stress at the Poiseuille value, due to the narrow interior of the tube connectors onto which the ends of the scaffold is mounted. The CFD simulations predict, that this flow redevelopment region, increases in length at higher flow rates. This has to be taken into consideration, when tissue culture at higher flow rates or with unsupplemented aqueous medium is required. This study has also presented a test method for the estimation of the radial compliance by direct pressurisation of the scaffold. The read out of the pressure and diameter width complies with the ISO requirements on accuracy. However, the current graft frame design that is used during culture does not allow for fixed longitudinal preload. Currently, the only strategy to adhere to all requirements, is to use a different graft frame during mechanical characterisation.

7 **Outlook**

The focus of the further development of the bioreactor should be on the completion of ISO compliancy regarding the mechanical characterisation, which includes the development of a graft frame that exerts a continuous preload during pressurisation. Depending on the need for higher shear forces, one limitation of the present bioreactor design, comprising the limited usable scaffold length, could be addressed by looking into other lab ware or by a custom design of the culture chamber. Another important step would be enabling the assessment of porous scaffolds with impermeable liners, which could be carried out with the use of balloons, such as those used in percutaneous transluminal angioplasty. This would enable the radial compliance estimation of porous electrospun scaffolds, which are currently subject to investigation in our research group. The separation of the intraluminal and extraluminal circuit is an important capability of the presented bioreactor, which enables the culture and assessment of multilayered TEVGs. Multi-layered electrospun TEVGs can be adapted to possess a different porosity and fibre microarchitecture on each side, which are tailored to the cells that populate the respective sides of a blood vessel wall (Ju et al. 2017; Wu et al. 2018). Fibre size, porosity, and orientation influence cell-specific cell infiltration and organisation in fibrous threedimensional scaffolds (Ju et al. 2010; Lowery et al. 2010; Soliman et al. 2010). This could be utilised to create electrospun scaffolds with longitudinal fibre alignment on the inner side tailored to ECs and circumferentially aligned fibres on the outer side with high porosity tailored to SMCs or fibroblasts (Ju et al. 2010; Whited and Rylander 2014). The circuit separation featured in the present bioreactor design would offer a suitable tool for the in vitro culture of such multi-layered TEVGs.

Bibliography

- Ando J, Yamamoto K. 2009. Vascular Mechanobiology: Endothelial Cell Responses to Fluid Shear Stress. Circulation Journal 73(11):1983-1992.
- Arndt JO, Klauske J, Mersch F. 1968. The diameter of the intact carotid artery in man and its change with pulse pressure. Pflüger's Archiv für die gesamte Physiologie des Menschen und der Tiere 301(3):230-240.
- Ayres C, Bowlin GL, Henderson SC, Taylor L, Shultz J, Alexander J, Telemeco TA, Simpson DG. 2006. Modulation of anisotropy in electrospun tissue-engineering scaffolds: Analysis of fiber alignment by the fast Fourier transform. Biomaterials 27(32):5524-34.
- Barron V, Lyons E, Stenson-Cox C, McHugh P, Pandit A. 2003. Bioreactors for cardiovascular cell and tissue growth: a review. Annals of biomedical engineering 31(9):1017-1030.
- Bilodeau K. 2004. Conception et validation d'un bioréacteur spécifique à la régénération du tissu artériel sous contraintes mécaniques.
- Bono N, Meghezi S, Soncini M, Piola M, Mantovani D, Fiore GB. 2017. A Dual-Mode Bioreactor System for Tissue Engineered Vascular Models. Annals of biomedical engineering 45(6):1496-1510.
- Braghirolli DI, Helfer VE, Chagastelles PC, Dalberto TP, Gamba D, Pranke P. 2017. Electrospun scaffolds functionalized with heparin and vascular endothelial growth factor increase the proliferation of endothelial progenitor cells. Biomed Mater 12(2):025003.
- Canny J. 1986. A computational approach to edge detection. IEEE Transactions on pattern analysis and machine intelligence(6):679-698.
- Cao Y, Croll TI, Cooper-White JJ, O'Connor AJ, Stevens GW. 2004. Production and surface modification of polylactide-based polymeric scaffolds for soft-tissue engineering. Methods Mol Biol 238:87-112.
- Carrel A, Lindbergh CA. 1938. The culture of organs. The American Journal of the Medical Sciences 196(5):732.
- Chien S. 1970. Shear dependence of effective cell volume as a determinant of blood viscosity. Science 168(3934):977-979.
- Chow T. 1980. The effect of particle shape on the mechanical properties of filled polymers. Journal of Materials Science 15(8):1873-1888.
- Coble R, Kingery W. 1956. Effect of porosity on physical properties of sintered alumina. Journal of the American Ceramic Society 39(11):377-385.
- Dewey C, Bussolari S, Gimbrone M, Davies PF. 1981. The dynamic response of vascular endothelial cells to fluid shear stress. Journal of biomechanical engineering 103(3):177-185
- Diamantouros SE. 2011. A Pulsatile Bioreactor System for Durability Testing and Compliance Estimation of Vascular Grafts [PhD. Thesis]. Aachen: RWTH.
- Diamantouros SE, Hurtado-Aguilar LG, Schmitz-Rode T, Mela P, Jockenhoevel S. 2013. Pulsatile perfusion bioreactor system for durability testing and compliance estimation of tissue engineered vascular grafts. Ann Biomed Eng 41(9):1979-89.
- Drilling S, Gaumer J, Lannutti J. 2009. Fabrication of burst pressure competent vascular grafts via electrospinning: effects of microstructure. J Biomed Mater Res A 88(4):923-34.
- Duda RO, Hart PE. 1972. Use of the Hough transformation to detect lines and curves in pictures. Communications of the ACM 15(1):11-15.
- Egorova AD, DeRuiter MC, de Boer HC, van de Pas S, Gittenberger-de Groot AC, van Zonneveld AJ, Poelmann RE, Hierck BP. 2012. Endothelial colony-forming cells show a mature transcriptional response to shear stress. In Vitro Cell Dev Biol Anim 48(1):21-9.
- El-Kurdi MS, Vipperman JS, Vorp DA. 2009. Design and subspace system identification of an ex vivo vascular perfusion system. Journal of biomechanical engineering 131(4):041012.
- Engbers-Buijtenhuijs P, Buttafoco L, Poot AA, Dijkstra PJ, de Vos RA, Sterk LM, Geelkerken RH, Vermes I, Feijen J. 2006. Biological characterisation of vascular grafts cultured in a bioreactor. Biomaterials 27(11):2390-7.
- Ford MD, Alperin N, Lee SH, Holdsworth DW, Steinman DA. 2005. Characterization of volumetric flow rate waveforms in the normal internal carotid and vertebral arteries. Physiological measurement 26(4):477.

- Gstraunthaler G, Seppi T, Pfaller W. 1999. Impact of culture conditions, culture media volumes, and glucose content on metabolic properties of renal epithelial cell cultures. Cellular physiology and biochemistry 9(3):150-172.
- Gusic RJ, Myung R, Petko M, Gaynor JW, Gooch KJ. 2005. Shear stress and pressure modulate saphenous vein remodeling ex vivo. J Biomech 38(9):1760-9.
- Hahn MS, McHale MK, Wang E, Schmedlen RH, West JL. 2007. Physiologic pulsatile flow bioreactor conditioning of poly(ethylene glycol)-based tissue engineered vascular grafts. Ann Biomed Eng 35(2):190-200.
- Hinderer S, Shen N, Ringuette L-J, Hansmann J, Reinhardt DP, Brucker SY, Davis EC, Schenke-Layland K. 2015. In vitro elastogenesis: instructing human vascular smooth muscle cells to generate an elastic fiber-containing extracellular matrix scaffold. Biomedical Materials 10(3):034102.
- Hinderer S, Sudrow K, Schneider M, Holeiter M, Layland SL, Seifert M, Schenke-Layland K. 2018. Surface functionalization of electrospun scaffolds using recombinant human decorin attracts circulating endothelial progenitor cells. Sci Rep 8(1):110.
- Hinderliter PM, Minard KR, Orr G, Chrisler WB, Thrall BD, Pounds JG, Teeguarden JG. 2010. ISDD: a computational model of particle sedimentation, diffusion and target cell dosimetry for in vitro toxicity studies. Particle and fibre toxicology 7(1):36.
- Hoenicka M, Wiedemann L, Puehler T, Hirt S, Birnbaum DE, Schmid C. 2010. Effects of shear forces and pressure on blood vessel function and metabolism in a perfusion bioreactor. Annals of biomedical engineering 38(12):3706-3723.
- Hokanson DE, Mozersky DJ, Sumner DS, McLeod Jr FD, Strandness Jr DE. 1972. Ultrasonic arteriography: A noninvasive method of arterial visualization. Radiology 102(2):435-435.
- Huang Z-M, Zhang YZ, Kotaki M, Ramakrishna S. 2003. A review on polymer nanofibers by electrospinning and their applications in nanocomposites. Composites Science and Technology 63(15):2223-2253.
- Inoquchi H, Tanaka T, Maehara Y, Matsuda T. 2007. The effect of gradually graded shear stress on the morphological integrity of a huvec-seeded compliant small-diameter vascular graft. Biomaterials 28(3):486-95.
- Isenberg BC, Williams C, Tranquillo RT. 2006. Small-diameter artificial arteries engineered in vitro. Circ Res 98(1):25-35.
- ISO. 2016. 7198:2016 Cardiovascular implants and extracorporeal systems Vascular prostheses — Tubular vascular grafts and vascular patches. International Organization for Standardization, Geneva, Switzerland.
- Ju YM, Ahn H, Arenas-Herrera J, Kim C, Abolbashari M, Atala A, Yoo JJ, Lee SJ. 2017. Electrospun vascular scaffold for cellularized small diameter blood vessels: A preclinical large animal study. Acta Biomater 59:58-67.
- Ju YM, Choi JS, Atala A, Yoo JJ, Lee SJ. 2010. Bilayered scaffold for engineering cellularized blood vessels. Biomaterials 31(15):4313-21.
- Kasyanov Y, Sistino JJ, Trusk TC, Markwald RR, Mironov V. 2005. Perfusion Bioreactors for cardiovascular tissue engineering. In: Chaudhuri J, Al-Rubeai M, editors. Bioreactors for Tissue Engineering: Principles, Design and Operation: Springer Science & Business Media. p 285-308.
- Kelleher CM, Vacanti JP. 2010. Engineering extracellular matrix through nanotechnology. Journal of the Royal Society Interface:rsif20100345.
- Kelly BA, Chowienczyk P. 2002. Vascular compliance. In: Hunt BJ, Poston L, Halliday AW, Schachter M, editors. An introduction to vascular biology: from basic science to clinical practice: Cambridge University Press. p 33-48.
- Kennedy KM, Bhaw-Luximon A, Jhurry D. 2017. Cell-matrix mechanical interaction in electrospun polymeric scaffolds for tissue engineering: Implications for scaffold design and performance. Acta Biomater 50:41-55.
- Keyence Corp. 2006. LS-7000 Series High-Speed, High-accuracy Digital Micrometer Catalog.
- Khorshidi S, Solouk A, Mirzadeh H, Mazinani S, Lagaron JM, Sharifi S, Ramakrishna S. 2016. A review of key challenges of electrospun scaffolds for tissue-engineering applications. J Tissue Eng Regen Med 10(9):715-38.
- Kielty CM. 2006. Elastic fibres in health and disease. Expert reviews in molecular medicine 8(19):1-23.
- Kim TG, Shin H, Lim DW. 2012. Biomimetic scaffolds for tissue engineering. Advanced Functional Materials 22(12):2446-2468.

- Konig G, McAllister TN, Dusserre N, Garrido SA, Iyican C, Marini A, Fiorillo A, Avila H, Wystrychowski W, Zagalski K. 2009. Mechanical properties of completely autologous human tissue engineered blood vessels compared to human saphenous vein and mammary artery. Biomaterials 30(8):1542-1550.
- Kutikhin AG, Sinitsky MY, Yuzhalin AE, Velikanova EA. 2018. Shear stress: An essential driver of endothelial progenitor cells. Journal of molecular and cellular cardiology.
- Langewouters G, Wesseling K, Goedhard W. 1984. The static elastic properties of 45 human thoracic and 20 abdominal aortas in vitro and the parameters of a new model. Journal of biomechanics 17(6):425-435.
- Laterreur V, Ruel J, Auger FA, Vallieres K, Tremblay C, Lacroix D, Tondreau M, Bourget JM, Germain L. 2014. Comparison of the direct burst pressure and the ring tensile test methods for mechanical characterization of tissue-engineered vascular substitutes. J Mech Behav Biomed Mater 34:253-63.
- Leeson C, Robinson M, Francis J, Robson M, Channon K, Neubauer S, Wiesmann F. 2006. Cardiovascular magnetic resonance imaging for non-invasive assessment of vascular function: validation against ultrasound. Journal of Cardiovascular Magnetic Resonance 8(2):381-387.
- Levesque P, Gauvin R, Larouche D, Auger FA, Germain L. 2011. A computer-controlled apparatus for the characterization of mechanical and viscoelastic properties of tissue-engineered vascular constructs. Cardiovascular Engineering and Technology 2(1):24-34.
- Li WJ, Laurencin CT, Caterson EJ, Tuan RS, Ko FK. 2002. Electrospun nanofibrous structure: a novel scaffold for tissue engineering. Journal of Biomedical Materials Research Part A 60(4):613-621.
- Lowery JL, Datta N, Rutledge GC. 2010. Effect of fiber diameter, pore size and seeding method on growth of human dermal fibroblasts in electrospun poly(epsilon-caprolactone) fibrous mats. Biomaterials 31(3):491-504.
- Marieb EN, Hoehn K. 2015. Human Anatomy & Physiology, Global Edition: Pearson Education Limited.
- Martin I, Wendt D, Heberer M. 2004. The role of bioreactors in tissue engineering. Trends Biotechnol 22(2):80-6.
- Maschhoff P, Heene S, Lavrentieva A, Hentrop T, Leibold C, Wahalla M-N, Stanislawski N, Blume H, Scheper T, Blume C. 2017. An intelligent bioreactor system for the cultivation of a bioartificial vascular graft. Engineering in Life Sciences 17(5):567-578.
- Matthews JA, Wnek GE, Simpson DG, Bowlin GL. 2002. Electrospinning of collagen nanofibers. Biomacromolecules 3(2):232-238.
- Maxwell JA, Anliker M. 1968. The dissipation and dispersion of small waves in arteries and veins with viscoelastic wall properties. Biophysical journal 8(8):920.
- McClure MJ, Sell SA, Ayres CE, Simpson DG, Bowlin GL. 2009. Electrospinning-aligned and random polydioxanone-polycaprolactone-silk fibroin-blended scaffolds: geometry for a vascular matrix. Biomed Mater 4(5):055010.
- Melchiorri AJ, Bracaglia LG, Kimerer LK, Hibino N, Fisher JP. 2016. In Vitro Endothelialization of Biodegradable Vascular Grafts Via Endothelial Progenitor Cell Seeding and Maturation in a Tubular Perfusion System Bioreactor. Tissue Eng Part C Methods 22(7):663-70.
- Morrison C, Macnair R, MacDonald C, Wykman A, Goldie I, Grant M. 1995. In vitro biocompatibility testing of polymers for orthopaedic implants using cultured fibroblasts and osteoblasts. Biomaterials 16(13):987-992.
- Nichols M, Townsend N, Scarborough P, Rayner M. 2014. Cardiovascular disease in Europe 2014: epidemiological update. European heart journal 35(42):2950-2959.
- Obi S, Masuda H, Shizuno T, Sato A, Yamamoto K, Ando J, Abe Y, Asahara T. 2012. Fluid shear stress induces differentiation of circulating phenotype endothelial progenitor cells. Am J Physiol Cell Physiol 303(6):C595-606.
- Opie LH, Paterson DJ. 2004. Blood Pressure and Peripheral Circulation. In: Opie LH, editor. Heart physiology: from cell to circulation. Fourth Edition ed: Lippincott Williams & Wilkins. p 431 459.
- Pauly HM, Kelly DJ, Popat KC, Trujillo NA, Dunne NJ, McCarthy HO, Haut Donahue TL. 2016.

 Mechanical properties and cellular response of novel electrospun nanofibers for

- ligament tissue engineering: Effects of orientation and geometry. J Mech Behav Biomed Mater 61:258-270.
- Piola M, Prandi F, Bono N, Soncini M, Penza E, Agrifoglio M, Polvani G, Pesce M, Fiore GB. 2013. A compact and automated ex vivo vessel culture system for the pulsatile pressure conditioning of human saphenous veins. J Tissue Eng Regen Med 10(3):E204-15.
- Pörtner R, Nagel-Heyer S, Goepfert C, Adamietz P, Meenen NM. 2005. Bioreactor design for tissue engineering. J Biosci Bioeng 100(3):235-45.
- Pugsley M, Tabrizchi R. 2000. The vascular system: An overview of structure and function. Journal of pharmacological and toxicological methods 44(2):333-340.
- Rakhorst G, Ploeg R. 2008. Biomaterials in modern medicine: the Groningen perspective: World Scientific Publishing Company.
- Rittgers SE, Karayannacos PE, Guy JF, Nerem RM, Shaw GM, Hostetler JR, Vasko JS. 1978. Velocity distribution and intimal proliferation in autologous vein grafts in dogs. Circulation research 42(6):792-801.
- Rnjak-Kovacina J, Weiss AS. 2011. Increasing the pore size of electrospun scaffolds. Tissue Eng Part B Rev 17(5):365-72.
- Shimizu N, Yamamoto K, Obi S, Kumagaya S, Masumura T, Shimano Y, Naruse K, Yamashita JK, Igarashi T, Ando J. 2008. Cyclic strain induces mouse embryonic stem cell differentiation into vascular smooth muscle cells by activating PDGF receptor β. Journal of applied physiology 104(3):766-772.
- Soliman S, Pagliari S, Rinaldi A, Forte G, Fiaccavento R, Pagliari F, Franzese O, Minieri M, Di Nardo P, Licoccia S and others. 2010. Multiscale three-dimensional scaffolds for soft tissue engineering via multimodal electrospinning. Acta Biomater 6(4):1227-37.
- Song L, Zhou Q, Duan P, Guo P, Li D, Xu Y, Li S, Luo F, Zhang Z. 2012. Successful development of small diameter tissue-engineering vascular vessels by our novel integrally designed pulsatile perfusion-based bioreactor. PLoS One 7(8):e42569.
- Stock UA, Vacanti JP. 2001. Cardiovascular physiology during fetal development and implications for tissue engineering. Tissue Eng 7(1):1-7.
- Stylianopoulos T, Bashur CA, Goldstein AS, Guelcher SA, Barocas VH. 2008. Computational predictions of the tensile properties of electrospun fibre meshes: effect of fibre diameter and fibre orientation. Journal of the mechanical behavior of biomedical materials 1(4):326-335.
- Tallawi M, Rosellini E, Barbani N, Cascone MG, Rai R, Saint-Pierre G, Boccaccini AR. 2015. Strategies for the chemical and biological functionalization of scaffolds for cardiac tissue engineering: a review. J R Soc Interface 12(108):20150254.
- Thompson CA, Colon-Hernandez P, Pomerantseva I, MacNeil BD, Nasseri B, Vacanti JP, Oesterle SN. 2002. A novel pulsatile, laminar flow bioreactor for the development of tissue-engineered vascular structures. Tissue engineering 8(6):1083-1088.
- Tirtaatmadja V, Dunstan DE, Boger DV. 2001. Rheology of dextran solutions. Journal of Non-Newtonian Fluid Mechanics 97(2-3):295-301.
- Tosun Z, McFetridge PS. 2013. Improved recellularization of ex vivo vascular scaffolds using directed transport gradients to modulate ECM remodeling. Biotechnol Bioeng 110(7):2035-45.
- Valiño G, Suárez C, Rico J, Álvarez B, Blanco D. Comparison between a laser micrometer and a touch trigger probe for workpiece measurement on a cnc lathe; 2012. Trans Tech Publ. p 49-54.
- Vito RP, Dixon SA. 2003. Blood vessel constitutive models—1995–2002. Annual review of biomedical engineering 5(1):413-439.
- Wang C, Cen L, Yin S, Liu Q, Liu W, Cao Y, Cui L. 2010. A small diameter elastic blood vessel wall prepared under pulsatile conditions from polyglycolic acid mesh and smooth muscle cells differentiated from adipose-derived stem cells. Biomaterials 31(4):621-30.
- Wang W, Kratz K, Behl M, Yan W, Liu Y, Xu X, Baudis S, Li Z, Kurtz A, Lendlein A. 2015. The interaction of adipose-derived human mesenchymal stem cells and polyether ether ketone. Clinical hemorheology and microcirculation 61(2):301-321.
- Wechezak A, Viggers R, Sauvage L. 1985. Fibronectin and F-actin redistribution in cultured endothelial cells exposed to shear stress. Laboratory investigation; a journal of technical methods and pathology 53(6):639-647.

- Wenz L, Merritt K, Brown S, Moet A, Steffee A. 1990. In vitro biocompatibility of polyetheretherketone and polysulfone composites. Journal of biomedical materials research 24(2):207-215.
- Whited BM, Rylander MN. 2014. The influence of electrospun scaffold topography on endothelial cell morphology, alignment, and adhesion in response to fluid flow. Biotechnol Bioeng 111(1):184-95.
- WHO. 2015. WHO Mortality Database (retrieved on 29-05-2018). http://www.who.int/healthinfo/statistics/mortality_rawdata/en/index.html
- Williams DF. 2008. On the mechanisms of biocompatibility. Biomaterials 29(20):2941-2953.
- Wolf F, Rojas Gonzalez DM, Steinseifer U, Obdenbusch M, Herfs W, Brecher C, Jockenhoevel S, Mela P, Schmitz-Rode T. 2018. VascuTrainer: A Mobile and Disposable Bioreactor System for the Conditioning of Tissue-Engineered Vascular Grafts. Ann Biomed Eng.
- Wong S-C, Baji A, Leng S. 2008. Effect of fiber diameter on tensile properties of electrospun poly(ε-caprolactone). Polymer 49(21):4713-4722.
- Wright G. 1997. Mechanical simulation of cardiac function by means of pulsatile blood pumps. Journal of cardiothoracic and vascular anesthesia 11(3):299-309.
- Wu SP, Ringgaard S, Oyre S, Hansen MS, Rasmus S, Pedersen EM. 2004. Wall shear rates differ between the normal carotid, femoral, and brachial arteries: an in vivo MRI study. Journal of Magnetic Resonance Imaging: An Official Journal of the International Society for Magnetic Resonance in Medicine 19(2):188-193.
- Wu T, Zhang J, Wang Y, Li D, Sun B, El-Hamshary H, Yin M, Mo X. 2018. Fabrication and preliminary study of a biomimetic tri-layer tubular graft based on fibers and fiber yarns for vascular tissue engineering. Mater Sci Eng C Mater Biol Appl 82:121-129.
- Yamamoto K, Takahashi T, Asahara T, Ohura N, Sokabe T, Kamiya A, Ando J. 2003. Proliferation, differentiation, and tube formation by endothelial progenitor cells in response to shear stress. Journal of applied physiology 95(5):2081-2088.
- Zhang X, Reagan MR, Kaplan DL. 2009. Electrospun silk biomaterial scaffolds for regenerative medicine. Adv Drug Deliv Rev 61(12):988-1006.

Appendix

A. Norms

I. ISO 7198:2016

- a) The length of the tested prosthesis should have a length of more than 10 times its diameter.
- b) The test conditions should approximate the in vivo environment. The determination of the compliance has to be carried out at 37 ± 2 °C and with a pulsatile frequency of 60 ± 10 bpm.
- c) Three pressure ranges have to be considered to account for nonlinear elastic properties: 50 - 90 mmHg, 80 - 120 mmHg, and 110 - 150 mmHg.
- The transducer should be able to measure the pressure to an accuracy of 2 mmHg.
- e) The device that measures the extension of the diameter of the graft should be capable of measuring the diameter to an accuracy of 0.02 mm.
- The vascular graft should have a longitudinal preload of 0.294 N to 0.588 N, corresponding to a suspended mass of 30 g to 60 g.
- If and elastic, non-permeable liner is used in the case of porous scaffolds, the diameter of the liner at 16 kPa should be significantly greater than the nominal pressurised diameter of the vascular graft to be measured.
- h) If the external diameter is directly measured, the internal diameter is calculated by subtracting the unloaded graft wall thickness. If the wall thickness significantly changes under pressurisation, the pressurised internal radius shall be calculated from the volume and length.
- The compliance shall be calculated according to:

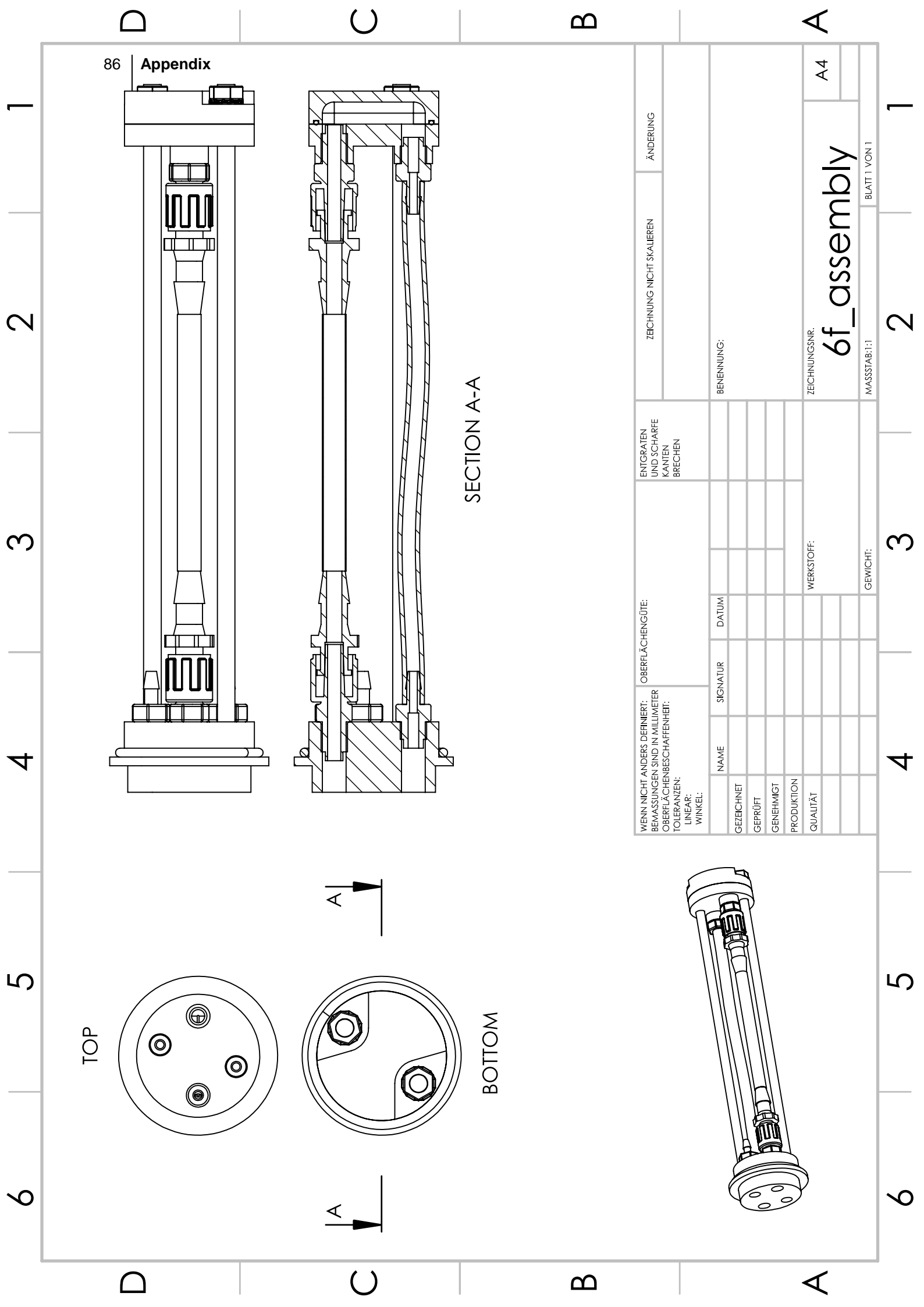
$$C = \frac{\Delta d/d_{p_1}}{\Delta p} = \frac{d_{p_2} - d_{p_1}}{d_{p_1} (p_2 - p_1)}$$

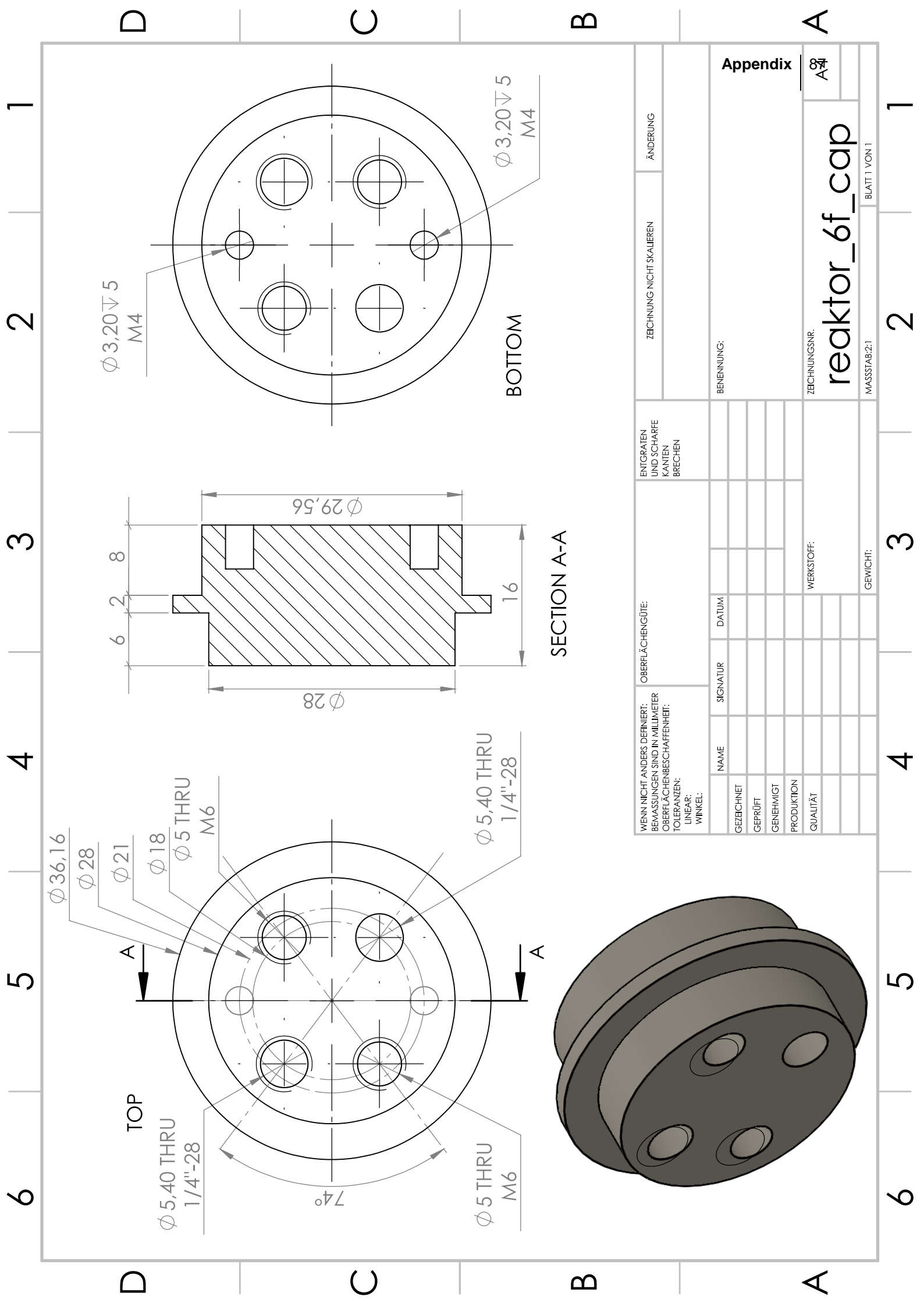
II. EN ISO 10993-5:2009

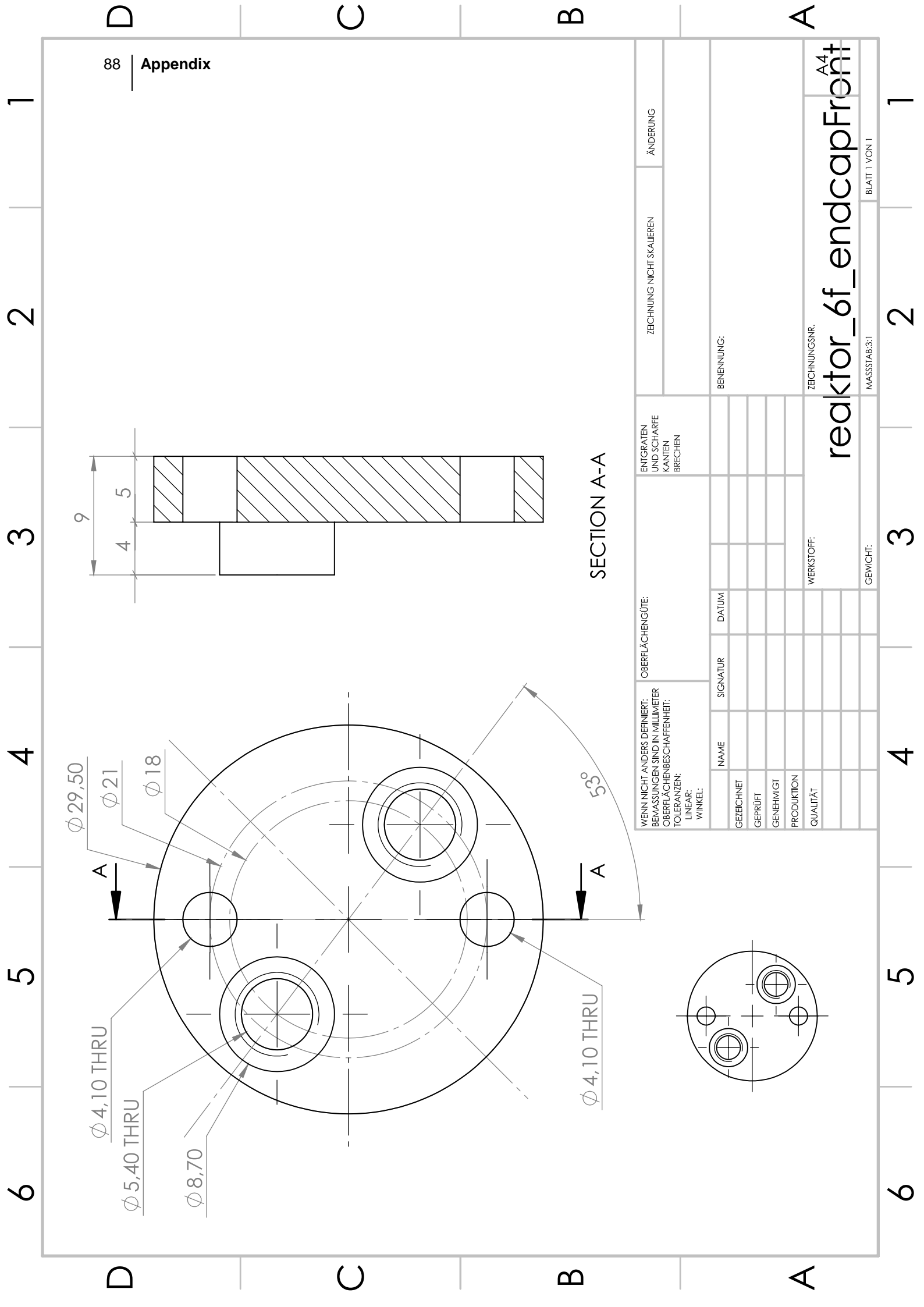
ISO 10993 covers the biological evaluation of medical devices. It consists of a total of 20 parts, of which part 5 describes a number of testing schemes to assess the in vitro cytotoxicity of medical devices. This includes the preparation of samples, cells, and guidelines for the exposure of the cells to the test samples or their extracts. Furthermore, it includes a number of assay protocols for the quantitative evaluation of the cytotoxicity tests. Two possible approaches for a cytotoxicity test are mentioned: either by testing a cell culture indirectly on an extract, or by testing a cell culture on the test sample itself. In both cases, the test should include three controls (positive, blank, and negative) and a minimum of three repetitions.

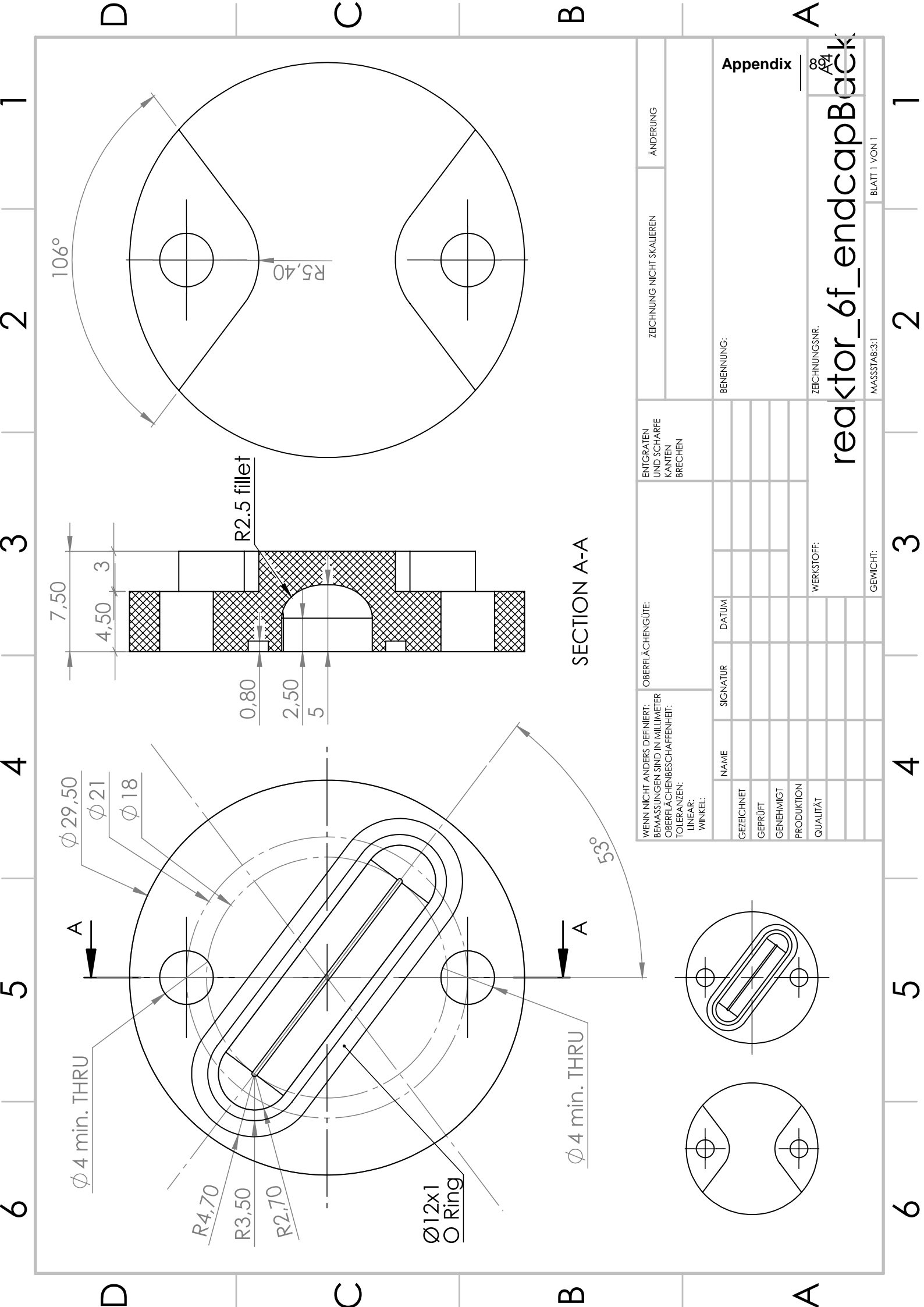
B. CAD Drawings

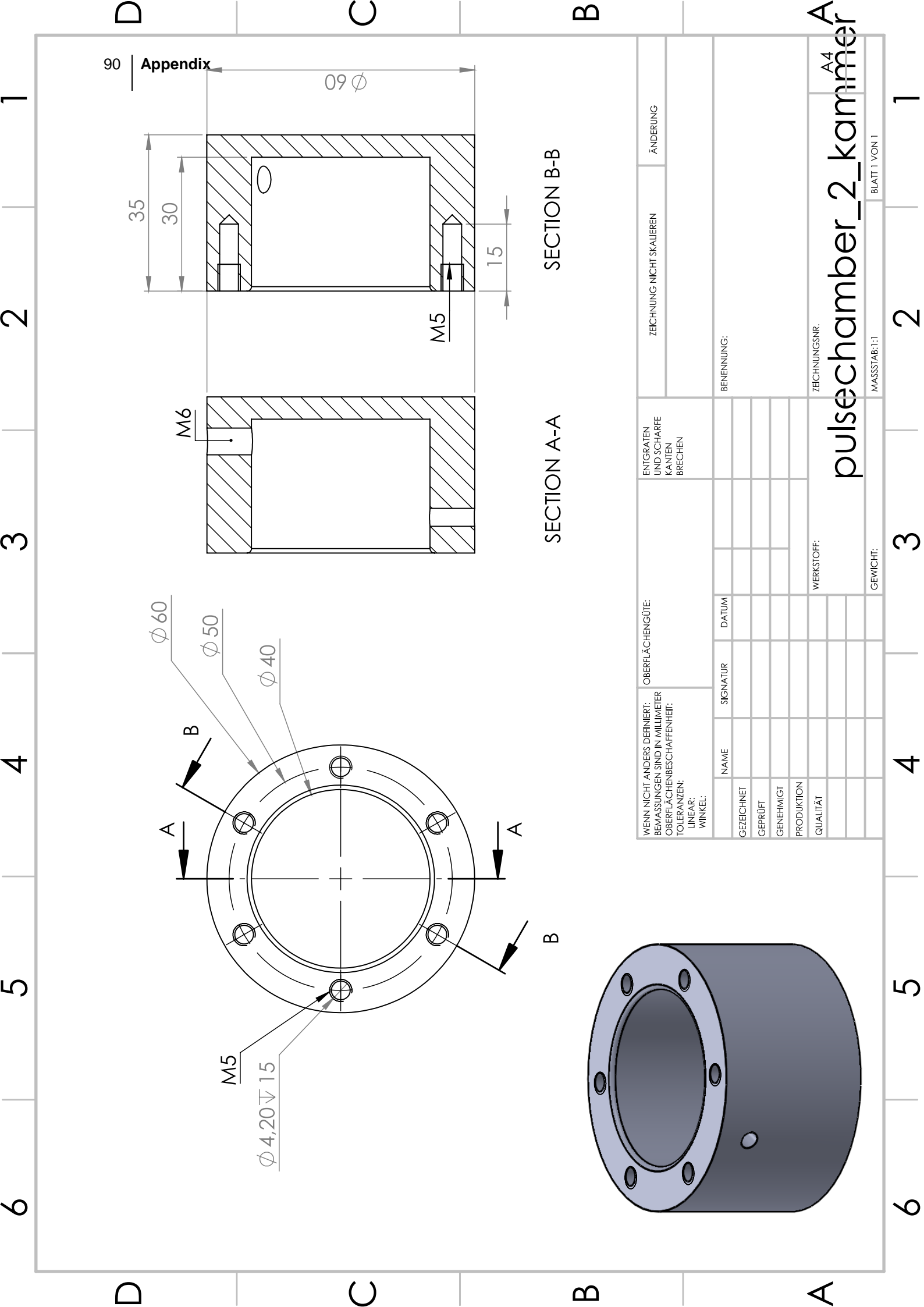
The following pages feature the full-sized DIN A4 CAD drawings.

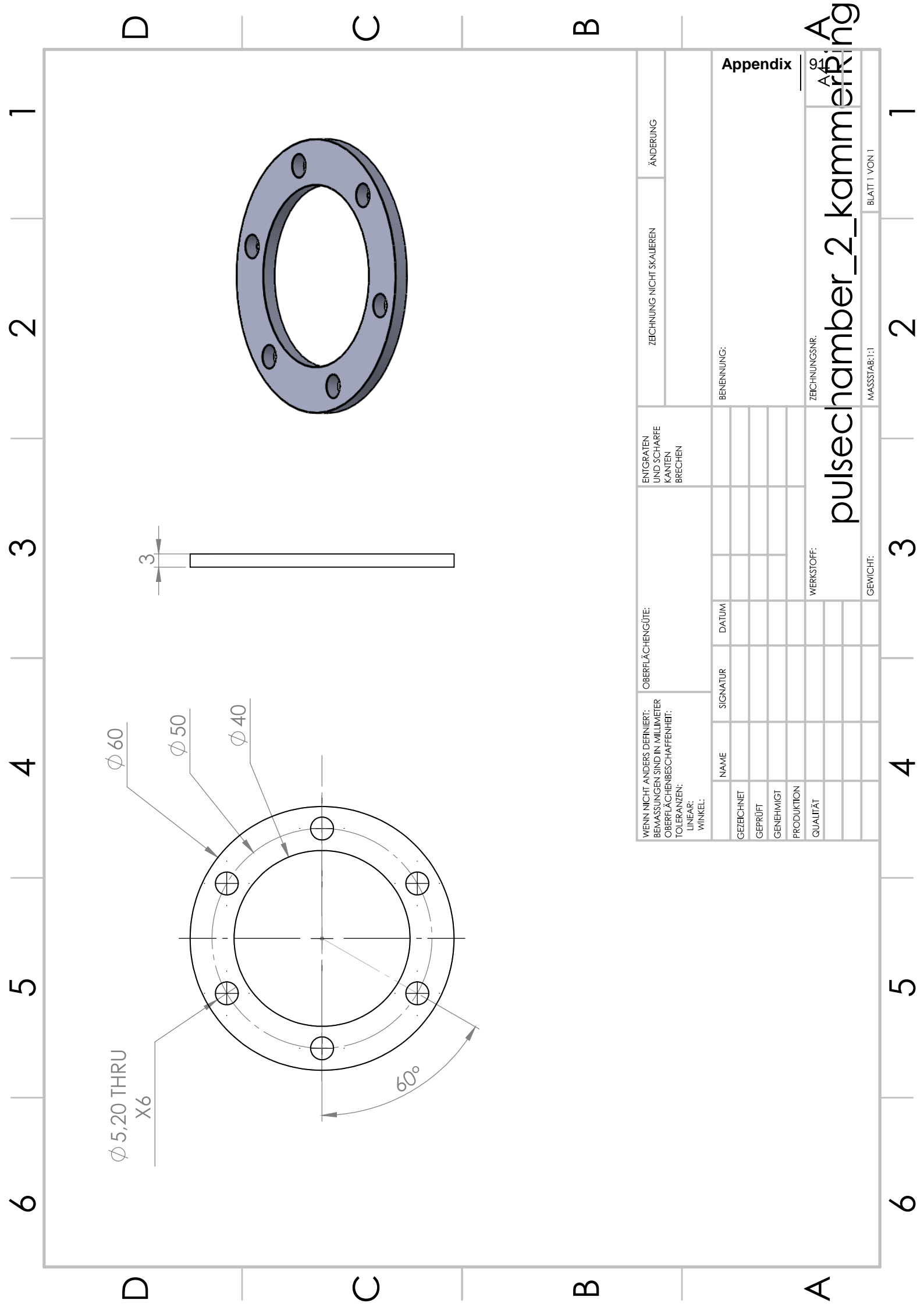












C. Code

Vessel dilation measurement (Algorithm 1: Real-time Hough Transform)

Language: C++

```
/* -----
Vessel Dilatation Measurement
Created by: Dmitri Visser
Based on Hough Transform Demo, retrieved from:
https://docs.opencv.org/2.4/doc/tutorials/imgproc/imgtrans/hough_lines/hough_lines.html
#include <opencv2/core.hpp>
#include <opencv2/videoio.hpp>
#include <opencv2/highgui.hpp>
#include <opencv2/imgproc/imgproc.hpp>
#include <iostream>
#include <stdio.h>
#include <vector>
#include <numeric>
#include <iomanip>
#include <sstream>
#include <chrono>
#include <Windows.h>
using namespace std;
// Capture Device Initialisation int deviceID = 0; // 0 = open default camera
int apiID = cv::CAP ANY;
                              // 0 = autodetect default API
cv::VideoCapture cap;
// Create OpenCV Matrices that store the frames
cv::Mat imgMatGray, imgMatRGB;
// Create images for the crop outs: imgMat0 and imgMat1
cv::Mat imgMat0, imgMat1, imgMatEdges0, imgMatEdges1;
\ensuremath{//} Define the crop outs. One will be on the left side,
// another on the right side.
int safeRegion = 10;
int centerMargin = 50;
int rectangleWidth = 240;
// The lines that will be found within the crop outs will
// be stored in: lines0 and lines1.
vector<cv::Vec2f> lines0, lines1;
vector<cv::Vec4i> linesp0, linesp1;
// Brightness/Contrast Adjustment
cv::Mat lut(1, 256, CV_8U);
int alpha = 50;
int beta = 128;
int foo = 0;
uchar *p = lut.data;
// Hough Transform Initialisation
cv::Mat standard_hough, probabilistic_hough;
int min_threshold = 50;
int max_trackbar = 150;
int s_trackbar = max_trackbar;
int thresholdP = 50;
int minLineLength = 50;
int maxLineGap = 50;
int houghModeProb = 1;
int main(int, char**)
{
        const char* windowName = "Diameter Measurement";
       SetConsoleTitle("Diameter Measurement Output");
       // Store current timestamp
       auto begin = chrono::high_resolution_clock::now();
       // Initialise capture device
       cap.open(deviceID + apiID);
       if (!cap.isOpened()) {
```

```
cerr << "E: Unable to open camera\n";</pre>
          return -1;
 cout << "Camera grabbing started" << endl</pre>
           << "Press any key to terminate" << endl;</pre>
 // Create window which will show the image and the measurements
 cv::namedWindow(windowName, cv::WINDOW_AUTOSIZE);
 cv::createTrackbar("ROI Width", windowName, &rectangleWidth, 400, NULL); cv::createTrackbar("ROI Margin", windowName, &safeRegion, 50, NULL);
 // Create window to adjust the image
const char* paramWindowName = "Parameters";
 cv::namedWindow(paramWindowName, cv::WINDOW_AUTOSIZE);
cv::namedWindow(paramWindowName, cv::WINDOW_AUTOSIZE);
cv::createTrackbar("Contrast", paramWindowName, &alpha, 100, NULL);
cv::createTrackbar("Brightness", paramWindowName, &beta, 255, NULL);
cv::createTrackbar("N Tresh", paramWindowName, &s_trackbar, max_trackbar, NULL);
cv::createTrackbar("N/P Mode", paramWindowName, &houghModeProb, 1, NULL);
cv::createTrackbar("P Thresh", paramWindowName, &thresholdP, 150, NULL);
cv::createTrackbar("P Min Line", paramWindowName, &minLineLength, 500, NULL);
cv::createTrackbar("P Max Gap", paramWindowName, &maxLineGap, 200, NULL);
 while(true)
 {
           // Grab colour frame from camera and store it into matrix 'imgMatRGB'
           cap.read(imgMatRGB);
           if (imgMatRGB.empty()) {
                    cerr << "E: Blank frame grabbed\n";</pre>
                    break:
          }
           // Convert imgMatRGB to a grayscale image.
           cv::cvtColor(imgMatRGB, imgMatGray, CV_BGR2GRAY);
           // Apply contrast and brightness adjustments
           // Since the OpenCV API for the GUI only supports trackbars with
           // positive integer numbers, the contrast and brightness parameters
           // are converted and cast to doubles here.
           imgMatGray.convertTo(imgMatGray, -1, 0.5 + (double)alpha / 100, beta - 128);
           // Crop out the two rectangles
          imgMat0 = imgMatGray(rectangleLeft);
           imgMat1 = imgMatGray(rectangleRight);
           // Apply the Canny edge detection algorithm on the cropouts.
          cv::Canny(imgMat0, imgMatEdges0, 50, 200, 3);
cv::Canny(imgMat1, imgMatEdges1, 50, 200, 3);
cv::imshow("Left", imgMatEdges0);
cv::imshow("Right", imgMatEdges1);
           cv::cvtColor(imgMatGray, standard_hough, CV_GRAY2BGR);
           // Store horizontal positions of the lines in a vector
           vector<float> leftHorPosition, rightHorPosition;
           float leftPositionSum = 0;
           float rightPositionSum = 0;
           // Reset number of found lines
           lines0.resize(0), lines1.resize(0);
           linesp0.resize(0), linesp1.resize(0);
           if ((bool)houghModeProb == true)
           {
                     // Hough Transform for both crop outs
                    cv::HoughLinesP(imgMatEdges0, linesp0, 1, CV_PI / 180, min_threshold + thresholdP, minLineLength,
maxLineGap);
                    cv::HoughLinesP(imgMatEdges1, linesp1, 1, CV_PI / 180, min_threshold + thresholdP, minLineLength,
maxLineGap):
                    leftHorPosition.resize(linesp0.size());
                    rightHorPosition.resize(linesp1.size());
                    for (size_t i = 0; i < linesp0.size(); i++)</pre>
                              cv::Vec4i l = linesp0[i];
                              leftHorPosition[i] = (float)(1[0] + 1[2]) / 2 + safeRegion;
```

```
leftPositionSum += leftHorPosition[i];
                              cv::Point(1[2] + safeRegion, 1[3] + safeRegion), cv::Scalar(0, 255, 0), 3,
CV AA);
                      }
                      for (size_t i = 0; i < linesp1.size(); i++)</pre>
                              cv::Vec4i l = linesp1[i];
                              rightHorPosition[i] = (float)(1[0] + 1[2]) / 2 + 640 - rectangleWidth - safeRegion;
                              rightPositionSum += rightHorPosition[i];
                              cv::line(standard_hough, cv::Point(1[0] + 640 - rectangleWidth - safeRegion, 1[1] +
safeRegion),
                                      cv::Point(1[2] + 640 - rectangleWidth - safeRegion, 1[3] + safeRegion),
cv::Scalar(0, 255, 0), 3, CV_AA);
               else {
                       // Hough Transform for both crop outs
                      cv::HoughLines(imgMatEdges0, lines0, 1, CV_PI / 180, min_threshold + s_trackbar, 0, 0);
                      cv::HoughLines(imgMatEdges1, lines1, 1, CV_PI / 180, min_threshold + s_trackbar, 0, 0);
                      leftHorPosition.resize(lines0.size());
                      rightHorPosition.resize(lines1.size());
                      for (size_t i = 0; i < lines0.size(); i++)</pre>
                              float r = lines0[i][0], t = lines0[i][1];
                              double cos_t = cos(t), sin_t = sin(t);
double x0 = r * cos_t, y0 = r * sin_t;
                              double alpha = 1000;
                              leftHorPosition[i] = x0 + rectangleWidth / 2 + safeRegion;
                              leftPositionSum += leftHorPosition[i];
                              cvRound(y0 - alpha * cos_t) + safeRegion);
                              cv::line(standard_hough, pt1, pt2, cv::Scalar(255, 0, 0), 3, cv::LINE_AA);
                      }
                      // Repeat for the right-hand side
                       for (size_t i = 0; i < lines1.size(); i++)</pre>
                              float r = lines1[i][0], t = lines1[i][1];
                              double cos_t = cos(t), sin_t = sin(t);
double x0 = r * cos_t, y0 = r * sin_t;
                              double alpha = 1000;
                              rightHorPosition[i] = x0 + 640 - rectangleWidth / 2 - safeRegion;
                              rightPositionSum += rightHorPosition[i];
                              cv::Point pt1(cvRound(x0 + alpha * (-sin_t) + 640 - rectangleWidth - safeRegion),
                              cvRound(y0 + alpha * cos_t) + safeRegion);
cv::Point pt2(cvRound(x0 - alpha * (-sin_t) + 640 - rectangleWidth - safeRegion),
                                      cvRound(y0 - alpha * cos_t) + safeRegion);
                              cv::line(standard_hough, pt1, pt2, cv::Scalar(255, 0, 0), 3, cv::LINE_AA);
                      }
               }
               // Draw the rectangular regions of the crop outs on the screen
               cv::rectangle(standard_hough, rectangleRight, cv::Scalar(0, 0, 255), 2); cv::rectangle(standard_hough, rectangleLeft, cv::Scalar(0, 0, 255), 2);
               if ((lines0.size() > 0 && lines1.size() > 0) || (linesp0.size() > 0 && linesp1.size() > 0))
                      // When lines are found by the Houghtransform,
                       // compute the distance between them and output to the console.
                      // Calculate timestamp of the measurement.
                       auto end = chrono::high_resolution_clock::now();
                      auto duration = end - begin;
```

```
auto ms = std::chrono::duration_cast<std::chrono::milliseconds>(duration).count();
                  // Calculate averages
                 float rightAverage = rightPositionSum / rightHorPosition.size();
float leftAverage = leftPositionSum / leftHorPosition.size();
                  // Output measurement to console.
                 // === OUTPUT COMMA SEPARATED ===
                                                                                              // Timestamp
                          << rightAverage - leftAverage << ", "</pre>
                                                                             // Diameter
                          << rightAverage << ", "
<< leftAverage << ", "</pre>
                                                                                              // Average position 1
                                                                                      // Average position 2
                          << s_trackbar << endl;
                                                                                     // Threshold setting
                 // Display measurement on the screen.
float diff = 0.0;
                  diff = rightAverage - leftAverage;
                  stringstream stream0,stream1;
stream0 << "DIFF: " << fixed << setprecision(1) << diff << "px";</pre>
                 string disp0 = stream0.str();
//string disp1 = stream1.str();
                  cv::putText(standard_hough, disp0, cv::Point(20, 40), cv::FONT_HERSHEY_SIMPLEX, 1, cv::Scalar(0, 0,
180), 2);
         else {
                  // When no edges are found in the crop outs,
                  // display the following message.
                  string disp0 = "No edges found.";
                  cv::putText(standard_hough, disp0, cv::Point(10, 150), cv::FONT_HERSHEY_SIMPLEX, 1, cv::Scalar(0, 0,
143), 2);
         cv::imshow(windowName, standard_hough);
         if (cv::waitKey(5) >= 0)
}
return 0;
}
```

Vessel dilation measurement (Algorithm 2: Width measurement by thresholding) П.

Language: Matlab

```
% Read recorded video file
filename = 'Film-80.avi';
actualDuration = 87.63;
vidObj = VideoReader(filename);
vidObj = vidObj.Height;
vidWidth = vidObj.Width;
k = 1:
nFrames = round(vidObj.Duration * vidObj.FrameRate);
diamPixels = zeros(nFrames, 1);
while hasFrame(vidObj)
     fprintf('Processing frame %i of %i\n',k,nFrames)
     \$ Read only first channel, since image is grayscale \$ Convert read data to a binary image
     cdata = readFrame(vidObj);
     binary = imbinarize(cdata(:, :, 1));
     \mbox{\$} Find left- and right-hand side of region where the transmission
     \mbox{\ensuremath{\$}} is below threshold for every horizontal frame row.
     width = zeros(vidHeight, 1);
for j = 1:1040 % Video frame has 1040 rows
          lhs = find(binary(j,:) < 0.5, 1, 'first');
rhs = find(binary(j,:) < 0.5, 1, 'last');
          width(j) = rhs - lhs;
     % Calculate mean width for current frame
     diamPixels(k) = mean(width);
     k = k+1:
end
clearvars -except diamPixels vidHeight vidWidth nFrames actualDuration
%% Calculate shift
\mbox{\%} Overlay oressure readings and recorded video
pressTime = datenum(pressTimestring,'dd-mm-yyyy HH:MM:ss.FFF');
pressTime = 24 .* 60 .* 60 .* (pressTime - pressTime(1));
diamTime = linspace(0, actualDuration, nFrames)';
close all
figure
hold on
yyaxis left
plot(pressTime, pressBits);
yyaxis right
plot(diamTime, diamPixels);
%% Compliance
% Calculate the pressure based on the last calibration of the pressure
% transducer.
x1 = -4.8533;
x2 = 0.042095;
pressMMHG = x1 + pressBits .* x2;
\$ Calculate the relative time, starting at 0 seconds and interpolate the \$ pressure data. This ensures that the time of the datapoints of the
\mbox{\ensuremath{\$}} pressure reading correspond to the video frames and can be correlated in
% the next step.

diamTime = linspace(0, actualDuration, nFrames)' - shift;
yi = interplq(pressTime,pressMMHG,diamTime);
% Define data subset to be analysed.
% [start_time end_time] in seconds
subset = [30 65];
idx1 = find(diamTime > subset(1), 1, 'first');
idx2 = find(diamTime < subset(2), 1, 'last');</pre>
% Calculate thickness
OD_tube = 7;
ID_tube = 6;
thickness = (OD_tube - ID_tube)/2;
% Calculate inner diameter based on thickness
```

III. Read wall shear stress from CFD data

Language: Matlab

```
wss = []; wssNorm = [];
tauInlet = zeros(1,length(data));
poisValue = zeros(1,length(data));
poisPositions = zeros(1,length(data));
r1 = 0.0015;  % Radius at entrance
r2 = 0.0025;  % Radius at scaffold
x1 = 43.15e-3; % Set this as starting x coordinate
               % Length of scaffold region of interest
1 = 55e-3;
% == GO THROUGH CASES AND EXTRACT WSS VALUES
for i = 1:length(data)
    % Take the region of interest as a subset and group the nodes according
    % to their x-position.
    % Subset 1: Everything from inlet until return channel
    subset1 = data[i]( data[i](:,3) > -0.005 , :);
    xlayers = unique(subset1(:,2),'rows');
    \% Calculate wall shear stress as a mean value of the nodes for every
    % slice in the yz plane.
wss = [wss; zeros(1,length(xlayers))];
    for j = 1:length(xlayers)
        wss(i,j) = mean(subset1( subset1(:,2) == xlayers(j) ,5));
    end
    \% Create a normalised wall shear stress profile
    tauInlet(i) = mean(wss(i, 5:40));
    wssNorm = [wssNorm; wss(i,:) ./ tauInlet(i) ./ (r1/r2).^3];
    % Extract position where the wall shear stress redevelops 95% of
    % the Poiseuille value.
    poisValue(i) = tauInlet(i) .* (r1/r2)^3;
    idx = bitand(xlayers >= x1, xlayers < x1+1);</pre>
    subset2 = wssNorm(i, idx);
    subset2_x = xlayers(idx);
    poisPositions(i) = find(subset2 < 0.95, 1, 'last');</pre>
end
```

D. MTS raw data

Plate 1:

PEEK1	BLIND
PEEK2	PC
PEEK3	NC

Plate 2:

Д	L1
Δ	L2
Δ	L3

	1	2	3	4	5	6	7	8	9	10	11	12
A	0,486	0,502	0,517	0,092	0,092	0,089	0,384	0,382	0,384	0,091	0,089	0,084
В	0,415	0,419	0,408	0,050	0,055	0,053	0,327	0,334	0,329	0,282	0,050	0,071
С	0,454	0,462	0,466	0,096	0,093	0,094	0,110	0,111	0,108	0,125	0,103	0,103
D	0,426	0,419	0,406	0,055	0,056	0,052	0,063	0,067	0,055	0,050	0,048	0,068
Ε	0,508	0,508	0,497	0,095	0,100	0,099	0,366	0,371	0,387	0,088	0,101	0,102
F	0,414	0,438	0,445	0,058	0,057	0,057	0,349	0,333	0,322	0,048	0,051	0,070
G	0,041	0,042	0,040	0,040	0,040	0,040	0,040	0,040	0,041	0,041	0,041	0,042
Н	0,041	0,042	0,041	0,041	0,041	0,042	0,043	0,041	0,042	0,042	0,042	0,042
	1	2	3	4	5	6	7	8	9	10	11	12
Α	0,432	2 0,420	3	4 0,092	5 0,094	6 0,098	7	8 0,042	9 0,043	10 0,043	11 0,043	12 0,042
A B												
	0,432	0,420	0,467	0,092	0,094	0,098	0,042	0,042	0,043	0,043	0,043	0,042
В	0,432	0,420	0,467	0,092	0,094	0,098	0,042	0,042	0,043	0,043	0,043	0,042
B C	0,432 0,321 0,395	0,420 0,322 0,418	0,467 0,348 0,416	0,092 0,052 0,098	0,094 0,058 0,097	0,098 0,057 0,093	0,042 0,042 0,041	0,042 0,041 0,041	0,043 0,042 0,042	0,043 0,041 0,042	0,043 0,041 0,041	0,042 0,042 0,044
B C D	0,432 0,321 0,395 0,326	0,420 0,322 0,418 0,338	0,467 0,348 0,416 0,353	0,092 0,052 0,098 0,071	0,094 0,058 0,097 0,048	0,098 0,057 0,093 0,051	0,042 0,042 0,041 0,044	0,042 0,041 0,041 0,042	0,043 0,042 0,042 0,043	0,043 0,041 0,042 0,040	0,043 0,041 0,041 0,041	0,042 0,042 0,044 0,044
B C D	0,432 0,321 0,395 0,326	0,420 0,322 0,418 0,338	0,467 0,348 0,416 0,353 0,412	0,092 0,052 0,098 0,071 0,095	0,094 0,058 0,097 0,048 0,090	0,098 0,057 0,093 0,051	0,042 0,042 0,041 0,044 0,043	0,042 0,041 0,041 0,042 0,042	0,043 0,042 0,042 0,043	0,043 0,041 0,042 0,040 0,041	0,043 0,041 0,041 0,041 0,041	0,042 0,042 0,044 0,044